MASONRY INFILL REINFORCED CONCRETE FRAMES UNDER CYCLIC LOADING

Mr. Jarun Srechai

A Dissertation Submitted in Partial Fulfillment of the Requirements
for the Degree of Doctor of Philosophy Program in Civil Engineering
Department of Civil Engineering
Faculty of Engineering
Chulalongkorn University
Academic Year 2013

โครงอาคารคอนกรีตเสริมเหล็กที่มีผนังอิฐก่อภายใต้แรงแบบวัฏจักร

นายจรัญ ศรีชัย

วิทยานิพนธ์นี้เป็นส่วนหนึ่งของการศึกษาตามหลักสูตรปริญญาวิศวกรรมศาสตรดุษฎีบัณฑิต
สาขาวิชาวิศวกรรมโยธา ภาควิชาวิศวกรรมโยธา
คณะวิศวกรรมศาสตร์ จุฬาลงกรณ์มหาวิทยาลัย
ปีการศึกษา 2556

Thesis Title	MASONRY INFILL REINFORCED CONCRETE FRAMES UNDER CYCLIC LOADING
By	Mr. Jarun Srechai
Field of Study	Civil Engineering
Thesis Advisor	Professor Panitan Lukkunaprasit, Ph.D.
Thesis Co-Advisor	Assistant Professor Arnon Wongkaew, Ph.D.

Accepted by the Faculty of Engineering, Chulalongkorn University in Partial Fulfillment of the Requirements for the Doctoral Degree

.....Dean of the Faculty of Engineering
(Professor Bundhit Eua-arporn, Ph.D.)

THESIS COMMITTEE

.....Chairman
(Professor Thaksin Thepchatri, Ph.D.)

.....Thesis Advisor
(Professor Panitan Lukkunaprasit, Ph.D.)

.....Thesis Co-Advisor
(Assistant Professor Arnon Wongkaew, Ph.D.)

.....Examiner
(Assistant Professor Chatpan Chintanapakdee, Ph.D.)

.....Examiner
(Assistant Professor Anat Ruangrassamee, Ph.D.)

.....External Examiner
(Associate Professor Sutat Leelataviwat, Ph.D.)

จรัญ ศรีชัย : โครงอาคารคอนกรีตเสริมเหล็กที่มีผนังอิฐก่อภายใต้แรงแบบวัฏจักร. (MASONRY INFILL REINFORCED CONCRETE FRAMES UNDER CYCLIC LOADING) อ.ที่ปรึกษาวิทยานิพนธ์หลัก: ศ. ดร.ปณิธาน ลักคุณะประสิทธิ์, อ.ที่ปรึกษาวิทยานิพนธ์ร่วม: ผศ. ดร.อานนท์ วงษ์แก้ว, 133 หน้า.

การศึกษาวิจัยนี้นำเสนอผลการศึกษาสมรรถนะในการต้านทานแผ่นดินไหวของโครงอาคารคอนกรีตเสริมเหล็กที่มีผนังอิฐก่อโดยวิธีการทดสอบและการวิเคราะห์ อีกทั้งเสนอวิธีการเสริมความแข็งแรงโครงสร้างที่เหมาะสมสำหรับโครงสร้างดังกล่าวเพื่อเพิ่มสมรรถนะของโครงสร้างให้ดีขึ้น ในส่วนของการศึกษาโดยวิธีการทดสอบจะใช้โครงอาคารคอนกรีตเสริมเหล็กที่มีผนังอิฐก่อขนาด 3/4 เท่าของโครงสร้างจริง มีความกว้าง 1 ช่วงเสา สูง 1 ชั้น และผนังอิฐก่อของตัวอย่างทดสอบที่ไม่มีการปรับปรุงโครงสร้างนั้นมีอัตราส่วนความกว้างต่อความสูงเท่ากับ 2 ซึ่งการศึกษาวิจัยในครั้งนี้ได้ทำการทดสอบตัวอย่างทดสอบทั้งหมดจำนวน 4 ตัวอย่างภายใต้แรงกระทำทางด้านข้างแบบวัฏจักรร่วมกับแรงกระทำในแนวดิ่งที่มีขนาดคงที่ ในส่วนของการศึกษาโดยการวิเคราะห์นั้น จะประเมินสมรรถนะของตัวอย่างทดสอบทั้งหมดโดยการวิเคราะห์ด้วยวิธีผลักด้านข้างแบบสถิตไร้เชิงเส้น โดยจำลองผนังอิฐก่อด้วยชิ้นส่วนรับแรงอัดในแนวทแยงเทียบเท่าแบบสามชิ้นต่อหนึ่งแนวทแยงมุมของผนังอิฐก่อ ในส่วนของโครงอาคารคอนกรีตเสริมเหล็กนั้นจะจำลองโดยใช้ชิ้นส่วนที่มีจุดหมุนพลาสติกเชิงดัดและเชิงเฉือนที่ปลายทั้งสอง

จากผลการศึกษาโดยวิธีทดสอบพบว่าเสาของตัวอย่างทดสอบที่ไม่มีการปรับปรุงโครงสร้างเกิดการวิบัติด้วยแรงเฉือนที่ระยะการเคลื่อนตัวทางด้านข้างต่ำมากโดยมีค่าเพียงร้อยละ 0.30 ของความสูง ซึ่งการวิบัติดังกล่าวเกิดขึ้นเนื่องจากมีแรงปริมาณมากจากผนังอิฐก่อถ่ายเข้าสู่เสาโดยตรงหลังจากผนังอิฐก่อบริเวณมุมที่รับแรงอัดเกิดความเสียหาย ด้วยการใช้รูปแบบการวิบัติดังกล่าวเป็นแนวทางในการปรับปรุงโครงสร้างให้กับตัวอย่างทดสอบโดยการแยกผนังอิฐก่อออกจากเสาของโครงอาคารและใช้หูช้างเหล็กในการถ่ายแรงปฏิสัมพันธ์ระหว่างผนังและคานของโครงอาคารโดยตรง ด้วยวิธีการนี้จะสามารถขจัดแรงจากผนังที่ถ่ายเข้าสู่เสาออกไปได้อย่างสิ้นเชิง วิธีการปรับปรุงโครงสร้างดังกล่าวสามารถเพิ่มสมรรถนะของโครงสร้างให้กับตัวอย่างทดสอบได้อย่างมากเมื่อเปรียบเทียบกับตัวอย่างทดสอบที่ไม่มีการปรับปรุงโครงสร้าง โดยความสามารถในการเคลื่อนตัวทางด้านข้างของตัวอย่างทดสอบที่ได้รับการปรับปรุงโครงสร้างมีค่าเพิ่มขึ้น 5 เท่าของตัวอย่างทดสอบที่ไม่มีการปรับปรุงโครงสร้าง อีกทั้งยังคงความสามารถในการต้านทานแรงทางด้านข้างและสติฟเนสของโครงสร้างไว้ได้เกือบทั้งหมด ผลการทดสอบแสดงให้เห็นว่าการเสริมเหล็กตะแกรงปริมาณเล็กน้อยในผนังอิฐก่อ (อัตราส่วนของพื้นที่หน้าตัดเหล็กเสริมต่อผนังอิฐก่อเท่ากับร้อยละ 0.11) ทำให้ตัวอย่างทดสอบมีความสามารถในการเคลื่อนตัวทางด้านข้างเพิ่มขึ้นถึง 8 เท่าเมื่อเทียบกับตัวอย่างทดสอบที่ไม่มีการปรับปรุงโครงสร้าง ผลการศึกษาโดยการวิเคราะห์ของโครงอาคารคอนกรีตเสริมเหล็กที่มีผนังอิฐก่อแสดงให้เห็นว่ากำลังยึดเหนี่ยวของผนังอิฐก่อที่กำหนดโดยมาตรฐาน ASCE 41-06 นั้นมีค่าต่ำกว่าค่าที่แท้จริงของผนังอิฐก่อที่ใช้ในตัวอย่างทดสอบของการศึกษานี้ และระยะเคลื่อนตัวด้านข้าง ณ ตำแหน่งที่ผนังอิฐก่อมีกำลังต้านทานสูงสุดที่เหมาะสมสำหรับใช้ในแบบจำลองของตัวอย่างทดสอบที่มีการปรับปรุงโครงสร้างแล้ว มีค่าเป็นสองเท่าของค่าที่กำหนดโดยมาตรฐาน ASCE 41-06 เมื่อใช้แบบจำลองที่มีการปรับแก้ความสัมพันธ์ของแรงและการเสียรูปที่เหมาะสมแล้วในการวิเคราะห์โครงอาคารคอนกรีตเสริมเหล็กที่มีผนังอิฐก่อ พบว่าความสัมพันธ์ระหว่างแรงและการเคลื่อนตัวด้านข้างที่จำลองได้มีความสอดคล้องกับผลการทดสอบ

ภาควิชา วิศวกรรมโยธา ลายมือชื่อนิสิต .....

สาขาวิชา วิศวกรรมโยธา ลายมือชื่อ อ.ที่ปรึกษาวิทยานิพนธ์หลัก .....

ปีการศึกษา 2556 ลายมือชื่อ อ.ที่ปรึกษาวิทยานิพนธ์ร่วม .....

5171873721 : MAJOR CIVIL ENGINEERING
KEYWORDS: NON-DUCTILE FRAME / REINFORCED CONCRETE / UN-REINFORCED MASONRY INFILL / CYCLIC TEST / SEISMIC PERFORMANCE / RETROFIT

JARUN SRECHAI: MASONRY INFILL REINFORCED CONCRETE FRAMES UNDER CYCLIC LOADING. ADVISOR: PROF. PANITAN LUKKUNAPRASIT, Ph.D., CO-ADVISOR: ASST. PROF. ARNON WONGKAEW, Ph.D., 133 pp.

This study involves experimental and analytical investigations on the seismic performance of masonry infill non-ductile reinforced concrete (RC) frames. An innovative retrofit scheme is proposed for enhancing seismic performance of such structures. Four ¾ scaled models of single bay, single story, non-ductile RC frames infilled with masonry panels were tested under lateral cyclic load and constant vertical load. The aspect ratio of the masonry infill panel (width to height) in the un-retrofitted specimen is 2.0. As for the analytical investigation, nonlinear static pushover analyses of the tested specimens are performed based on an equivalent three diagonal struts approach. The surrounding frame is modelled using discrete elements with flexural and shear plastic hinges lumped at the ends, and the infill panel modelled using compression-only bar elements.

Experimental results indicate that shear failure occurs prematurely in the columns of the un-retrofitted specimen at a very small drift ratio of 0.30% due to the large strut force exerted by the unreinforced masonry (URM) infill panel on those columns following corner crushing of the URM panel. Guided by such failure, the URM panel is separated from the columns and steel brackets are provided to transfer the interactive forces between the panel and the beams, thereby totally eliminating transfer of large strut force to the columns. The proposed scheme results in much enhanced performance of the retrofitted structure over the un-retrofitted one, with the drift capacity increased 5 folds while retaining most of the strength and stiffness. Moreover, premature severe shear damage in the columns was totally eliminated. With slight steel wire mesh reinforcement (reinforcement ratio of 0.11%) provided in the infill panel, the test specimen could attain a drift capacity of 8 times that of the un-retrofitted one. The analytical study of masonry infill RC frames reveals that the ASCE 41-06 specified cohesive capacity of masonry infill is too conservative for the specimens tested, and the drift associated with the peak lateral capacity of the retrofitted masonry infill should be taken as twice the value specified in the standard. With proper adjustments made for specifying the lateral load-deformation of the URM infill, reasonable agreement in the simulated lateral load-displacement relation of the URM infilled RC frame with the experimental results is obtained.

Department:	Civil Engineering	Student's Signature	.....
Field of Study:	Civil Engineering	Advisor's Signature	.....
Academic Year:	2013	Co-Advisor's Signature	.....

ACKNOWLEDGEMENTS

The author is grateful for the scholarship and research fund from the Commission on Higher Education of Thailand-AUN/SEED-Net and Faculty of Engineering, Burapha University, Thailand (No.CA2/2553). This scholarship and research fund provided a great opportunity for the author to study in Ph.D. program and completing the research. The author would also like to acknowledge and to express deep the support from the Center of Excellence in Earthquake Engineering and Vibration, Chulalongkorn University. The appreciation for an exchange doctoral student scholarship from the European Commission funded project EU-NICE. With this support, I had a great time to carry out my research with Prof. Enrico Spacone at the University of Chieti-Pescara, Italy.

I also wish to express my deepest gratitude to my dissertation advisor, Prof. Panitan Lukkunaprasit, for his continuous guidance and encouragement throughout this study. His invaluable support and care made it possible to complete this study without any problem. Great appreciation is also extended to Asst. Prof. Arnon Wongkaew and Assoc. Prof. Sutat Leelataviwat as well as the dissertation's committee for reviewing the report and offering helpful suggestions and valuable comments.

The assistance of Dr. Boonrat Lohwongwatana in preparing the material for test specimens construction and the assistance of Building 33 Company Limited in casting the test specimens are greatly appreciated. My sincere thanks go to the technicians of the Department of Civil Engineering and graduate students for their help in conducting experiments.

Finally, I would like to attribute all of the achievement to my family for their encouragement, suggestions, and generous comforts throughout all the phases of my Ph.D. study.

CONTENTS

Page

Page

Page

LIST OF TABLES

Page

LIST OF FIGURES

Page

CHAPTER I
INTRODUCTION

1.1 Research Significance

Reinforced concrete (RC) frames with un-reinforced masonry (URM) infill panels is a common structural system in developing countries, especially in low rise buildings. In practical design, the effect of the URM infill panel is commonly ignored due to the complexity involved in modeling. Earthquake reconnaissance in past earthquakes in high seismic prone countries has witnessed poor performance of such structural system, especially when the RC frames are detailed as non-ductile (Sezen et al., 2003, Kyriakides and Billington, 2008). Undesirable abrupt shear failure of the bounding columns or beam-column joints often follows due to transfer of the huge strut force resisted by the infill to the columns following corner crushing of the panel. This is true not only in strong earthquakes, but also in moderate shaking such as that in Chiang-Rai, Thailand caused by the Mw6.9 Tarlay earthquake in Myanmar on March 24, 2011. Model tests as well as full scale tests on real buildings have also yielded similar results (e.g., Bertero and Brokken, 1983, Mehrabi et al., 1996, Al-Chaar et al., 2002, Lee and Woo, 2002, Corte et al., 2008, Shing et al., 2009). It is important to note that such failure can occur at a relatively small story drift, in the order of 0.3%. On the other hand, there have been test results as well as incidents of actual performance of such buildings in earthquakes which demonstrate beneficial effect of un-reinforced infills (Hassan and Sozen, 1997, Mostafaei and Kabeyasawa, 2004, Pinto and Taucer, 2006, Gómez-Martínez et al., 2012). The benefit or detrimental effects of URM panels on building performance have been clearly reviewed by Pujol and Fick (2010) and Fardis and Panagiotakos (1997).

Laboratory tests with masonry reinforced with steel wire mesh, carbon fiber reinforced polymers (CFRP) or the like have demonstrated the potential of transforming the brittle masonry panel to a more ductile one suitable for retrofitting. However, past attempts have accomplished limited success.

As described previously, the URM infill panel provided the significant effects on structural response in both beneficial and un-beneficial. Based on the relevant previous studies, the sophisticated interaction between masonry infill panel and surrounding RC frames caused the difficulty in the structural response prediction. Moreover, several failure modes could occur in the both masonry infill panel and

surrounding RC frame depends upon the properties of URM infill panel and surrounding RC fame. Those failure modes could have a significant effect on the lateral resistance capacity of such structures.

1.2 Objectives of Research

This research focuses on investigating the structural response of un-retrofitted and retrofitted masonry-infilled non-ductile reinforced concrete frames under cyclic loading, which the aim to effectively utilize the masonry walls for seismic resistance. Although emphasis was placed on experimental studies, push over analyses based on a well recognized model were also performed. The main objectives of the research are:

1) To evaluate the structural behavior of masonry-infilled non-ductile reinforced concrete frames under cyclic loading.
2) To propose a suitable retrofitting scheme for non-ductile reinforced concrete frames with un-reinforced masonry infill panels, in the light of experimental results of an un-retrofitted specimen.
3) To verify the accuracy of the proposed analytical modeling to predict the seismic performance of masonry-infilled non-ductile reinforced concrete frames.

1.3 Scope of Research

The structural response of non-ductile reinforced concrete frames with masonry infill panels is evaluated. Both experimental and analytical approaches were considered in this research. The scopes of the research are:

1) Only the in-plane behavior of non-ductile RC frames with solid masonry infill panel is considered.
2) Static cyclic load tests of a single-bay, single-story, sub-assemblage of the prototype are conducted on near full size specimens. With configuration restraints in the testing facility, the scale of 3/4 is employed.
3) Only solid URM panels with solid brick units are considered.
4) The analytical study involves a nonlinear static pushover procedure under monotonic loading only. It is based on a well recognized strut and tie model involving three struts.

1.4 Research Methodology

The major process of the research can be summarized as follows:

1) The previous relevant studies were reviewed.
2) The prototype building, corresponding to an existing low-rise RC frames with masonry infill panels in Thailand, was designed for this research.
3) A sub-assemblage of a single-bay and single-story prototype building was selected for testing.
4) Based on the experimental results of an un-retrofitted specimen, a retrofitting scheme was proposed.
5) Three quarters scale specimens retrofitted with the proposed scheme were constructed and tested in the laboratory.
6) The experimental data were processed and the results discussed.
7) The two-dimensional analytical models for static pushover analyses of the un-retrofitted and retrofitted specimens were constructed and calibrated with the experimental results.

CHAPTER II
LITERATURE REVIEW

2.1 Introduction

Reinforced concrete frames with un-reinforced masonry infill panels are a common structural system in developing countries, especially in low-rise buildings. In practical design, the effect of the URM infill panel is commonly ignored. However, in reality, URM infill panels inevitably provide a significant effect on the seismic response of the structure. In this chapter, a summary of previous relevant studies is presented.

2.2 Behavior of RC frames with masonry infill panels

In this section the relevant studies on the behavior of RC frames with un-reinforced and reinforced masonry infill panel are summarized as follows.

2.2.1 RC frames with unreinforced masonry infill panels

Angel et al. (1994) investigated the seismic response of RC frames with URM infill panels. Eight full-scale models of a single-bay, single-story ductile RC frame with URM infill panel were tested. The URM panels consisted of clay brick or concrete block infills. The aspect ratio (the ratio of width to height of the infill panel) of each specimen was 1.54. In-plane displacement control cyclic loading was applied until cracking occurred in the URM panel. Then an out-of-plane load test was performed. Based on the experimental results, the initial lateral stiffness of the tested specimens was found to depend proportionally on the masonry compressive strength. The mortar properties provided a significant effect on the shear strength of the URM panel. The estimated lateral stiffness of the tested specimens using the diagonal strut analogy was close to the experimental results.

Mehrabi et al. (1996) reported experimental results of twelve 1/2-scale specimens of single-bay, single-story RC frames with weak and strong URM infill panels. The weak and strong infill panels were constructed of hollow and solid concrete blocks, respectively. Two types of RC frames designated as “weak frames” and “strong frames” were considered. The first one was designed for wind load only and the other was designed for seismic load. Various parameters including infill panel

aspect ratio of 1.5 and 2.0, two lateral loading patterns and two vertical loading patterns were employed. It was concluded that the infill panels provided a significant effect on the structural response of the tested frames. The lateral strengths of RC weak frames with weak and strong infill panels were 1.5 and 2.3 times, respectively, compared with the bare frame, whereas the corresponding lateral stiffness were approximately 15 and 50 times, respectively. Three main failure mechanisms of the tested specimens were observed, which depended strongly on the surrounding frame and infill panel strength ratios (Figure 2-1). Flexural failure of the RC frame and sliding along the bed-joint of the infill panel could be observed for weak frames infilled with weak panels. Brittle shear failure of the columns was predominant in the case of weak frame infilled with strong panel. In the case of a strong RC frame infilled with a strong URM panel, the corner crushing of the URM panel was observed as well as a diagonal strut mechanism was found to develop. The difference of vertical load patterns provided an insignificant effect on the tested frames, with 5% variation in the ultimate lateral resistance.

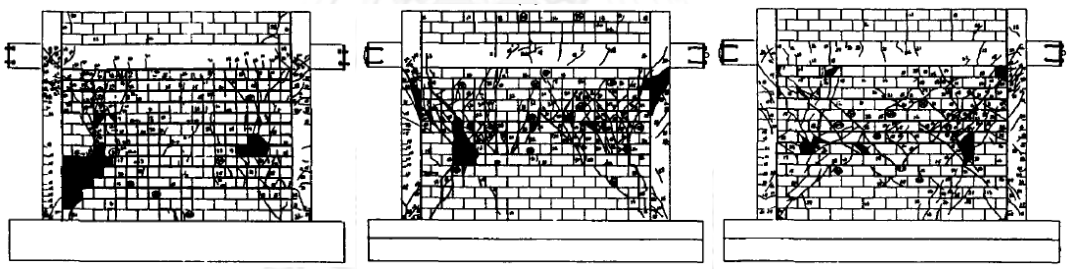

(a) (b) (c)

Figure 2-1. Failure mechanism of test specimens: (a) sliding of bed joint; (b) Shear failure of columns; (c) Conner crushing of masonry infill panel (Mehrabi et al. 1996)

Negro and Verzeletti (1996) performed pseudo-dynamic tests on the full-scale, four-story ductile RC building with and without URM infill panels. The URM infill panels were constructed with clay blocks. The story drift of the URM infilled specimen was reported to decrease by about 50%, compared with the bare RC building. On the other hand, the URM infilled specimen exhibited lower energy dissipation capability, compared with the tested specimen without URM infill panel.

Al-Chaar et al. (2002) reported the experimental results of five 1/2 scale specimens of single-story frames with different numbers of bays. The non-ductile RC

frames with concrete block and clay brick infill panels were used. In-plane monotonic loading, displacement control was employed in all specimens. For single-bay specimens, the lateral strength and stiffness were reported to increase by about 1.4-1.6 and 17-23 times, respectively, over the RC bare frame. In the case of multi-bay specimens, the lateral strength and stiffness of the tested specimens depended on the number of bays with a nonlinear relation. Compressive strength of the infill panel and number of bays provided significantly affect the failure mechanism of the specimens. The single-bay with concrete block infill panel specimen exhibited large diagonal crack in the infill panel, followed by shear failure of compressive column. On the other hand, the single-bay with clay brick infill panel specimen exhibited a strut action. For 2-bay specimen with concrete block infill panels diagonal cracks occurred followed by corner crushing and shear failure of the column.

Lee and Woo (2002) performed an experimental evaluation of the 1/5-scale, 3-story, 2-bay non-ductile RC frames with URM infill panels made of concrete. Earthquake simulation shake table and monotonic loading tests were conducted. First, the shake table tests of fully infill specimen were performed. Then some infill panels were removed and shake table test repeated followed by monotonic load test. The stiffness of the full infill and partial infill frames were reported as 18 and 4 times, respectively, compared with the RC bare frame. Only slightly damage was observed in the URM infill panels and RC frame. Under the monotonic load, the ultimate strength of the partial infill frame was 2 times of the RC bare frame. Sliding along the bed-joint of the URM panel occurred, resulting in a soft-story failure of the tested specimen.

Centeno et al. (2008) performed an experimental investigation on RC frames with URM infill panels. Two 1/2-scale, single-story, single-bay gravity load designed RC frames with URM infill panels were tested. The URM infill panel was constructed with hollow concrete blocks. Two types of testing protocols were considered. In-plane monotonic loading was employed for one specimen and shake table test with different levels of earthquake simulation was used for the other. In the case of monotonic load test, first diagonal cracks of infill panel occurred at 0.3% drift and sliding along the bed-joint of the URM infill panel was observed when story drift reached 1.0%. Lap splice at the base of the leeward RC column failure was observed at 1.65% drift. However, the tested specimen attained maximum load resistance without significant degradation of strength and stiffness until testing was terminated at 3.8% drift. At this state, lap slice failure and shear cracks were observed in both RC columns. Similar to the monotonic load test, first diagonal cracking of infill panel

indicated at 0.3% drift under shack table testing. However, significant stiffness degradation was observed in the strong earthquake simulation test because of severe damage of the URM infill panel at 0.9%.

Corte et al. (2008) reported experimental results of an actual non-ductile RC building with URM infill panels. The two-story building consisted of two bays and four bays in the loading and the orthogonal directions, respectively. Two cycles of fully reversed lateral loading were applied for small story drifts (story drift approximately lower than 0.25%), thereafter the building was pushed until the story drift reached 5%. URM infill cracks appeared at 0.2% story drift and became very large when the story drift reached 0.5%. Various failure modes of the URM panels such as diagonal tension crack, corner crushing, bed-joint sliding, and mix-modes were observed in various URM panels of the building. Flexural-shear damage of the columns due to the interaction of the URM infill panels was observed. After the testing of original building was completed, the building was repaired and the infill panels were rebuilt. Moreover, the infill panels were strengthened with fiber reinforced polymer (FRP) rods in the bed-joints of masonry panels. Similar to the test result of original building, the extensive flexural-shear cracks were observed in the RC columns. However, the strengthening technique exhibited a beneficial effect for preventing the diagonal tension crack of infill panels.

The influence of masonry strength on the structural response of the RC frames with URM infill panel was reported by Kakaletsis and Karayannis (2008). The 1/3-scale, single-story, single-bay ductile RC frames with weak and strong infill panels were tested under in-plane cyclic loading. The lateral strength and secant initial stiffness were reported to increase by 0.6 - 0.8 and 1.4 - 1.6 times, respectively, over the RC bare frame. Moreover, the brittle shear failure was not observed in the RC surrounding frames and the specimen with strong URM infill panels showed better performance, compared with the other one. However, the story drift capacity (at 20% drop in the lateral capacity) of the RC frames infilled with weak and strong panels decreased approximately of 0.4 and 0.15 times of the bare frame, respectively.

Pujol and Fick (2010) reported the cyclic load test results of a 3-dimentional full-scale, three-story non-ductile RC flat-plate structure infilled with URM panels. The structure consisted of two-bays in loading direction and one-bay in the orthogonal direction. The bay length was 6100 mm (center-to-center) in each direction and the story height was 3050 mm (floor-to-floor). Solid URM infill panels made of the clay bricks, were constructed in one bay of the loading direction in all

stories (Figure 2-2). The aspect ratio (W/H) of the URM infill panel was 2.0. The lateral strength and stiffness of the RC flat-plate structure with URM infill panels were reported to be 2 and 6 times, respectively, compared with the RC flat-plate structure without the URM infill panels. The first crack occurred in the URM infill panel at 0.15% story drift. Significant stiffness degradation resulted at 0.2% story drift due to severe damage in the URM infill panels. However, the story drift capacity (at 20% drop in the lateral capacity) of 1.5% was attained without brittle shear failure of the RC columns.

Figure 2-2. RC flat-plate structure with URM infill panels (Pujol et al. 2010)

Zovkic et al. (2013) investigated the influences of the masonry infill panel on the seismic behavior of ductile RC frames. Ten 2/5 scale, single-story sing-bay specimens were tested under lateral cyclic load. Various compressive strengths of masonry panel were considered. It was concluded that the masonry infill panel could increase initial stiffness of the tested specimens in the order of 5.8-6.5 times, over the RC bare frame. It was noted that the variation of masonry infill panel strengths had relatively insignificant effect on initial stiffness of the tested specimens. On the other hand, the lateral strength of the tested specimens was affected significantly by the masonry panel strength. The lateral strength of the tested specimens were reported to increase by about 10% - 30% depending on the masonry panel strength, over the RC bare frame. At 0.75% story drift, the influence of the masonry infill panels could be ignored due to severe damage was occurred. The experiment was terminated at 1.0% story drift with only minor damage observed in the RC surrounding frames.

2.2.2 RC frames with reinforced masonry infill panels

Laboratory tests on masonry infilled frames with masonry reinforced with steel wire mesh, carbon-fiber-reinforced polymers (CFRP) or the like have demonstrated the potential of transforming the brittle masonry panel to a more ductile one suitable for retrofitting. However, past attempts have accomplished limited success.

Bertero and Brokken (1983) investigated the effects of masonry and lightweight concrete infill panels on the behavior of RC buildings. Both experimental and analytical investigations were conducted. Eighteen 1/3 scale models of sub-assemblages of an 11 story-three bay building were tested under cyclic or monotonic load. The test specimens consisted of 3-1/2 stories and 1-1/2 bays. Both reinforced and un-reinforced masonry infill panels were employed, with reinforcement ratio of 0.15%, 0.40%, and 0.60% for the reinforced panels. The infill panels consisted of different materials including hollow clay brick, concrete block, split brick reinforced externally with welded wire fabric (WWF), and lightweight concrete panel. In the case reinforcement with WWF, the reinforcement was attached to surrounding RC frame with dowel bars. Experimental results revealed that the infill panels provided a significant effect on the structural response of the tested frames. The effective lateral stiffness of infilled frames ranged from 1.17 to 11.69 times when compared with the bare frame, depending upon infill panel type. The maximum lateral resistance of infilled frames ranged from 2.8 to 8.0 times that of the bare frame, which decreased significantly following cracking in the infill panels. In the worst case, after the infill panel cracked the lateral stiffness decreased in the order of 80% of the uncracked lateral stiffness. The effective viscous damping, on the other hand, increased to 12% after cracking which was equal to 6 times of the uncracked effective viscous damping. It was found that solid brick infills reinforced externally with welded wire fabric plastered with cement mortar exhibited superior performance over other types of infills. Buildings with such infills were estimated to be capable of resisting an earthquake with an effective peak ground motion of 0.4g. However, to effectively utilize the reinforced infill panels for retrofitting RC frames, the connection between infill panel and surrounding RC frame should be designed properly.

Calvi and Bolognini (2001) investigated the seismic response of RC frames with weak reinforced masonry infill panels. Nine full scale, single-bay, single-story ductile RC frames with clay block infill panels were tested. Two strengthening schemes were studied. The first one incorporated steel re-bars embedded in the mortar layers, and the second scheme employed steel wire mesh in the cover plaster of the masonry

infill panel. Various test protocols were employed for in-plane loading, some of which were followed by out-of-plane tests. It was concluded that the provision of reinforcement in the masonry panels, even in small amount, significantly enhanced the performance of the infilled frames tested as far as damage limit state was concerned. External meshes were found to be superior to the rebar type of reinforcement, resulting in a tremendous improvement in terms of strength, stiffness and energy dissipation capacities.

Acun and Sucuoglu (2006) reported the experimental results of three 1/3 scale, single-bay two-story non-ductile RC frames with masonry infill walls. The infill walls were strengthened with steel wire meshes and cover mortar. In addition, steel dowels were provided to transfer the interactive force between the masonry wall and the surrounding frame. Story drift capacities (at 20% drop in lateral load capacity) in the range of 0.7%-1.1% were achieved.

Erdem et al. (2006) performed an experimental study on 1/3-scale test specimens of two-story, three-bay non-ductile RC frames. The middle bay of one frame was filled with masonry infilled panels reinforced with diagonal CFRP strips. The lateral strength and stiffness were reported to increase by about 4 and 10 times, respectively, over the RC bare frame, but the story drift capacity was rather low, only in the order of 0.5%.

Altin et al. (2008) investigated the behavior of ten 1/3-scale test specimens of single-bay, single-story non-ductile RC frames with perforated clay brick infill strengthened with diagonal CFRP reinforcement of various widths attached to the masonry panel. They concluded that CFRP reinforcement could increase strength and stiffness of test specimens in the order of 0.54-1.61 times and 2.81-5.40 times, respectively, compared with the un-retrofitted specimen. However, after the ultimate load was reached the lateral load capacity suddenly dropped due to rupture or debonding of CFRP, resulting in relatively low drift capacity.

Billington et al. (2009) proposed a strengthening technique for masonry infilled non-ductile RC frames using steel wire mesh and Engineered Cementitious Composites (ECC). In addition, shear dowels were used to transfer the horizontal force between the masonry wall and the surrounding frame. Four 1/5 and one 2/3 scale models of single bay, single story non-ductile RC frames with masonry infill panels were tested. In the case of 1/5 scale specimens, their scheme was found to enhance the structural performance significantly, with drift ratios of 1.0%-4.0% achieved at 20% drop in lateral load capacity. However, in the case of the larger

test specimen (2/3-scale), brittle failure mechanism occurred. At 1.0% story drift, the lateral capacity of the test specimen significantly dropped due to separation between the cover plaster and the shear dowels. A similar retrofitting scheme was employed by Shing et al. (2009). The shake-table tests of two 2/3-scale, three-story, two-bay non-ductile RC frames with masonry infill panels were performed. The first specimen was infilled with un-retrofitted masonry panels and the other was infilled with retrofitted masonry panels. When the strong earthquake simulation was employed, shear failure of the first story columns was observed in the un-retrofitted specimen. At the similar level of earthquake simulation, only shear cracks could be observed in the exterior beam-column joint of the retrofitted specimen. It was concluded that the retrofitting scheme could enhance the seismic response of the tested specimen.

Yuksel et al. (2010) reported the experimental results of six 1/3 scale test specimens of single-bay, single-story non-ductile RC frames with hollow clay brick infills retrofitted with various configurations of CFRP (e.g., cross-braced, cross diamond-braced strips, etc.). With the CFRP retrofit investigated, strength increased in the order of 12% to 53% over the un-retrofitted infill wall frame, and the initial stiffness increased in order of 186% - 303%. However, all retrofitted specimens except one exhibited a sharp degradation in post-peak behavior due to debonding of CFRP connections, with drift capacity in the range of 1.0%-1.7%.

A similar investigation was conducted by Erol et al. (2012) with the masonry infilled non-ductile RC frames strengthened by diagonal CFRP strips. Cyclic load tests on six 1/2 scale specimens indicated that the lateral strength and the initial stiffness of the strengthened specimens increased in the range of 0.23 - 0.79 times and 0.77 - 1.62 times, respectively, compared with the un-strengthened specimen, while the drift capacity ranged from of 0.8% to 1.4%.

A few observations from the literature reviews, retrofitting schemes for RC frames with URM infills have been proposed by many researchers with the main objective of improving the ductility capacity of the assembly. However, past attempts have accomplished limited success. Firstly, most experiments were conducted with specimens of small sizes, ranging from 1/5 to 1/2 scales. Secondly, results from a larger size specimen appear to be significantly inferior to those from small sizes. Finally, the possibility of development of brittle shear failure in the boundary columns was not fully addressed in those studies. Some of those problems have been resolved by the retrofitting scheme proposed by Lukkunaprasit and Srechai

(2012). A comprehensive account of the scheme has been presented by Srechai and Lukkunaprasit (2013). Much of the materials in this paper is included in this dissertation for completeness.

2.2.3 Failure mechanism of RC frames with masonry infill panel

As described in the preceding section, a number of failure modes could occur in the both masonry infill panel and surrounding RC frame. Moreover, those failure modes depend on several parameters and difficult to predict. Paulay and Priestly (1992); FEMA (1998); Shing and Mehrabi (2002) and Asteris et al. (2011) identified five possible failure modes of masonry infill panel. These are as follows:

1) Flexural failure–an assembly fails in flexural mode without separation between surrounding frame and masonry infill panel. This mode could occur in the specimens with low aspect ratio (*W/H*) and low longitudinal reinforcement in the RC columns.
2) Sliding along the bed-joint of the masonry infill panel, frequently found in the frame with low shear strength masonry infill panel.
3) Diagonal crack of the infill panel.
4) Sliding of multi bed-joint of the infill panel. This usually occurs in infill panels with weak mortar joints.
5) Corner crushing of the infill panel, commonly found in the frame with low compressive strength masonry infill panel.

However, only sliding along the bed-joint and corner crushing of the masonry infill panels are normally considered as the predominant failure modes (Asteris et al., 2011). Flexural failure mode is not commonly found in typical low rise masonry infill frames. Sliding of multi bed-joint mode can be considered along with sliding along the bed-joint mode. When a diagonal crack forms, normally the load resistance capacity of masonry infill panel does not drop until other mode of failure occurs; so it is not define as a failure mode.

2.3 Analytical modeling of RC frames with masonry infill panels

As described in the preceding section, masonry infill panels have a significant effect on the behavior of RC structures with such infills. The sophisticated interaction

between masonry infill panel and surrounding RC frame and partial separations between the infill panel and surrounding frame cause difficulty in the structural modeling. Moreover, several failure modes could occur in both the masonry infill panel and the surrounding RC frame which greatly affect the structural performance. In the literature, a number of analytical approaches for RC frames with masonry infill panels have been proposed. An effective and simple approach known as the equivalent diagonal struts model is discussed in this section.

2.3.1 Effective width of an equivalent diagonal strut

As indicated in Asteris et al. (2011), an equivalent diagonal strut modeling to represent masonry infill panels (as illustrated in Figure 2-3) was introduced by Polyakov (1960). Several researchers (e.g., Holmes, 1961, Paulay and Priestly, 1992, Crisafulli, 1997) proposed that the effective width (*w*) of a diagonal strut is a fraction of the masonry panel diagonal length (*d*). It should be noted that the mechanical properties of both RC surrounding frame and masonry infill panel are excluded in the formulation. The most popular formulation for calculating effective width of a diagonal strut, proposed by Mainstone (1971) as given in Equation (2-1). This equation was recommended by standards (e.g., FEMA, 1998, FEMA, 2000, and ASCE, 2007) to evaluate the lateral stiffness of masonry infilled frames.

$$w = 0.175(h\lambda)^{-0.4}d \tag{2-1}$$

where λ is relative stiffness of the surrounding frame and masonry infill panel, proposed by Smith and Carter (1969), and it is given by

$$\lambda = \sqrt[4]{\frac{E_m t_w \sin 2\theta}{4EIh_w}} \tag{2-2}$$

where E and E_m are moduli of elasticity of the surrounding frame and masonry infill panel, respectively, I is moment of inertia of the column, t_w is thickness of infill panel, h_w is infill panel height, and θ is the inclination angle of the diagonal strut from the horizontal direction.

Earlier, Smith and Carter (1969) proposed a contact length between surrounding frame and masonry infill (Z) as given in Equation (2-3).

$$Z = \frac{\pi}{2\lambda} \tag{2-3}$$

A series of charts were given relating the diagonal strut effective width to the contact length (Z).

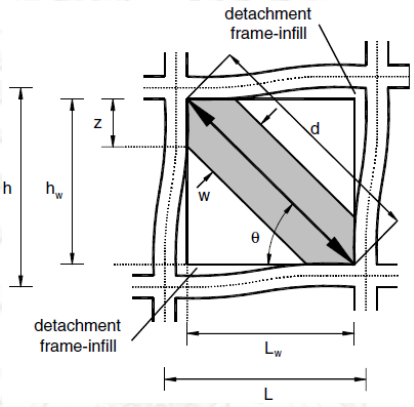

Figure 2-3. Diagonal strut for masonry infill panel (Asteris et al. 2011)

2.3.2 In-plane strength of masonry infill panel

The lateral resistance of masonry infill panel is governed by the failure mode. As described in the preceding section, a number of failure modes could occur in both the masonry infill panel and the surrounding RC frame. FEMA 306 (FEMA, 1998) proposed formulas for calculating lateral load resistance capacity of infill panel associated with different failure modes. Four possible failure modes of masonry infill panel including sliding-shear failure, compression failure, diagonal tension failure, and general shear failure were considered. The lateral load resistance capacity of those failure modes can be evaluated as described below.

1) Sliding-shear failure

This mode frequently occurs when the masonry infill panel is constructed with weak mortar joints, compared with masonry unit. The lateral load resistance capacity of this mode, V_{slide}, can be estimated by Mohr-Coulomb criterion as follows:

$$V_{slide} = (\tau_0 + \sigma_y \tan\phi) L_w t_w \quad (2\text{-}4)$$

where τ_0 is the cohesive capacity, σ_y is vertical stress of infill panel, ϕ is angle of sliding friction, L_w is length of infill panel, and t_w is thickness of infill panel. It should be noted that $tan\phi$ is equal to sliding friction coefficient (μ), and Equation 2-4 can be rewritten as

$$V_{slide} = \tau_0 L_w t_w + \mu N \quad (2\text{-}5)$$

where N is vertical load in the infill panel. Although no external load is imposed on the infill panel, vertical load in the infill panel is induced by the shortening strain of the panel caused by the lateral deformation, given by

$$N = \varepsilon L_w t_w E_m \quad (2\text{-}6)$$

The shortening strain (ε) of the panel can be expressed in terms of story drift angle as follows:

$$\varepsilon = \frac{\delta}{h} = \theta \frac{\Delta}{h} = \theta^2 \quad (2\text{-}7)$$

where δ is downward movement of the upper beam, h is story height, Δ is inter-story displacement, and θ is inter-story drift angle. By substituting Equations (2-6) and (2-7) into Equation (2-5), the lateral load resistance of infill panel associated with sliding along the bed-joint failure mode can be expressed as

$$V_{slide} = \tau_0 L_w t_w + \mu L_w t_w E_m \theta^2 \quad (2\text{-}8)$$

The cohesive capacity (τ_0) of the infill panel should be obtained from the test data. Alternatively, the following expression can be used (FEMA, 1998):

$$\tau_0 = \frac{f'_{m90}}{20} \quad (2\text{-}9)$$

where f'_{m90} is compressive strength of masonry prism in the horizontal direction. If the experimental data is not available, it can be set as 50% of the compressive strength in the vertical direction (f'_m).

2) Compression failure mode

This mode is frequently witnessed when the masonry infill panel is constructed with low compressive strength masonry units. The lateral load resistance capacity, V_{cc}, of such infill panel can be estimated as follows:

$$V_{cc} = wt_w f'_{m90} \cos\theta \quad (2\text{-}10)$$

where w is effective width of diagonal strut which can be calculated by Equation (2-1).

3) Diagonal tension failure mode

This mode generally this mode of failure is not defied as a failure mechanism of the URM panel (Paulay and Priestly, 1992) because the lateral load resistance associated with development of diagonal tension crack is not the ultimate capacity. Usually, the diagonal tension crack is followed by another failure mode such as compression failure. The lateral load resistance associated with diagonal tension crack, V_{cr}, of infill panel can be determined as follows:

$$V_{cr} = \frac{2\sqrt{2}L_w t_w \sigma_{cr}}{\left(\frac{L_w}{h_w}+\frac{h_w}{L_w}\right)} \quad (2\text{-}11)$$

where σ_{cr} is cracking capacity of masonry should be obtained from the test data. Alternatively, the following expressions can be used (FEMA, 1998).

$$\sigma_{cr} = \frac{f'_{m90}}{20} \quad (2\text{-}12)$$

or

$$\sigma_{cr} = 20\sqrt{f'_m} \tag{2-13}$$

It should be noted that the masonry compressive strength must be substituted into Equation 2-13 in psi unit.

4) General shear failure mode

The lateral load resistance of this failure mode is separated into two states including the initial shear (V_{mi}) and final shear (V_{mf}) capacities. For the final shear capacity the cyclic loading effect is taken into account. The lateral load resistance of both states can be calculated as follows:

$$V_{mi} = A_{vh}2\sqrt{f'_m} \tag{2-14}$$

$$V_{mf} = 0.3V_{mi} \tag{2-15}$$

where A_{vh} is net horizontal area of the infill panel and the masonry compressive strength must be substituted into Equation 2-14 in psi unit.

As indicated in Mostafaei and Kabeyasawa (2004), the load resistance capacity of infill panel associated with sliding-shear failure mode was proposed by Paulay and Priestly (1992). Similar to FEMA 306, Mohr-Coulomb criterion was used. However, vertical load in the infill panel was calculated from a vertical component of strut force, given by

$$N = R_c sin\theta \tag{2-16}$$

It should be noted that a horizontal component of strut force is the lateral load resistance capacity of infill panel.

$$V_{slide} = R_c cos\theta \tag{2-17}$$

Substituting Equations (2-16) and (2-17) into Equation (2-5), the lateral load resistance of infill panel can be expressed as

$$V_{slide} = \frac{\tau_0 L_w t_w}{(1-\mu tan\theta)} \quad (2\text{-}18)$$

The cohesive capacity (τ_0) can be assumed as $0.04f'_m$ and the friction coefficient (μ) can be calculated as follows:

$$\mu = 0.654 + 0.000515f'_j \quad (2\text{-}19)$$

where f'_j is compressive strength of the mortar (ksc)

For compression failure mode, Mostafaei and Kabeyasawa (2004) replaced f'_{m90} in Equation (2-10) by f'_m. Therefore, load resistance capacity of infill panel associated with corner crushing failure mode can be written as

$$V_{cc} = wt_w f'_m \cos\theta \quad (2\text{-}20)$$

where w is effective width of diagonal strut which can be calculated by Equation (2-3) and other parameters are described above.

Similar to FEMA 306, Mostafaei and Kabeyasawa (2004) adopted the formula proposed by Saneinejad and Hobbs (1995) to estimate the diagonal tension crack resistance capacity of the infill panel.

2.3.3 Single-strut and multiple-strut models

The applicability of the single-strut model to evaluate the overall seismic response of RC frame with masonry infill panel was demonstrated by several researchers (e.g., Dolšek and Fajfar, 2002, Magenes and Pampanin, 2004, Mostafaei and Kabeyasawa, 2004, Hashemi and Mosalam, 2007, Stavridis, 2009, and Uva et al., 2012). However, the single-strut model could not simulate the local response of the structures, especially the internal forces in the surrounding frame. As a result, the actual failure mechanism of the surrounding frame is not captured (Crisafulli, 1997, and Crisafulli

and Carr, 2007). Therefore, the multiple-strut models were proposed to resolve this problem.

Crisafulli (1997) reported the preliminary analytical results of masonry infill frames. Single-strut, two-strut, and three-strut models were analyzed and compared with the refined finite element model. All models were constructed with a different number of diagonal struts whose total effective area was the same. For the two-strut model, both diagonal struts had the same area. In the case of three-strut model, 50% and 25% of the total effective area were used for the central strut and off-diagonal struts, respectively. The eccentricity of off-diagonal struts equal to 1/3 and 1/2 times of the contact length were used for two-strut and three-strut model, respectively. The contact length of the infill panel and surrounding frame was calculated in accordance with Stafford Smith (1966). It was concluded that all models could estimate the lateral stiffness of the structures. However, the single-strut model under-estimated the internal forces in the surrounding frame. The three-strut model yielded the best performance in terms of internal force prediction, compared with the other strut models.

El-Dakhakhni et al. (2003) proposed an analytical model for predicting the structural response of masonry infilled steel frames and compared it with the experimental results. The three diagonal struts were used to represent the masonry infill panel. The strut widths of 50% and 25% of the total effective width were used for the central strut and the off-diagonal struts, respectively. The eccentricity of the off-diagonal struts was set equal to the contact length between infill panel and surrounding frames estimated in accordance with Saneinejad and Hobbs (1995). It was concluded that the proposed model could predict the lateral stiffness and strength of masonry infill steel frame up to failure state. Additionally, the internal forces and failure mechanism of the masonry infill steel frame were predicted with acceptable accuracy, compared with the experimental results.

Kaushik et al. (2008) performed the comparative study of single-strut and three-strut models to predict the structural response of masonry infill RC frames. These analytical models were analyzed and compared with the finite element model. Analytical results indicated that the overall response of the structures can be predicted by a single-strut model. However, a three-strut model provided the better result compared with a single-strut. Furthermore, a three-strut model could capture the internal forces and local failure of the surrounding RC frame.

Uva et al. (2012) evaluated the seismic performance of a seven-story RC frame with masonry infill panels. The influence of a single-strut and two-strut modes on the local behavior of the system was considered. They concluded that a single-strut model could not capture the local failure of the surrounding RC frame. On the other hand, brittle shear failure of the RC columns was observed in the two-strut model. As a result, the ultimate lateral strength of a two-strut model decreased to be 0.5 times of a single-strut model. This result clearly shows the influence of the number of diagonal struts on the structural response, especially when brittle shear failure occurred in the RC frame.

CHAPTER III
RETROFIT SCHEME, TEST SPECIMENS, AND TEST SETUP

3.1 Introduction

An experimental program was conducted to investigate the seismic performance of masonry infilled RC frames. Four 3/4-scale specimens of single-bay, single-story non-ductile RC frames with masonry infill panels were tested. Specimen design, test setup, and the retrofit scheme are presented in this chapter.

3.2 Prototype structure

An exterior RC frame of a three-bay, three-story, typical commercial building was selected as a prototype structure (illustrated in Figure 3-1). The existing building was originally designed to resist gravity load and wind load. The RC frame typically has non-ductile detailing, with minimum transverse reinforcement. The minimum design loads and capacity requirements in accordance with the Thailand design standard were followed. The frame was fully infilled with solid clay bricks with thickness of 100 mm (including cement plaster on each face). The expected compressive strength of concrete was 20.6 MPa. The tensile yield strength of deformed bars (designated SD30) was 300 MPa, and that of round bars (SR24) was 240 MPa. An interior, single-bay, single-story RC frame of the first story was selected as the prototype specimen. The details of the prototype specimen are shown in Figure 3-2.

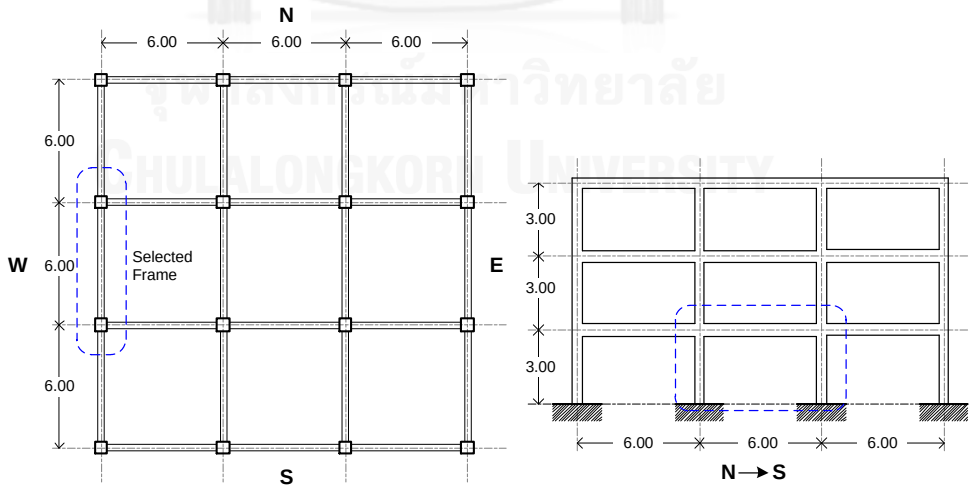

(a) (b)

Figure 3-1. Prototype structure: (a) floor plan; and (b) elevation

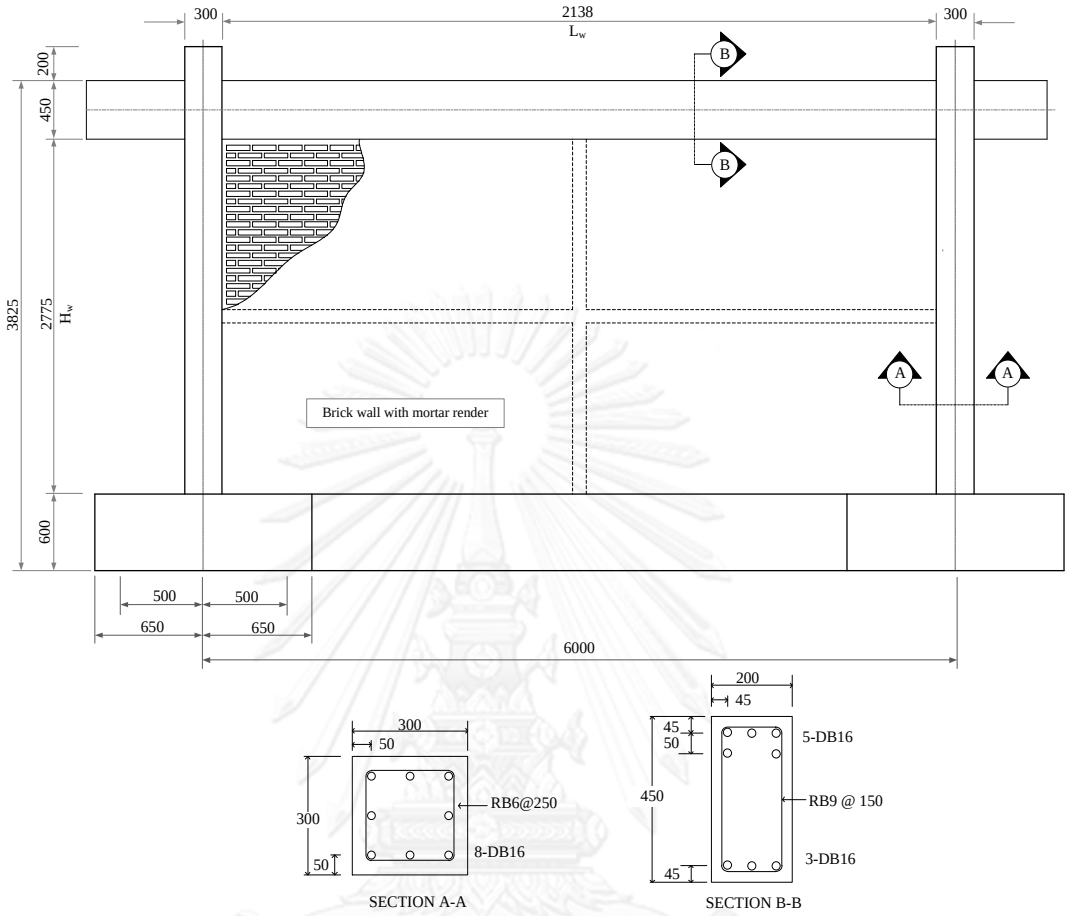

Figure 3-2. Prototype specimen

3.3 Retrofit scheme

As mentioned in the literature review, experimental results of URM infilled RC frames reveal that threatening shear cracks may occur in the columns and beam-column joints at a very small drift (in the or of 0.25%). Subsequently, undesirable abrupt shear failure of the RC columns and beam-column joints follow due to transfer of the large strut force resisted by the URM panel to the columns following corner crushing of the panel. Therefore, in order to effectively utilize the URM infills for seismic resistance, the following problems must be addressed and minimized:

1) Shear failure of the (non-ductile) RC columns and /or beam-column joints;
2) Crushing of the corners of the infill;
3) Sliding of horizontal bed joints in the infill.

All these modes of failure can lead to the relatively low ductility capacity of the structural system. Guided by failure mechanisms observed from the literature and experimental results, the following innovative scheme (shown in Figure 3-3) has been proposed by Lukkunaprasit and Srechai (2012) for resolving weaknesses of the non-ductile infilled URM RC frames:

1) The retrofitted masonry is separated from the vertical columns so that no shear force is transferred to them, eliminating totally the shear failure caused by the strut forces from the URM panel;
2) Steel brackets (depicted in Figure 3-4) are provided to transfer the interactive horizontal forces between the RC frame and the masonry panel;
3) The small vertical steel members (or other equivalent components) are anchored to the vertical boundaries of masonry infill to prevent the sliding joint failure of the masonry panel.
4) The corners of the infill are reinforced with wire meshes and high strength mortar.

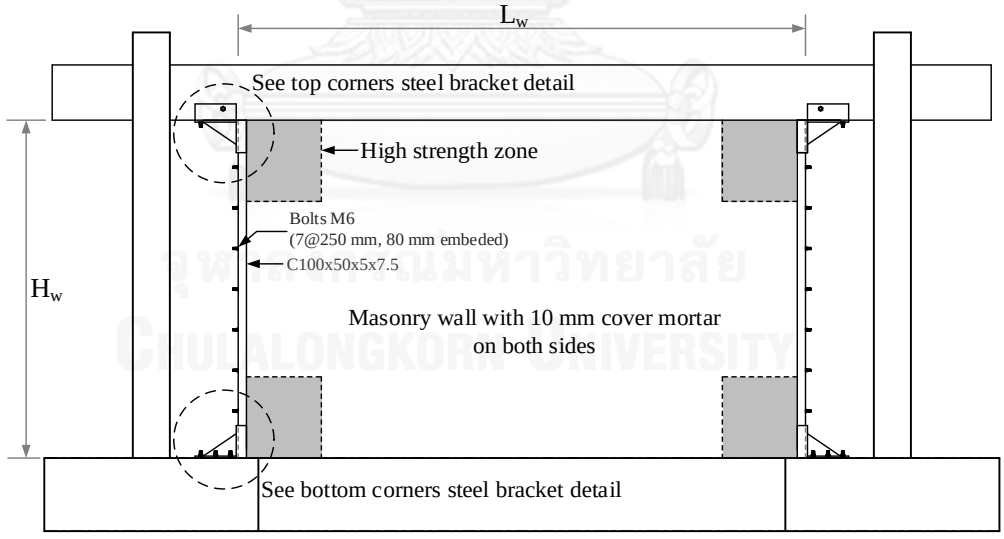

Figure 3-3. Retrofitting scheme of URM-infilled RC frames

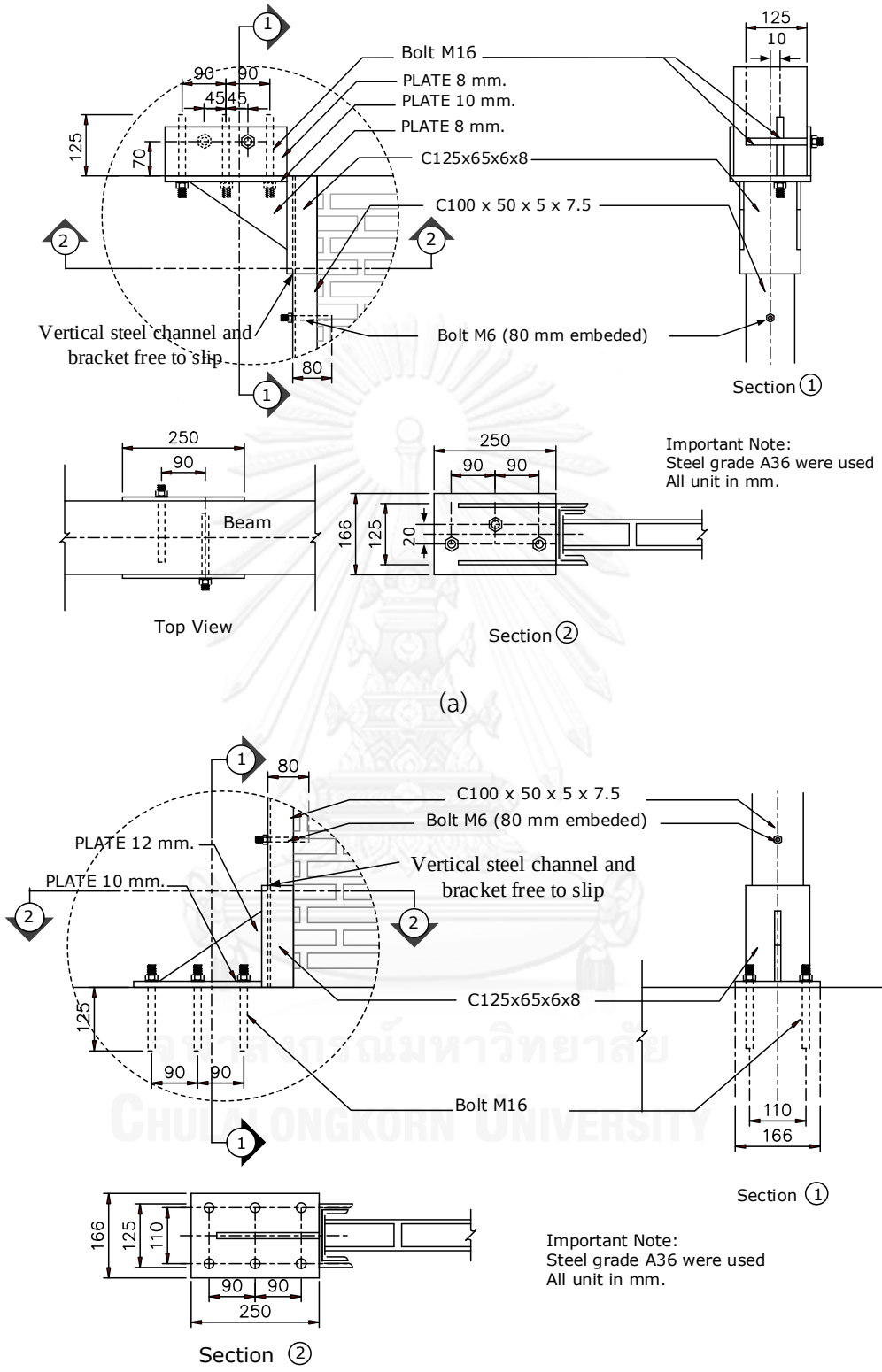

Figure 3-4. Steel bracket and connection detailing; (a) top corners bracket and (b) bottom corners bracket

3.3.1 Analytical study of the connection detail

Since the large strut forces exist at the corners of the URM panel, the connection detail between the panel and the steel brackets must have a significant influence to the behavior of the test specimen. Therefore, a preliminary analytical study of the connection between the URM panel and the steel brackets was conducted in order to provide a guide line for a selection of the appropriate connection details. An elastic finite element model of the retrofitted specimen was constructed as demonstrated in Figure 3-5. The surrounding frame, vertical steel members and steel brackets were modeled using the elastic frame elements. The beam-column joints were treated as rigid links. Meanwhile, the URM panel was generated using four nodes shell elements. To simplify the model, the compression spring elements were employed to connect the URM panel and the surrounding frame or the steel brackets. This element is capable of transforming only the compression load. The spring constant was assigned with the elastic modulus of the masonry prism of 3758 MPa. An elastic pushover analysis was performed using SAP2000 structural analysis software (CSI 2011). The lateral load corresponding to 80% of the estimated capacity was applied.

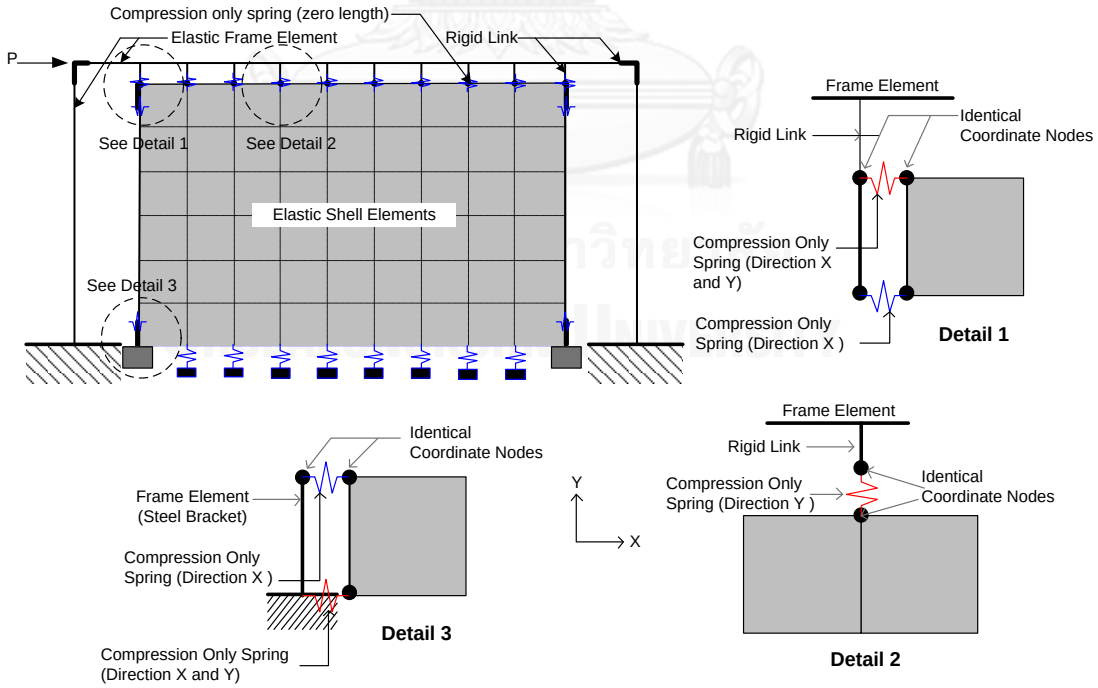

Figure 3-5. Preliminary finite elements model

The principal stresses in URM panels are represented as vectors in Figure 3-6. When the sliding between URM panel and steel brackets is allowed, the largest compressive stress concentrates at the corner of URM panel. Only small tensile stress in the order of 0.92 MPa develops in the URM panel. On the other hand, in the case of the URM panel was fixed to the steel brackets, the tensile stress increases tremendously by 4.3 times compared with the former case. In view of the low tensile strength of the brick assembly, it is obvious that the contact between the URM panel and steel brackets should allow free slip between them so as to minimize development of tensile stresses in the panel.

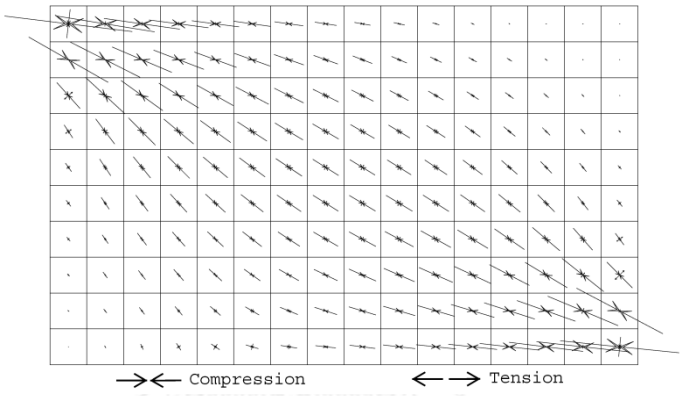

(a)

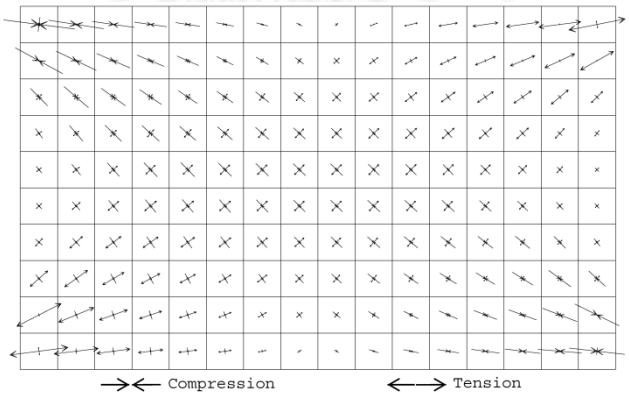

(b)

Figure 3-6. Principal stress distribution in URM panels: (a) the connection between vertical steel channel and steel bracket is free to slip; (b) the connection between vertical steel channel and steel bracket is fixed

3.4 Test specimens

Due to the limitation of the laboratory facilities and test setup, therefore the test specimens were scaled to 3/4 times of the prototype specimen. The structural dimensions, longitudinal reinforcement ratio (ρ), and transverse reinforcement ratio (ρ_s) were also scaled down to match the reduced size. Four 3/4 scale models of single bay, single story non-ductile RC frames with masonry infill panel consisting of one un-retrofitted and three retrofitted specimens were used in this study. The surrounding RC frame with identical detailing as illustrated in Figure 3-7 was used for all specimens. The comparison of structural indexes of the prototype and scaled specimens is listed in Table 3-1. The corresponding details of each specimen are described as follows.

Specimen MIRCF01 was the original un-retrofitted assembly with panel aspect ratio (panel width/height) of 2.0. The details of the specimens are shown in Figure 3-7 and Figure 3-8. The RC frame was of typical non-ductile details used in Thailand, with minimum transverse reinforcement. Low strength non-structural solid clay bricks were utilized to construct the 70 mm thick infill panel (including 10 mm cement plaster on each face). Widely spaced small dowel bars with short straight legs were embedded in the columns to connect the URM panel to the RC columns. This is a typical detail for constructing infill panels in Thailand. The construction sequence of the test specimen is illustrated in Figure 3-9 and can be described as follows. First, the footing of the test specimen was cast and followed by the construction of the RC frame. Then, the masonry infill panel including 50 × 80 mm horizontal and vertical lintels were constructed. Finally, the cement plaster was rendered on each face of the masonry infill panel. All material properties will be discussed in the next section.

Table 3-1. Details of RC members

Parameters	Prototype Structure	3/4-Scale Test Specimen
Specimen Dimensions	3000 x 6000 mm	2250 x 4500 mm
RC Beam		
Cross section	200 x 450 mm	150 x 340 mm
Top reinforcement	5-DB16 (ρ = 0.0136)	5-DB12 (ρ = 0.0136)
Bottom reinforcement	3-DB16 (ρ = 0.0081)	3-DB12 (ρ = 0.0081)
Transverse reinforcement	RB9@150 mm (ρ_s = 0.009)	RB6@100 mm (ρ_s = 0.009)
RC columns		
Cross section	300 x 300 mm	225 x 225 mm
Longitudinal reinforcement	8-DB16 (ρ = 0.018)	8-DB12 (ρ = 0.017)
Transverse reinforcement	RB6@250 mm (ρ_s = 0.0009)	RB4@150 mm (ρ_s =0.001)

Note: DBx denotes deformed bar of diameter x mm, RBx denotes round bar of diameter x mm.

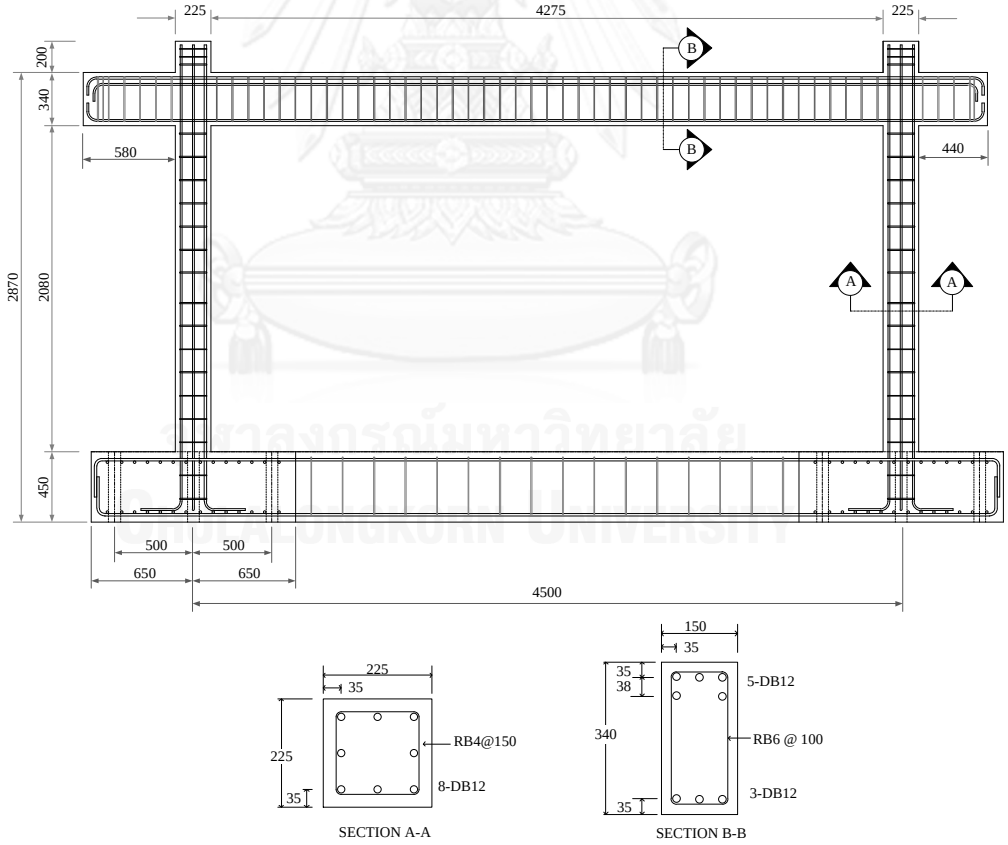

Figure 3-7. The RC frame of test specimens

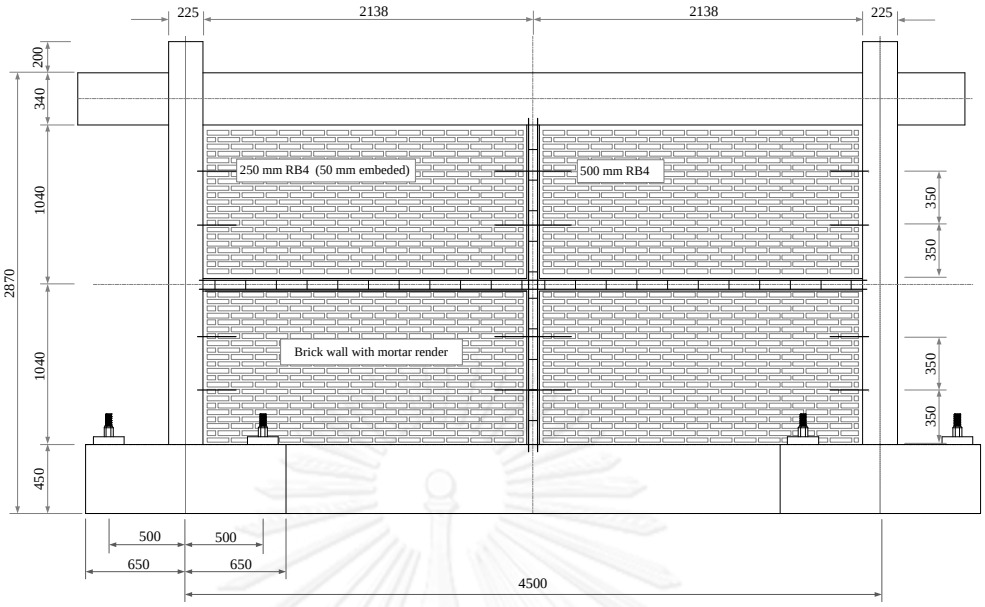

Figure 3-8. The infill panel detailing of test specimen MIRCF01

(a) (b)

(c)

Figure 3-9. Construction sequence of the test specimen MIRCF01: (a) RC frame casting; (b) URM panel assembly; and (c) URM panel plastering

Specimen MIRCF02 was retrofitted with the scheme proposed in previous section. After the experiment of specimen MIRCF01 was completed, the damaged RC frame was repaired and used for specimen MIRCF02. The concrete in the damaged regions of the columns (in the vicinity of the beam-column joint) was removed and recast (Figure 3-10). The cracks elsewhere in the RC frame were repaired with high pressure epoxy injection. However, the original steel reinforcement of the RC frame, some of which was significantly bent due to deformation from the previous testing, was retained. As for the URM panel, both ends of the panel of the tested specimen MIRCF01 adjacent to the columns were removed, leaving 80% of the original panel in the retrofitted specimen MIRCF02 (aspect ratio of the infill panel is equal to 1.6). High pressure epoxy grouting was then applied to the separation joints between the URM panel and the beam and footing. As indicated in Figure 3-11, the corners of the infill panel with a size of 500 mm × 500 mm were reinforced with chicken cage wire meshes with a reinforcement ratio of 0.29%, and high strength mortar was applied (with the original plaster chipped off). Then small vertical steel members (C-100×50×5×7.5) were anchored to the vertical boundaries of the masonry infill panel. Finally, steel brackets were provided to transfer the interactive horizontal forces between the RC frame and the masonry panel (Figure 3-12). The resistance capacity of the steel brackets was designed to satisfy with the ultimate lateral capacity of the infill panel. All material properties will also be discussed in the next section.

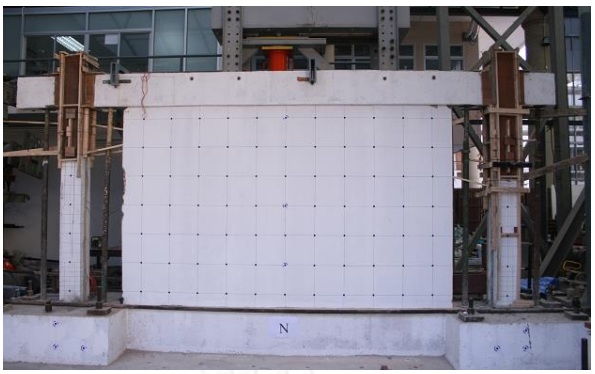

(a)

(b)

Figure 3-10. Construction sequence of the test specimen MIRCF02: (a) recasting of RC frame; and (b) reproduce the bound strength with epoxy injection

Figure 3-11. Reinforcement at the corners of infill panel

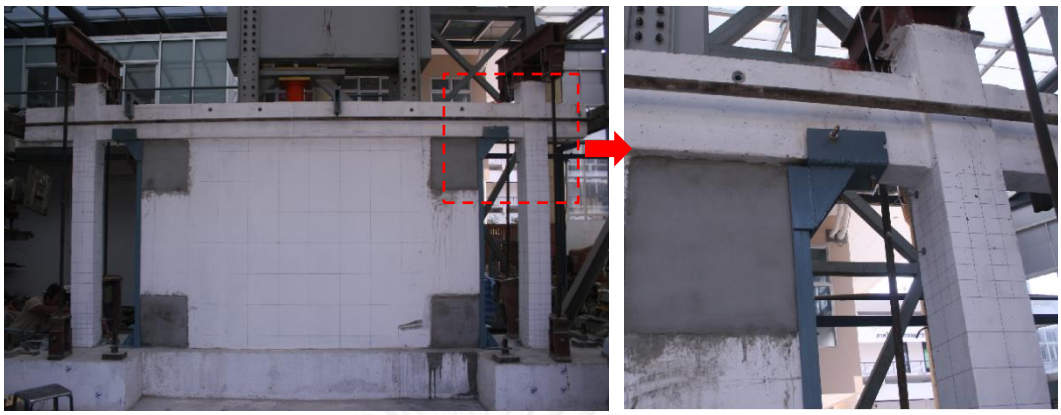

Figure 3-12. Retrofitted test specimen MIRCF02

Specimen MIRCF03 was a newly constructed assemblage with the panel aspect ratio (panel width/height) of 1.0. After the experiment of specimen MIRCF02 was completed, the damaged RC frame together with the damaged URM panel were demolished. The RC footing, however, was reused. The concrete in the column base regions of the RC footing was cored, 100 mm in depth, to provide the space for connecting the new longitudinal reinforcement of the columns. Then new steel rebars of the RC columns were welded to the original steel bars embedded in the footing. Subsequently, the RC frame was constructed. The URM infill panel with the width of 2080 mm was built. It should be noted that the retrofitting scheme used in test specimen MIRCF02 was also applied (i.e. corner strengthening, provision of boundary steel channels with load transfer brackets). The test specimen MIRCF03 is shown in Figure 3-13. All material properties will also be discussed in the next section.

Figure 3-13. Test specimen MIRCF03

Specimen MIRCF04 was retrofitted with the scheme proposed previously. Also the RC frame of specimen MIRCF04 was the repaired one. After the experiment of specimen MIRCF03 was completed, the upper portion of the RC frame (including the beam) was removed and recast (Figure 3-14). The cracks elsewhere in the RC frame were repaired with high pressure epoxy injection. Most of the original steel reinforcement of the RC columns were retained. However, the reinforcement with significant bent was replaced by the new one. Then, the reinforced infill panel with the panel aspect ratio of 1.6 was constructed. Steel wire mesh, 3 mm diameter with 200 × 200 mm mesh, was used to reinforce the masonry infill panel on each face (Figure 3-14). The corresponding reinforcement ratio becomes 0.11%. Again, the retrofitting scheme used in test specimen MIRCF02 was also applied (Figure 3-15). Small steel angles were provided to clamp the steel wire mesh to the surrounding RC frame in order to prevent the out-of-plane collapse of the infill panel.

Figure 3-14**.** URM of test specimen MIRCF04 reinforced with steel wire mesh

Figure 3-15. Test specimen MIRCF04 with small angles to prevent out-of-plane deformation

3.5 Material Properties

The material testing was conducted during the experimental program. Reinforcement steel, concrete, mortar, and masonry were included. These material properties are discussed as follows.

3.5.1 Reinforcement steel

Three types of reinforcement steel were used in each specimen. First, 12 mm diameter deformed bar (DB12), steel grade SD30 was used as a longitudinal reinforcement of the RC beam and RC columns. Second, 6 mm diameter round bar (RB6), steel grade SR24 was used as transverse reinforcement of the RC beam. Third, 4 mm diameter cold-drawn steel wire was used as transverse reinforcement of the RC columns. It should be noted that the last one was a high strength steel wire. The minimum yield strength was 485 MPa which was significantly higher than SR24 steel grade. Therefore a heat treatment was applied to reduce the yield strength of the cold-drawn steel wire to around 240 MPa. These wire are designated RB4. Tensile tests were conducted on three samples of each reinforcing steel type. The average tested results are summarized in Table 3-2.

Table 3-2. Reinforcement steel properties

Specimen	Steel Type	Yield Strength f_y (MPa)	Ultimate Strength f_u (MPa)	Modulus of Elasticity E_s (MPa)
MIRCF01	DB12	360.9	549.3	211157
	RB6	307.7	455.5	198531
	RB4	246.5	365.2	182368
MIRCF02	DB12	360.9	549.3	211157
	RB6	307.7	455.5	198531
	RB4	246.5	365.2	182368
MIRCF03	DB12	339.4	542.0	196074
	RB6	311.7	448.6	199123
	RB4	244.6	362.3	183453
MIRCF04	DB12	339.4	542.0	196074
	RB6	311.7	448.6	199123
	RB4	244.6	362.3	183453

3.5.2 Concrete

The ready mix concrete with the specific compressive strength of 20.6 MPa was used in this study. The compression test was conducted on the standard concrete cylinder, 150 mm diameter 300 mm height. At least three samples were tested for each component. The average tested results are summarized in Table 3-3.

Table 3-3. Concrete compressive strength

Specimen	Component	Compressive strength (MPa)		Remark
		28 days	Test date	
MIRCF01	Columns	19.4	20.0	
	Beam	18.6	19.6	
MIRCF02	Columns	19.4 -	21.5 20.8	Original concrete Repaired concrete
	Beam	18.6	20.2	
MIRCF03	Columns	20.1	21.9	
	Beam	19.5	19.5	
MIRCF04	Columns	20.1 -	21.9 21.6	Original concrete Repaired concrete
	Beam	-	21.6	Repaired concrete

3.5.3 Mortar, Cement plaster, and Masonry

The mortar and cement plaster are the important composition of masonry infill panels. For mortar, an average cement-to-sand ratio of 1: 2.8 and water-cement ratio of 0.45 by weight were used. The corresponding values for cement plaster were 1: 2.6 and 0.65 by weight, respectively. In addition the high strength cement plaster was applied at each corner of the retrofitted infill panels. The compression tests were conducted on the 50×50×50 mm cubes of those materials. At least three samples were tested according to ASTM C-109-02 standard. The average compressive strength of all materials at test date is summarized in Table 3-4.

The compressive strength of the masonry infill was evaluated by compression test. The masonry prisms, constructed with five units of clay brick and cement plaster on each face, were tested following the ASTM-C1314-07 standard. Failure pattern of the masonry prism is shown in Figure 3-16. Furthermore, diagonal tension or shear tests of the masonry assemblages were conducted. The masonry assemblages, 500 mm × 500 mm, including cement plaster on each face were tested according to ASTM E519-10 standard. Failure pattern of the masonry assembly is shown in Figure 3-16. The average compressive strength, shear strength and modulus of elasticity of the masonry panels are summarized in Table 3-5.

Table 3-4. Compressive strength of mortar and cement plasters

Specimen	Compressive strength (MPa)		
	Mortar	Cement Plaster	Corner Cement
MIRCF01	19.5	19.2	-
MIRCF02	20.0	19.6	33.4
MIRCF03	18.0	20.1	29.5
MIRCF04	17.4	16.8	28.4

Table 3-5. Compressive strength, shear strength and modulus of elasticity of masonry assembly

Specimen	Compressive strength f'_m (MPa)	Shear strength S_s (MPa)	Modulus of elasticity E_m (MPa)
MIRCF01	6.6	1.0	3757
MIRCF02	6.6	1.0	3757
MIRCF03	7.2	1.2	3692
MIRCF04	6.9	1.1	3509

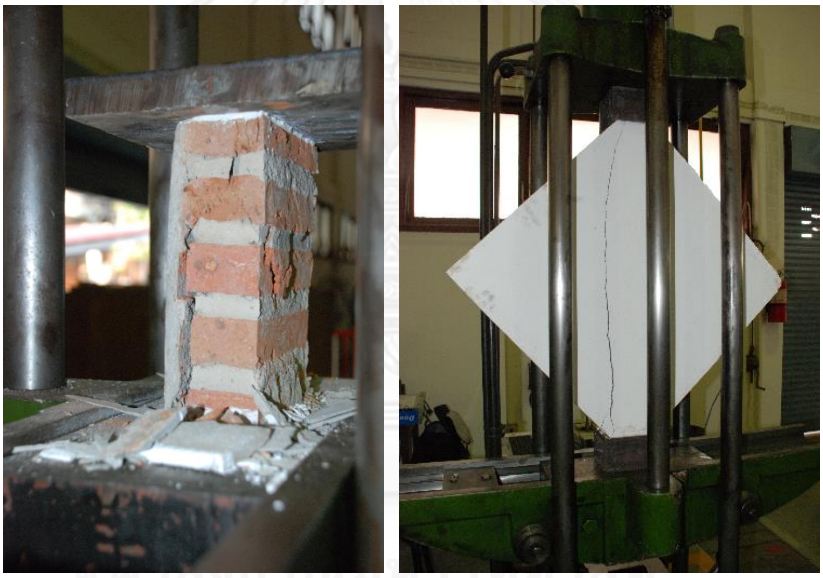

(a) (b)

Figure 3-16. Failure pattern of masonry: (a) compression test of masonry prism; (b) diagonal tension test of masonry assembly

3.6 Test setup and loading pattern

In this study, four 3/4 scale models of single-bay, single-story non-ductile RC frames with masonry infill panel were tested under horizontal cyclic load and a constant vertical load. Post tensioned rods were used to anchor the test specimen with the

strong floor. The horizontal cyclic load was applied at the center line of the RC beam by mean of a 1000 kN hydraulic actuator. The displacement-controlled loading sequence consisted of cycles of controlled displacements with drift ratios of 0.125%, 0.25%, 0.50%, 0.75%, 1.00%, 1.25%, 1.50%, 1.75%, 2.00% and 2.50% (Figure 3-17). Two cycles were repeated at each drift level to ensure stable hysteretic behavior was attained. The test was performed until the lateral load capacity was practically lost, or terminated if it was deemed unsafe to continue. The vertical loads were applied to the top of the columns through transfer cross beams. Each beam was connected to two high strength steel bars, one on each side of the cross beam. One of them was pulled down using a center hole hydraulic jack, thereby exerting a compressive vertical force on the column. Two such hydraulic jacks were provided, both connected to the same hydraulic pump. During the test those hydraulic jacks were manually controlled to maintain a constant vertical load within 5% tolerance. A vertical load of 20% of the nominal strength of columns based on the concrete gross section (approximately is 200 kN) was applied on the columns. The test setup configuration is illustrated in Figure 3-18.

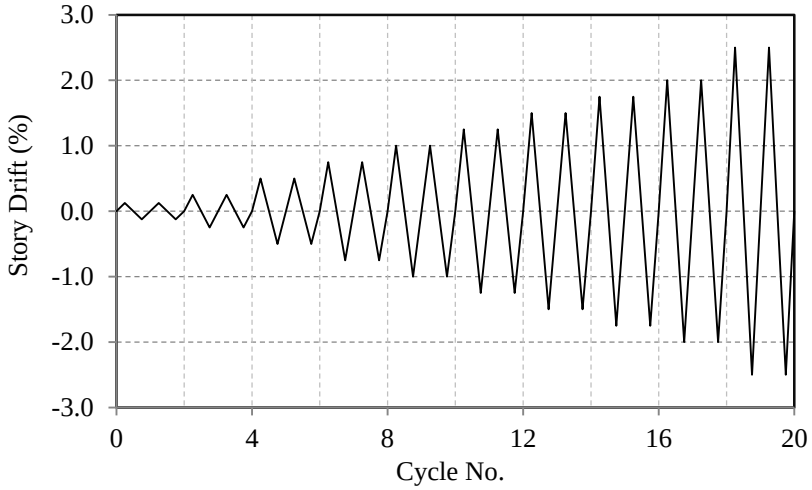

Figure 3-17. Horizontal cyclic load protocol

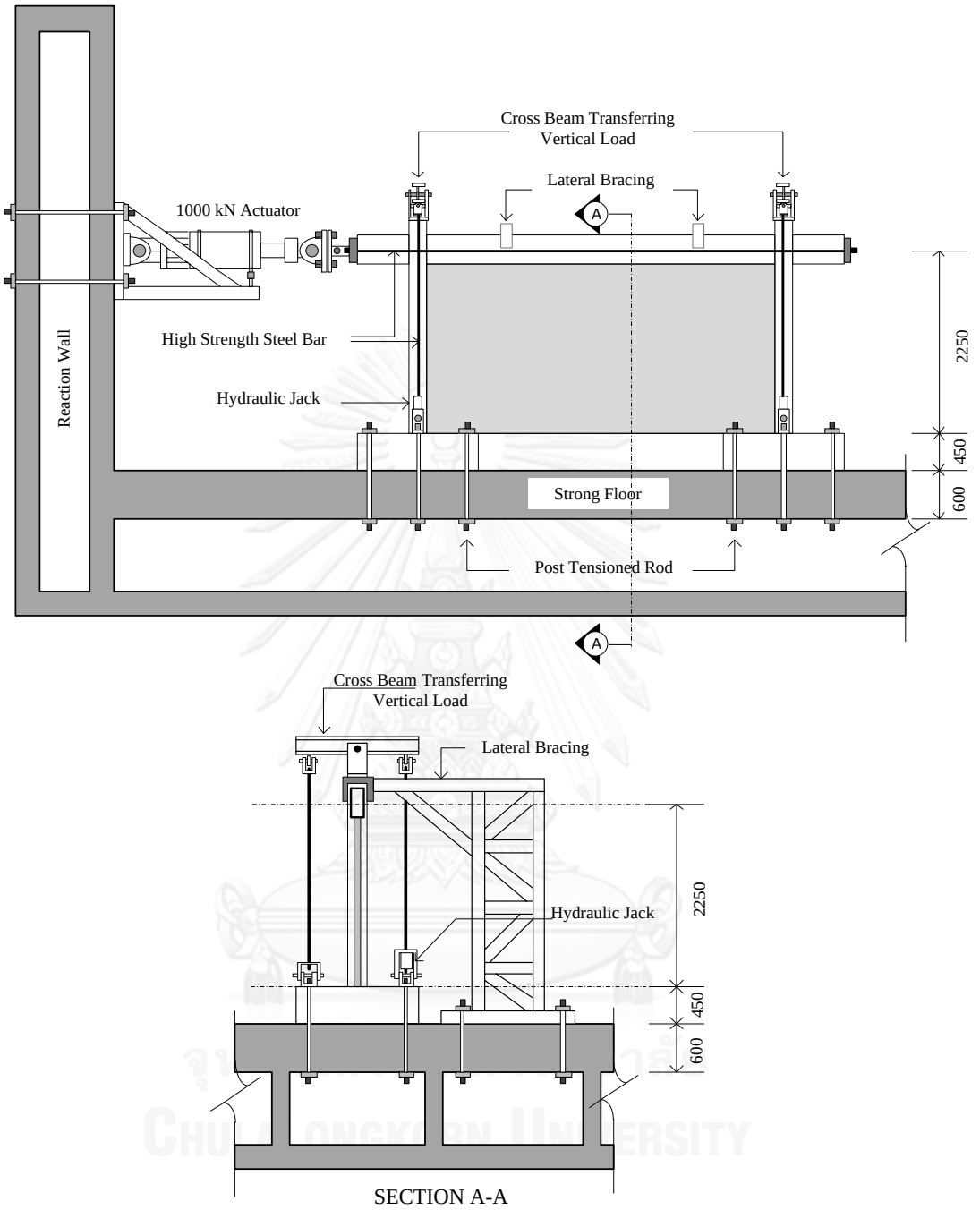

Figure 3-18. Test setup configuration

3.7 Instrumentations

Strains in the longitudinal and transverse steel reinforcements were monitored by strain gages. These strain gages were installed before concrete casting (Figure 3-19).

The expected critical regions were selected to monitor strains in the reinforcing bars during the test. The locations of strain gages are shown in Figure 3-20. Four abbreviations were indicated in the figure. The longitudinal and horizontal strain gages in the column reinforcing bars were named as SLCx and STCx, respectively. Similarly, the strain gages of the longitudinal and transverse reinforcing bars in the beam were called SLBx and STBx, respectively. The displacement transducers were used to measure the lateral displacement of the test specimens at the beam centerline and footing as well as the uplift of test specimen was monitored during the test.

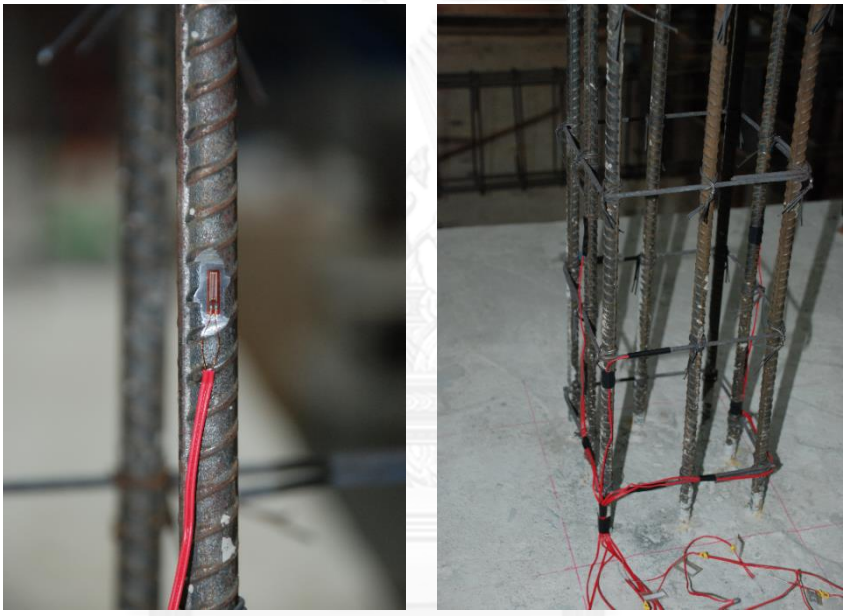

Figure 3-19. Strains measurement of reinforcing steel

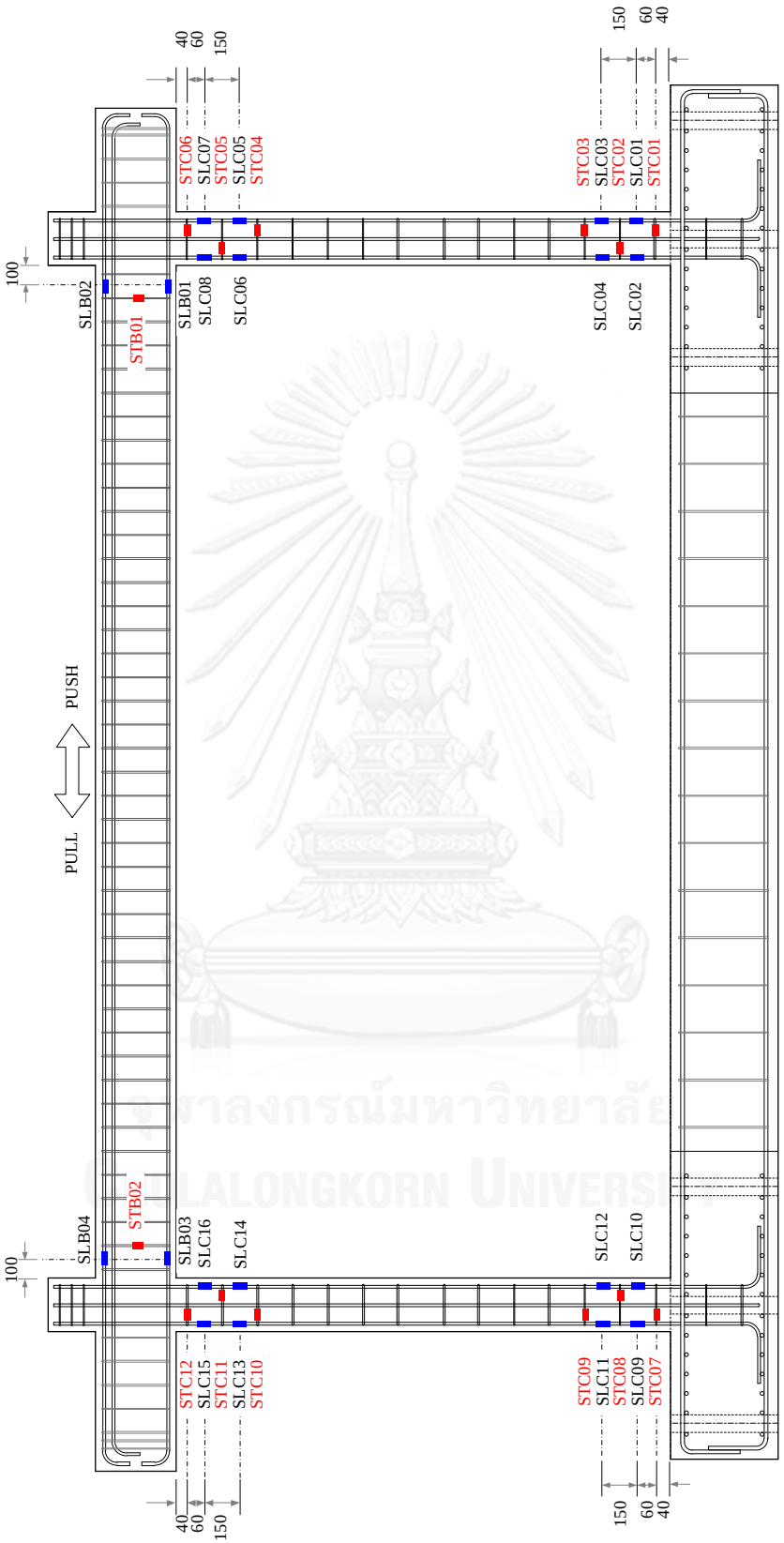

Figure 3-20. Strain gages location

CHAPTER IV
EXPERIMENTAL RESULTS AND DISCUSSION

In this chapter the experimental results of the tested specimens are presented and discussed. The main findings from the experiment are described as the following sections.

4.1 Crack patterns and failure modes

In the first cycle loading of the control specimen MIRCF01, separations between surrounding RC frame and URM infill panel were observed near the corners upon unloading (see Figure 4-1). Furthermore, tiny horizontal cracks occurred along the wall-beam and wall-footing interfaces of the specimen MIRCF01 at 0.125% drift ratio. At the first cycle of 0.25% drift, hairline shear cracks occurred in the columns and beam-to-column joints. In the second cycle of the same drift, those shear cracks widened rapidly. Crack widths of about 0.5 and 1.0 mm were observed in the columns and beam-to-column joints, respectively. Moreover, impending corner crushing was observed at one corner (see Figure 4-2). This frame assembly attained an average peak load of 292 kN at 0.33% drift, after which the capacity suddenly dropped to less than 40% at 0.5% drift (see Figure 4-3) with the formation of damaging shear cracks in RC columns and beam-column joints and corner crushing of the masonry infill as depicted clearly in Figure 4-4. It should be noted that the URM panel was essentially undamaged except for the crushed corners. In fact, the URM panel of this specimen was retained (with part of the panel adjacent to the columns removed as mentioned earlier) in the retrofitted specimen MIRCF02.

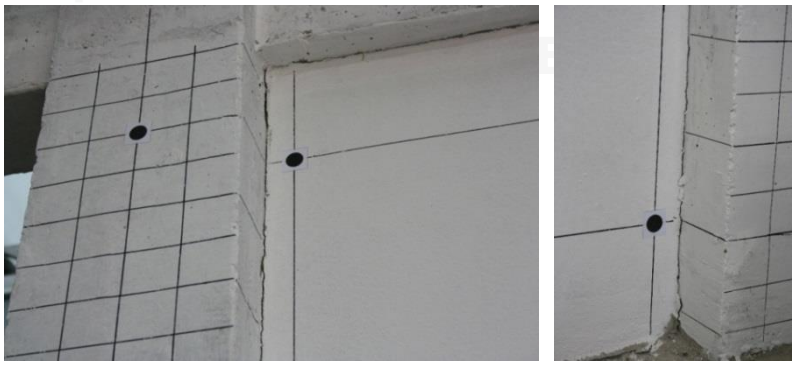

(a) (b)

Figure 4-1. The separations between surrounding RC frame and URM infill panel of specimen MIRCF01 at 0.125% drift; (a) top corner and (b) bottom corner

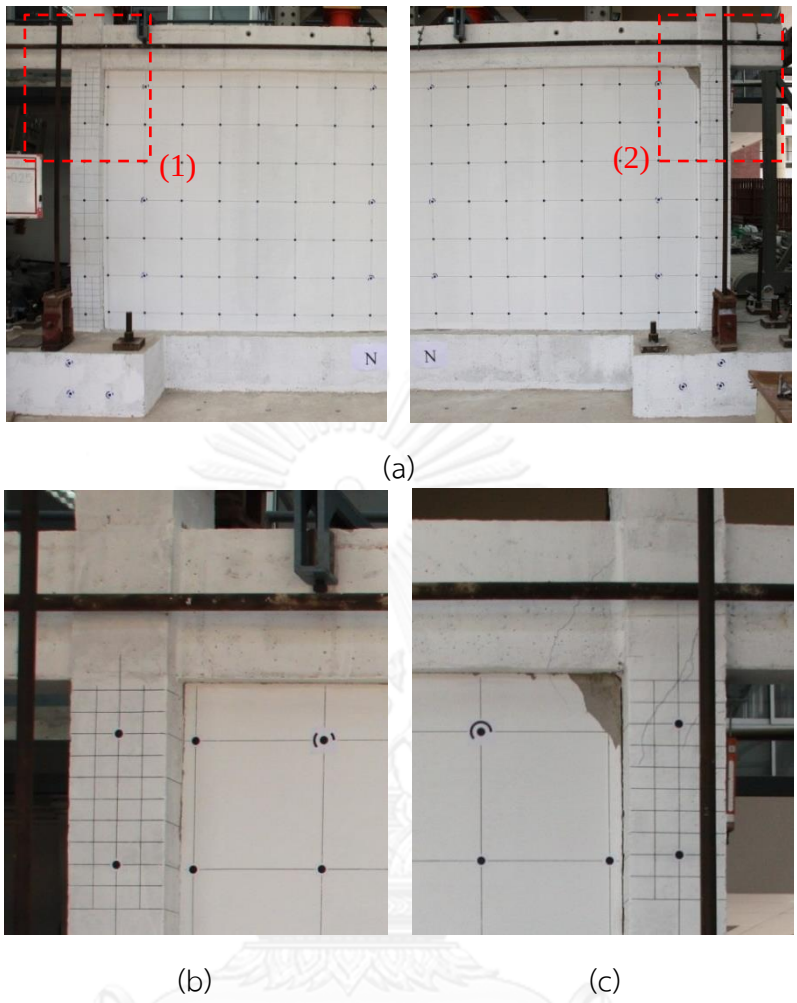

Figure 4-2. (a) Damage condition in the column and URM panel of specimen MIRCF01 at 0.25% drift; (b) and (c) closed up views of region (1) and (2), respectively

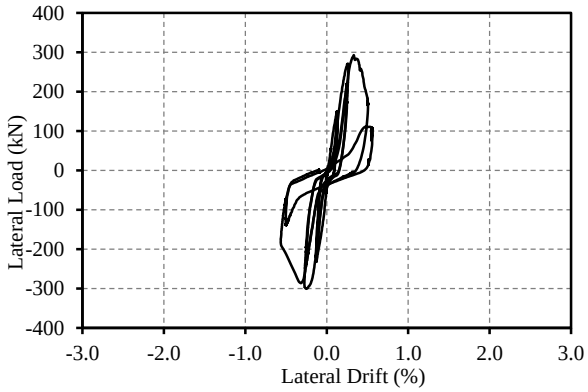

Figure 4-3. Hysteretic loops of specimen MIRCF01

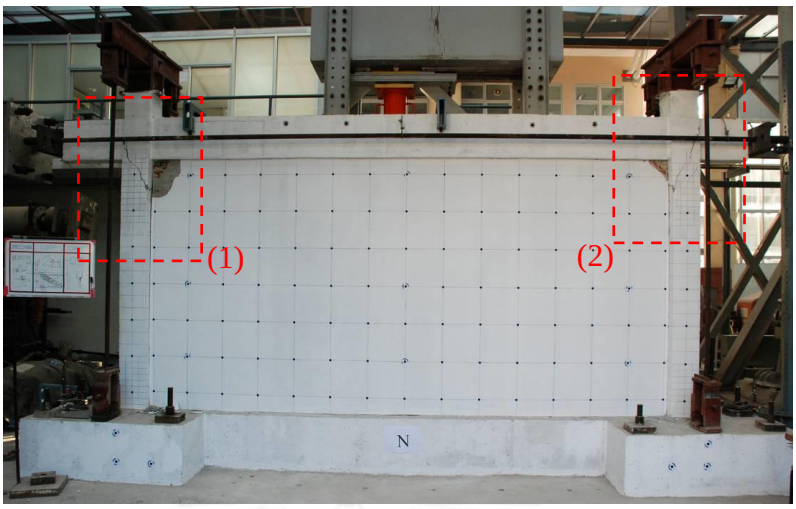

(a)

(b) (c)

Figure 4-4. (a) Damage condition in the column and URM panel of specimen MIRCF01 at 0.50% drift; (b) and (c) closed up views of region (1) and (2), respectively

Specimen MIRCF02, with the 20% removal of the URM panel adjacent to the columns exhibited remarkable improvement in performance over the original system. At 0.125% drift, hairline diagonal cracks started to develop in the panel (see Figure 4-5). When the test specimen was loaded to 0.25% drift, these cracks expanded. The diagonal cracks of the URM panel also occurred in the other direction. Moreover, minor flexural cracks in the columns were observed during the second cycle of the 0.25% drift increment. As shown in Figure 4-6, the compression strut mechanism could be clearly seen at about 0.50% drift. At this state, the width of diagonal cracks in the URM panel was approximately 5.0 mm. Visible hairline shear cracks occurred in

the beam near the load transfer brackets. The previously developed minor flexural cracks in the columns also extended in length. It can be seen from Figure 4-7 that the lateral resistance of specimen MIRCF02 slightly dropped as severe diagonal cracks of the URM panel developed. However, the lateral resistance picked up again when the test specimen was loaded to the 0.75% drift. At 1.0% drift, splitting of the boundary between the strengthened corner and the rest of the panel was observed. The largest diagonal crack in the infill panel widened to about 11 mm (see Figure 4-8). In addition, bending of the vertical steel channels could be obviously noticed at this state. The test specimen retained an average peak load of around 246 kN at 1.25% drift. The drift capacity of 1.5% was achieved at a sustainable lateral load of 80% of the peak load capacity (see Figure 4-7). Corner crushing was severe at 1.75% drift with the spalling of the wire mesh reinforced plaster. Furthermore, the vertical steel channels were severely bent (Figure 4-9) indicating the partial confinement action of the vertical steel channels in preventing joint sliding failure and in transferring the interactive forces between the infill panel and the steel brackets. The test was terminated at 2.0% story drift for safety reason since significant out-of-plane deformation was observed in the URM panel (Figure 4-10 (c)). Although severe damage occurred in the URM panel and the development of flexural cracks in the RC columns with minor flexural-shear cracks in the columns near the RC footing, these damages had no threat to cause collapse of the specimen (see Figure 4-10). Furthermore, only small shear cracks were observed in the RC beam near the load transfer brackets as indicated in Figure 4-11.

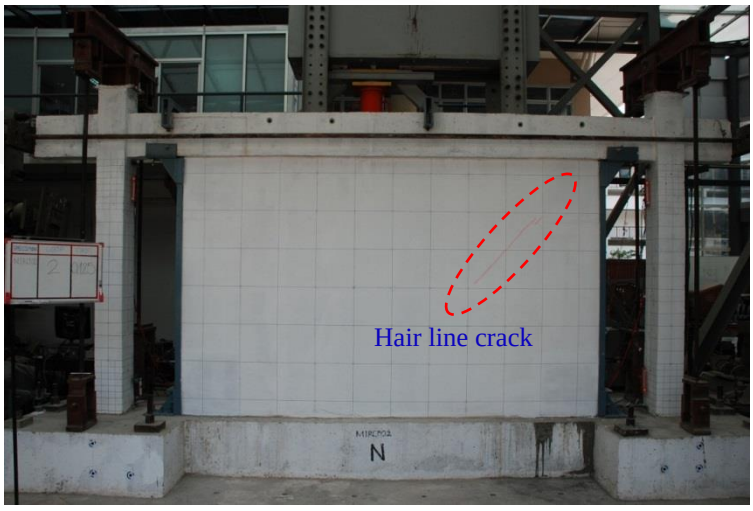

Figure 4-5. Retrofitted specimen MIRCF02 at 0.125% drift

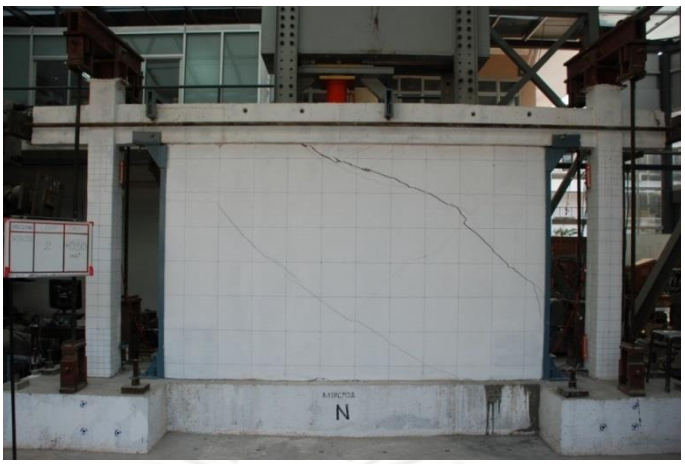

Figure 4-6. Retrofitted specimen MIRCF02 at 0.50% drift

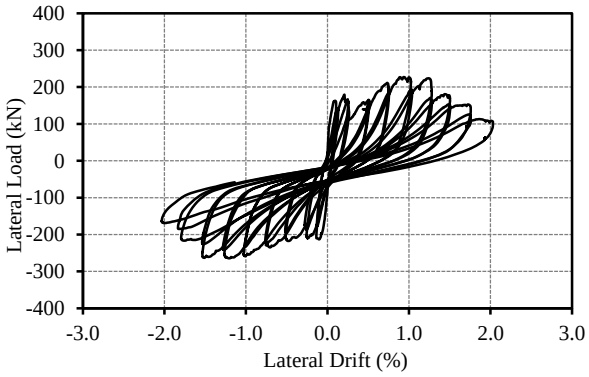

Figure 4-7. Hysteretic loops of the retrofitted specimen MIRCF02

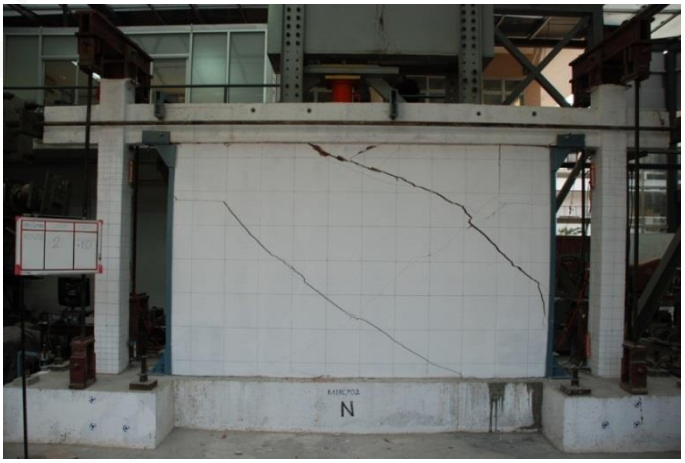

Figure 4-8. Damage condition of retrofitted specimen MIRCF02 at 1.00% drift

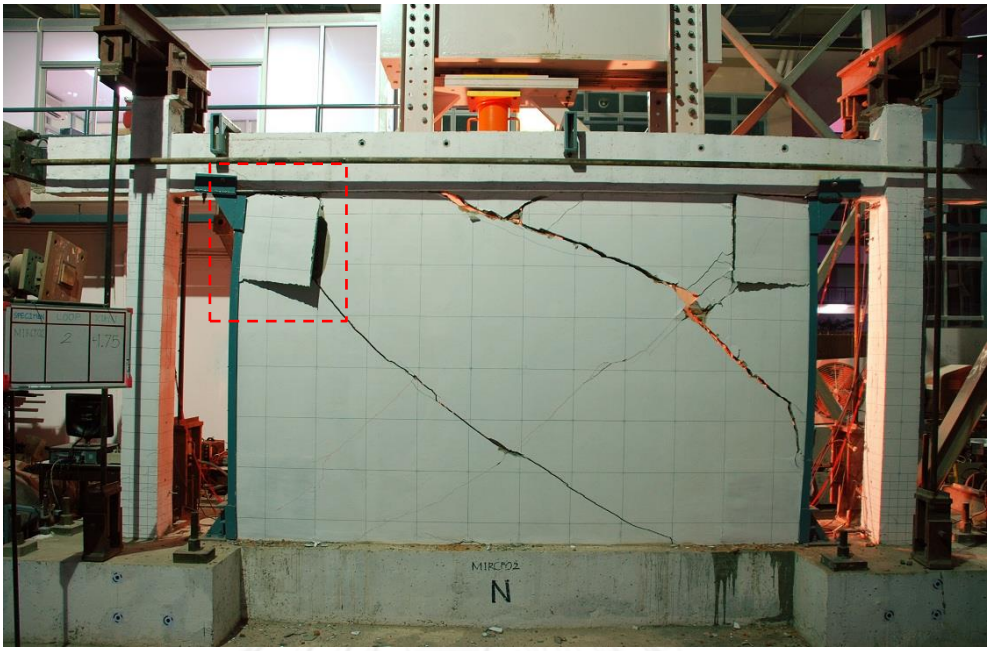

(a)

(b)

Figure 4-9. (a) Retrofitted specimen MIRCF02 at 1.75% drift; (b) severely deformed vertical steel channel

(a)

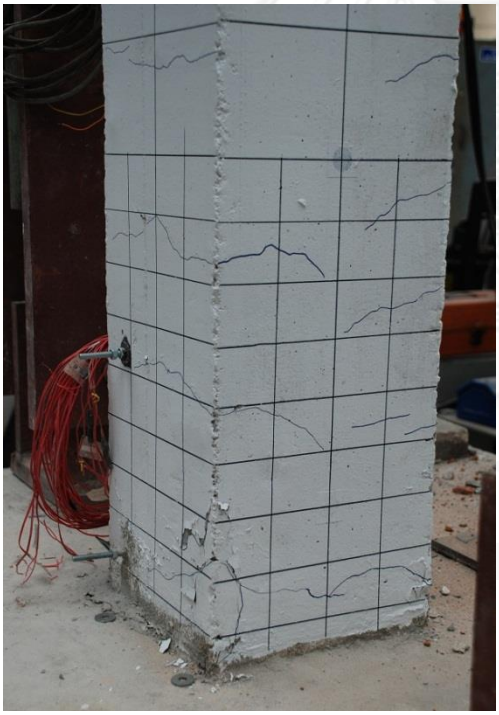

(b)

(c)

Figure 4-10. (a) Retrofitted specimen MIRCF02 at 2.00% drift; (b) damage condition in the column; and (c) out-of-plane deformation of the URM panel

Figure 4-11. Damage condition in the RC beam of specimen MIRCF02 at 2.00% drift

Specimen MIRCF03 with the 50% removal of the URM panel adjacent to the columns resulting in wall aspect ratio of 1.0 (Figure 4-12) exhibited a remarkable improvement in ductility capacity compared to the original system. However, the peak lateral load of specimen MIRCF03 decreased significantly compared to the un-retrofitted specimen. At 0.125% drift, the horizontal crack between the URM panel and the footing was observed. This crack opened rapidly when the test specimen was loaded to the 0.25% drift. Minor flexural cracks in the columns and beam-column joints were observed in the first cycle of the 0.50% drift. The crack width of about 1.0 mm was measured in the beam-column joint when the test specimen was subjected to 0.75% story drift. As depicted in Figure 4-13, visible shear and flexural-shear cracks were observed in the RC beam near the load transfer brackets at 1.0% story drift. Moreover, minor shear cracks also occurred in the beam-column joints at the same state. A rocking behavior was clearly observed in the specimen MIRCF03. The maximum gap between the URM panel and the footing was measured as 13 mm during the second cycle of 1.0% drift. The test specimen attained an average peak load of 173 kN at 1.50% drift. The drift capacity of 1.75% was achieved at a sustainable lateral load of 80% of the peak (see Figure 4-14). Impending crushing of concrete in the column occurred near the beam-column joint at 1.75% drift as shown in Figure 4-15. It should be noted that more flexural and shear cracks developed in RC columns compared to MIRCF02. At a drift of 2.0%, a large diagonal crack occurred in the URM panel resulting in moderate drop of the lateral resistance

of the test specimen. At this state, the maximum width of diagonal crack in the infill panel was about 6.0 mm. The gap at the base of the wall was measured as 26 mm. The damage condition of specimen MIRCF03 at 2.0% story drift is shown in Figure 4-16. At a drift of 2.5%, severe crushing and splitting of concrete in the column near the beam-column joint was observed. After that the longitudinal steel bars in the column buckled (see Figure 4-17). The gap at the base of the wall due to rocking was as large as 30 mm at this state.

Figure 4-12. Retrofitted specimen MIRCF03

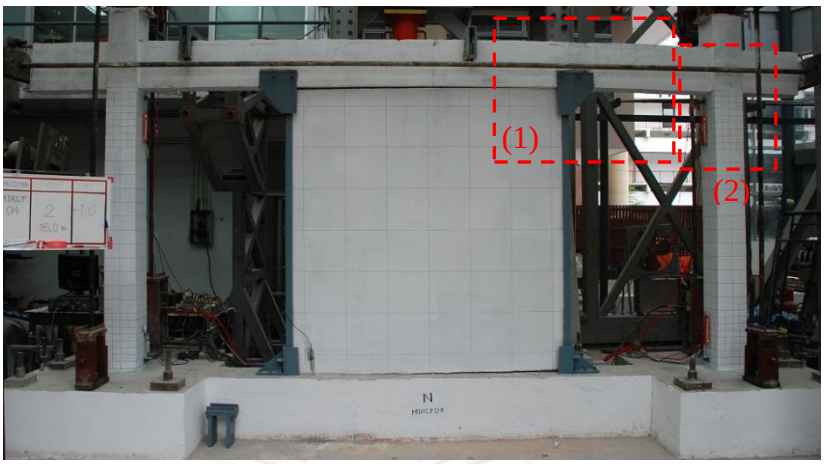

(a)

(b) (c)

Figure 4-13. (a) Damage condition of specimen MIRCF03 at 1.00% drift; (b) and (c) closed up views of region (1) and (2), respectively

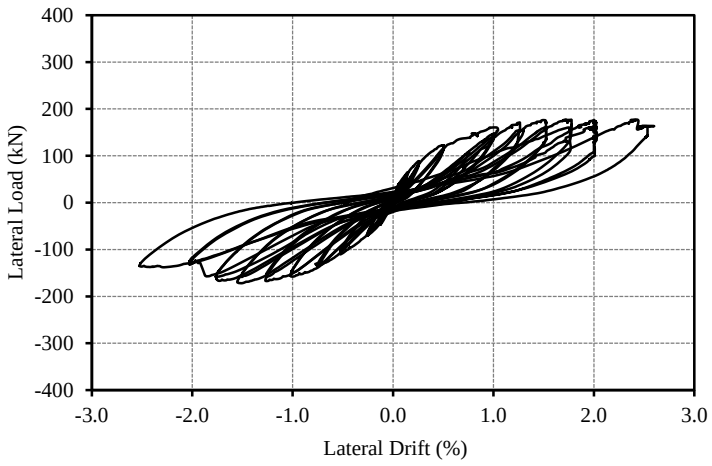

Figure 4-14. Hysteretic loops of the retrofitted specimen MIRCF03

Figure 4-15. Splitting of concrete in the RC column at 1.75% drift

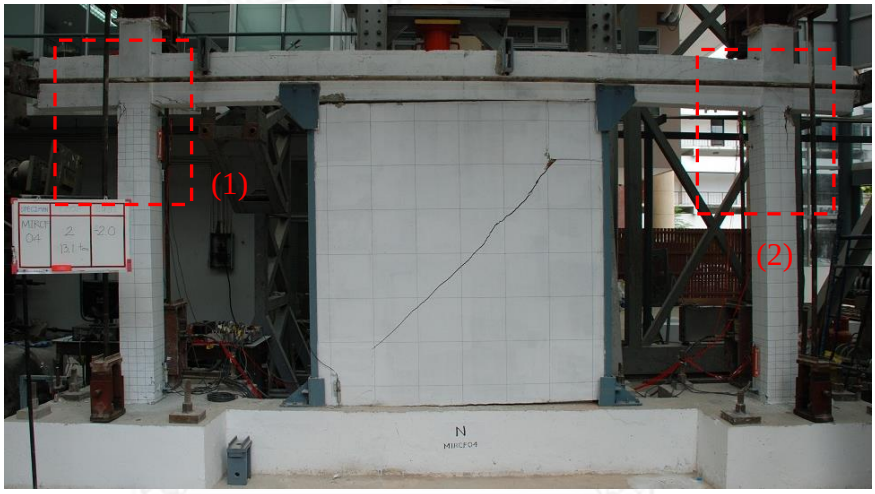

(a)

(b) (c)

Figure 4-16. (a) Damage condition of specimen MIRCF03 at 2.00% drift; (b) and (c) closed up views of region (1) and (2), respectively

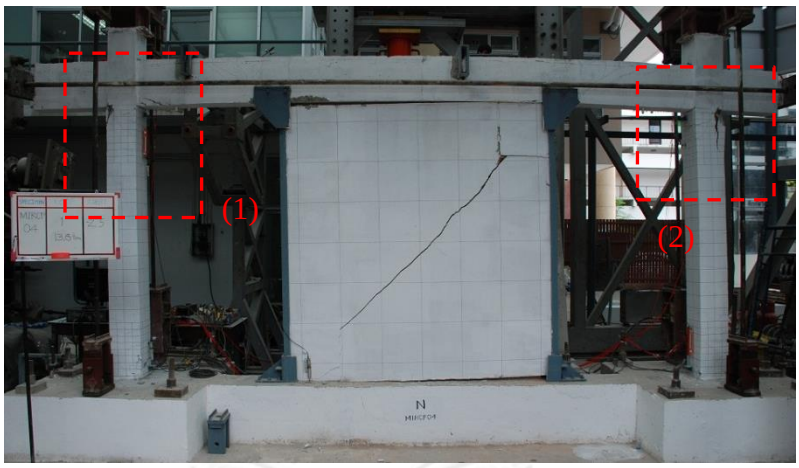

(a)

(b) (c)

Figure 4-17. Damage condition of specimen MIRCF03 at 2.50% drift; (b) and (c) closed up views of region (1) and (2), respectively

Specimen MIRCF04, with the same configuration as specimen MIRCF02 except for a slight steel reinforcement in the masonry infill panel, exhibited a remarkable improvement in performance over specimen MIRCF02. At 0.125% drift, small diagonal cracks started to develop in the panel (see Figure 4-18). The crack width of about 0.5 mm was measured. When the test specimen was loaded to 0.25% drift, hairline flexural cracks were observed in the RC columns. As shown in Figure 4-19, a slight corner crushing of the infill panel developed at 0.50% drift. Moreover, at this state the steel wires which were attached to the surrounding RC frame pulled out due to sliding of the infill panel. A small diagonal crack was observed at the corner of the

infill panel during the first cycle to 0.75% drift. Also, visible flexural-shear cracks occurred in the RC columns (see Figure 4-20). During the second cycle of 0.75% drift, the largest crack in the RC columns widened to roughly 0.5 mm. The test specimen approximately maintained an average peak load of 230 kN at 1.25% drift up to 2.00% drift. The specimen could sustain a drift capacity of 2.0% at the lateral load of over 80% of the peak load (see Figure 4-21). At 1.75% drift, the largest crack in the RC columns was about 1.0 mm. Also, the gap between the wall and footing due to rocking was 4 mm. Figure 4-22 shows the damage condition of test specimen MIRCF04 at 1.75% drift. It was observed that with a slight steel wire mesh reinforcement in the infill panel, the damage of the infill panel was reduced considerably. The out-of-plane deformation of the infill panel of specimen MIRCF04 decreased considerably, compared with specimen MIRCF02. At 2.0% drift, crushing of concrete in the RC column near the footing and spalling of cement plaster at the corner of infill panel were observed (see Figure 4-23). At this state, the test specimen was able to sustain a lateral load of about 90% of the peak capacity. However, the flexural-shear failure occurred abruptly at the lower part of the RC column during the second cycle of 2.5% drift as depicted in Figure 4-24.

Figure 4-18. Damage condition of specimen MIRCF04 at 0.125% drift

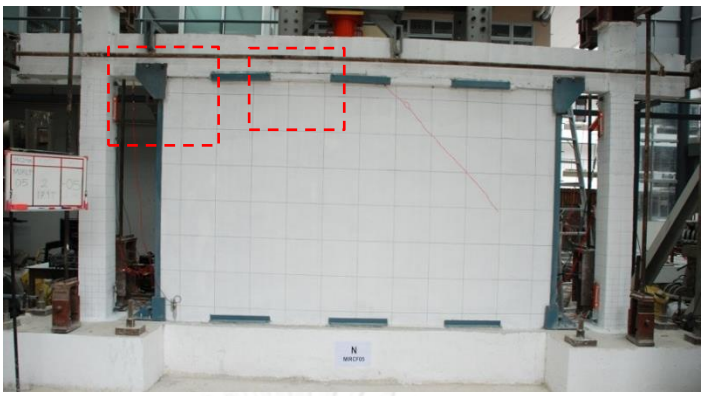

(a)

(b) (c)

Figure 4-19. (a) Damage condition of specimen MIRCF04 at 0.50% drift; (b) a slight corner crushing of infill panel; and (c) steel wires pulled out

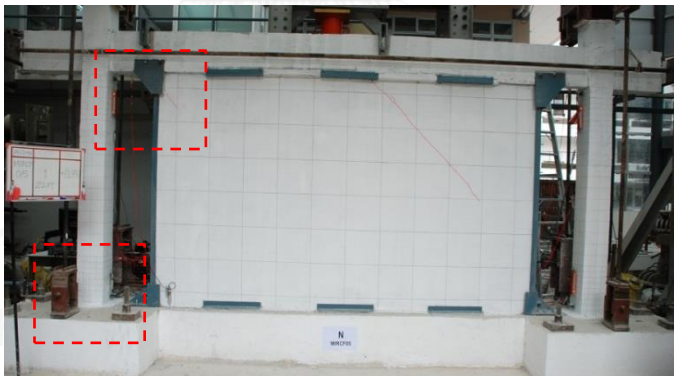

(a)

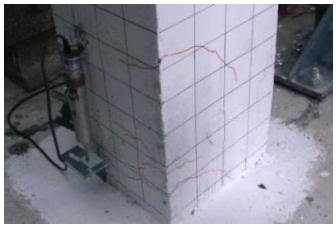

(b) (c)

Figure 4-20. (a) Damage condition of specimen MIRCF04 at 0.75% drift; (b) flexural-shear cracks; and (c) small diagonal cracks at the corner of infill panel

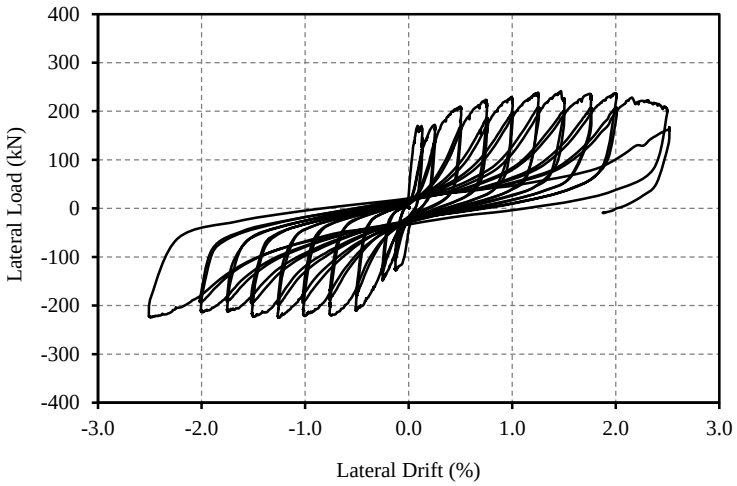

Figure 4-21. Hysteretic loops of the retrofitted specimen MIRCF04

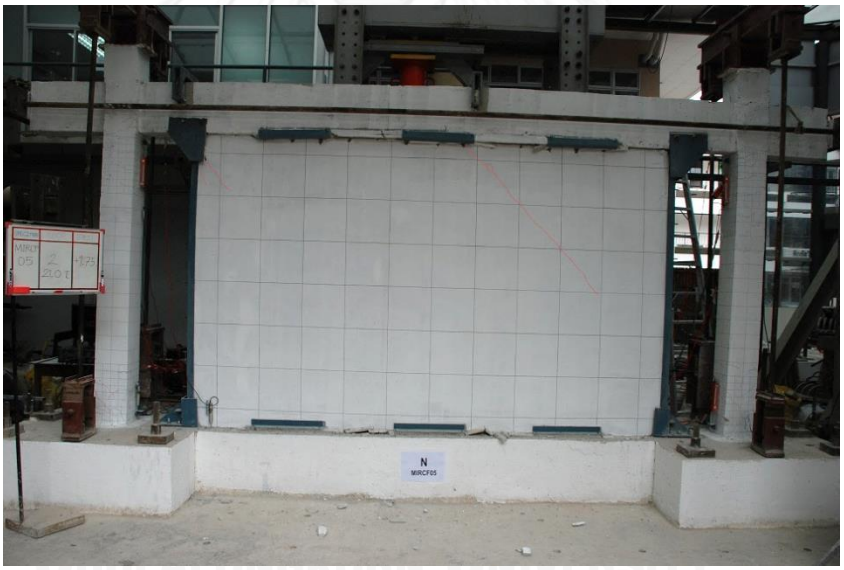

Figure 4-22. Damage condition of specimen MIRCF04 at 1.75% drift

(a)

(b)

Figure 4-23. Damage condition of specimen MIRCF04 at 2.0% drift: (a) Splitting of concrete in the column and (b) corner crushing of the infill panel

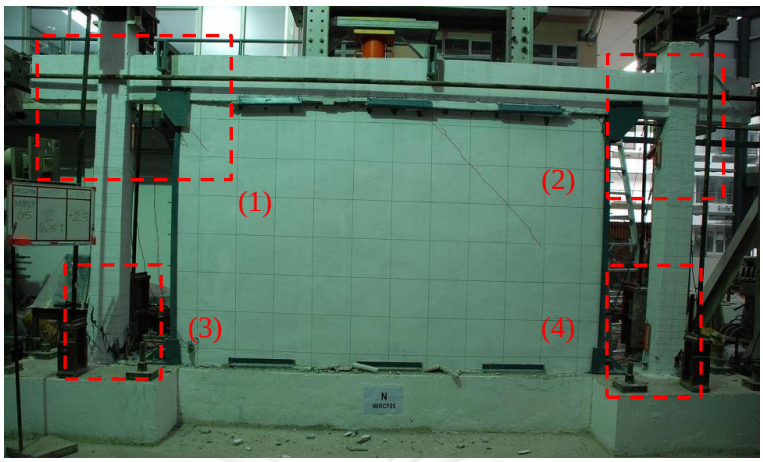

(a)

(b)

(c)

(d)

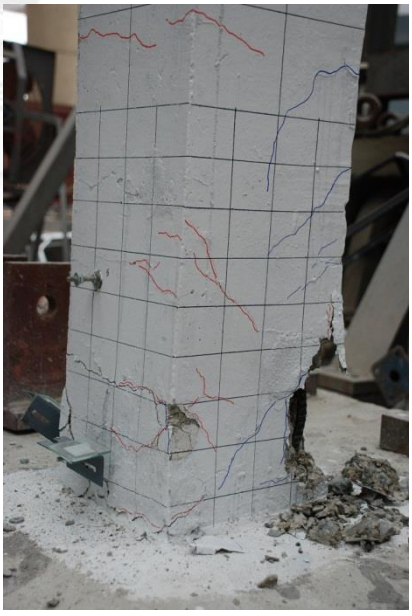

(e)

Figure 4-24. (a) Damage condition of specimen MIRCF04 at 2.5% drift; (b) to (e) closed up views of region (1) to (4), respectively

4.2 Lateral strength and lateral stiffness

The hysteretic loops of test specimen MIRCF01 is presented in Figure 4-25. As can be seen, the test specimen remained in the linear range up to 0.25% drift. Subsequently, the visible nonlinear behavior started to develop due to slight damage of the URM panel and the surrounding RC frame. After the peak load of 292 kN was achieved at 0.33% drift, the load capacity suddenly dropped to 120 kN, approximately a 60% decrease from the peak load. This was caused by the formation of shear cracks in the RC columns and beam-column joints as well as corner crushing of the URM panel. Specimen MIRCF02, with the 20% removal of the URM panel adjacent to the columns and the proposed retrofitting scheme, exhibited a remarkable improvement in performance over the un-retrofitted one. The nonlinear behavior was initiated by a diagonal crack of the infill panel at 0.125% drift. It can be seen from Figure 4-26 that the lateral resistance of specimen MIRCF02 slightly dropped due to severe diagonal cracks of the URM panel at 0.50% drift. However, the lateral load gradually increased when the specimen was loaded to a larger drift level. The tested specimen attained an average peak load of around 246 kN at 1.25% drift. Then the load capacity gradually dropped. Moreover, the drift capacity of 1.5% was achieved at a sustainable lateral load of 80% of the peak capacity.

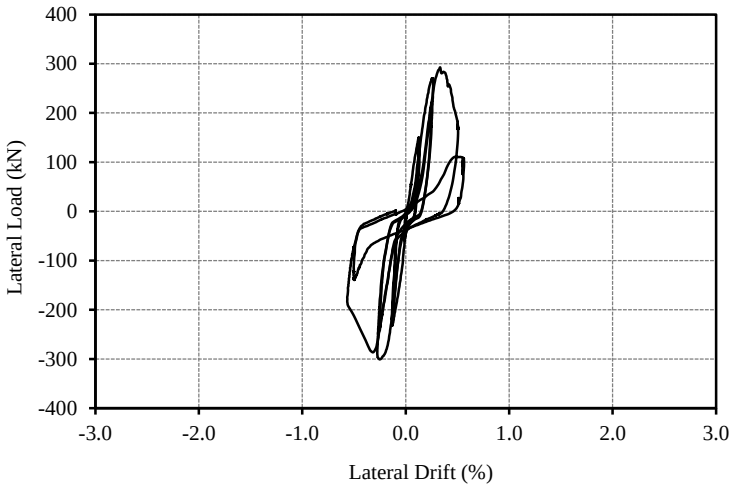

Figure 4-25. Hysteretic loops of the retrofitted specimen MIRCF01

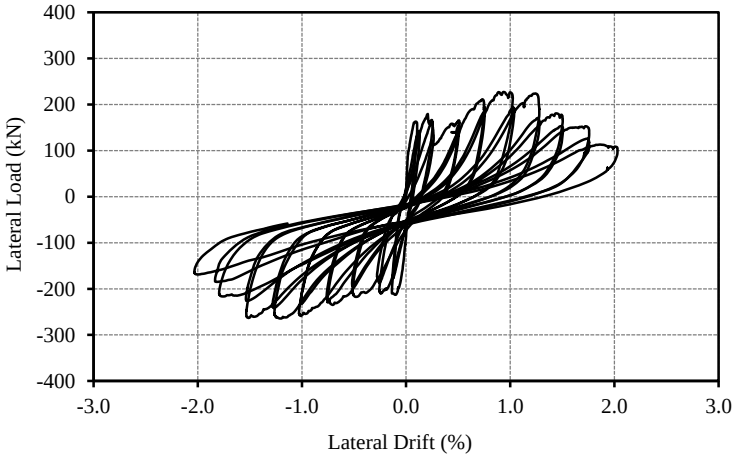

Figure 4-26. Hysteretic loops of the retrofitted specimen MIRCF02

Although the displacement capacity of the retrofitted specimen MIRCF03 was significantly improved over the un-retrofitted specimen, its peak lateral load, however, decreased significantly compared to the un-retrofitted specimen as shown in Figure 4-27. In the elastic response range, the lateral resistance of specimen MIRCF03 gradually increased with a lateral stiffness smaller than both specimens MIRCF01 and MIRCF02. Obviously, the contribution of the smaller infill panel on the lateral resistance of specimen MIRCF03 was much less than those of specimens MIRCF01 and MIRCF02. The visible nonlinear behavior started to develop due to the slight damage to the surrounding frame and rocking of the URM panel. The test specimen attained an average peak load of around 173 kN at 1.50% drift. The drift capacity of 1.75% was achieved at a sustainable lateral load of 80% of the peak capacity. It should be noted that the strength deterioration of specimen MIRCF03 developed with slower rate compared to specimen MIRCF02. The reason is that the infill panel of specimen MIRCF02 suffered more extensive damage.

With the steel wire mesh reinforcement utilized in the infill panel, specimen MIRCF04 exhibited the most superior performance among the tested specimens. The hysteretic loops of specimen MIRCF04 is shown in Figure 4-28. The nonlinear behavior was started by a diagonal crack in the infill panel during the 0.125% drift increment. The test specimen attained an average peak load of around 230 kN at 1.25% drift and maintained this load up to 2.0% drift. The drift capacity of 2.0% was achieved at a sustainable lateral load over 80% of the peak capacity. However, the test specimen lost its lateral capacity during the second cycle to 2.5% drift due to flexural-shear failure and crushing of the columns.

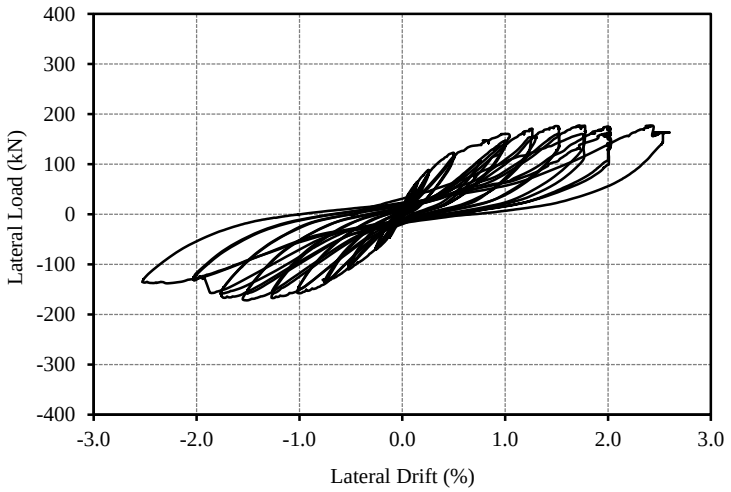

Figure 4-27. Hysteretic loops of the retrofitted specimen MIRCF03

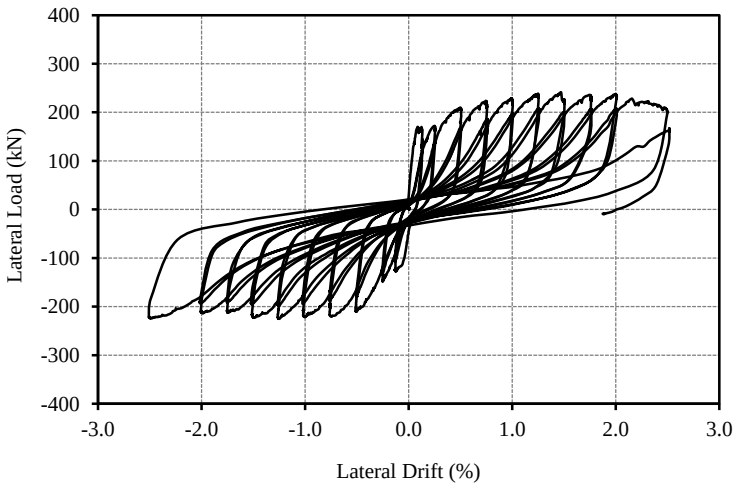

Figure 4-28. Hysteretic loops of the retrofitted specimen MIRCF04

The lateral load versus drift ratio envelope curves of the tested specimens are demonstrated in Figure 4-29. The average peak lateral load of the retrofitted specimens MIRCF02 and MIRCF04 were 0.84 and 0.79 times of specimen MIRCF01, respectively. On the other hand, the drift capacities at a sustainable lateral load of 80% of the peak load of the retrofitted specimens MIRCF02 and MIRCF04 were 6 and 8 times, respectively. It should be noted that both retrofitted specimens reached their average peak strength at about the same drift. However, specimen MIRCF04 exhibited less strength degradation compared to specimen MIRCF02. Although the average peak strength of retrofitted specimen MIRCF03 was only 0.59 times of the

un-retrofitted specimen MIRCF01, the drift capacity was about 7 times higher. It is interesting to note that reduction in the URM panel cross-sectional area results in decrease in the peak lateral load approximately in proportion to the area reduction of URM panel cross-sectional area for the specimen tested in which the URM infill contributed significantly to the lateral load capacity of the assemblage.

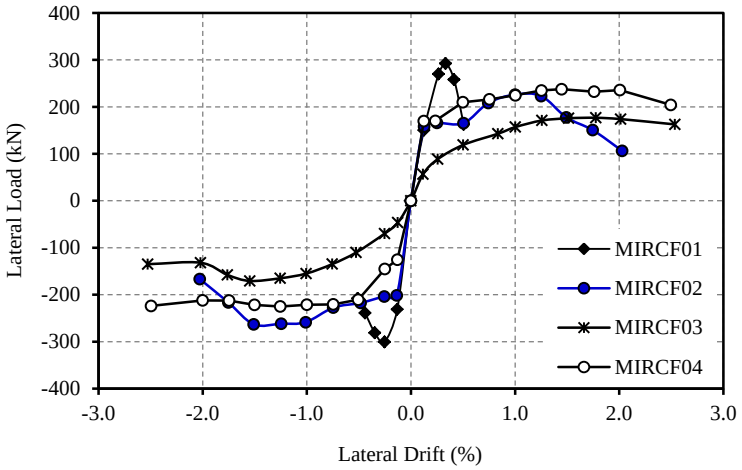

Figure 4-29. Envelopes of the hysteretic curves

Figure 4-30 shows the secant stiffness versus drift ratio of the tested specimens. At 0.125% drift, the secant stiffness of the retrofitted specimen MIRCF02 drift was roughly 94% of the secant stiffness of the un-retrofitted specimen MIRCF01. Although 20% of the URM infill panel was removed, the secant stiffness of specimen MIRCF02 approximately decreased by 6% only compared to specimen MIRCF01. The reason can be explained as follows. A pre-test to 10 kN lateral load was performed on specimen MIRCF01 for checking the data acquisition and the measurement system. Moreover, for specimen MIRCF02 high pressure epoxy injection was employed to seal the separation between the URM panel and the surrounding frame interface which occurred after testing specimen MIRCF01. This procedure may have increased the bond strength between URM infill panel and surrounding RC frame of specimen MIRCF02. Therefore, both these two factors may lead to favorable effect on the secant stiffness of specimen MIRCF02 in comparison with MIRCF01. A different result was observed in the retrofitted specimen MIRCF04. At the 0.125% drift, the secant stiffness of specimen MIRCF04 was approximately 82% of the specimen MIRCF01. However, the secant stiffness at 0.25% drift of both specimens MIRCF02

and MIRCF04 were similar and significantly lower than the un-retrofitted specimen. With the removal of 50% of URM infill panel (specimen MRCF03), the secant stiffness at 0.125% drift was only 30% of the un-retrofitted specimen. It is important to note that a significant reduction in stiffness of specimen MIRCF03 was caused by the large reduction in the URM panel width and a significant rocking motion of URM panel.

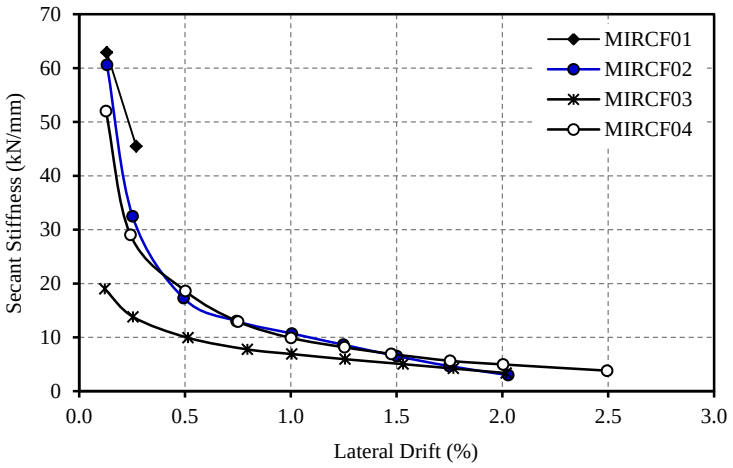

Figure 4-30. Secant stiffness variation with lateral drift

4.3 Energy dissipation and equivalent viscous damping ratio

One desirable characteristic of seismic resistant structures is the ability to dissipate energy to reduce structural damage. The structural energy dissipation capacity can be calculated from the area under the load displacement hysteretic loops. In this study a numerical integration scheme based on the trapezoidal rule was used to determine the area under the hysteretic loops. The cumulative energy dissipation with increasing loading cycles of all specimens is presented in Figure 4-31. It is observed that all retrofitted specimens achieved higher total energy dissipation capacities than the un-retrofitted specimen. Specimens, MIRCF02 and MIRCF04, have similar energy dissipation capacities up to 1.75% drift. In the case of specimen MIRCF03, its energy dissipation capacity was slight lower than that of the other specimens up to 0.25% drift. However, beyond this state the energy dissipation capacity of specimen MIRCF03 was considerable lowest among the other retrofitted specimens. At 0.5% drift, the cumulative energy dissipation of specimen MIRCF03 was only 0.25 and 0.28 times of specimens MIRCF02 and MIRCF04, respectively.

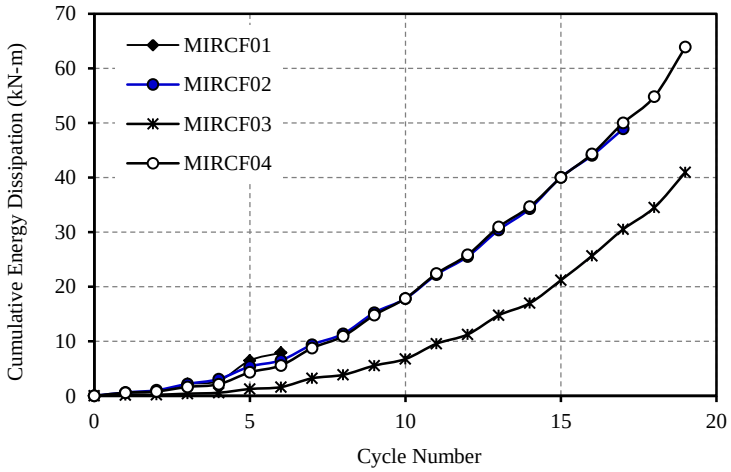

Figure 4-31. Cumulative energy dissipation with loading cycles

An equivalent viscous damping, ξ_{eq}, of a structure is a useful parameter for assessing seismic response. For a structural component subjected to cyclic load, the energy dissipation under hysteretic loop can be correlated with the equivalent viscous damping as follows (Priestley et al., 1996):

$$\xi_{eq} = \frac{E_i}{4\pi E_e} \tag{4-1}$$

where E_e is the strain energy stored in an equivalent linear elastic system when the maximum displacement is reached at each cycle, and E_i is the energy dissipation of each cycle.

An equivalent viscous damping versus drift ratio of the tested specimens is shown in Figure 4-32. Both retrofitted specimens MIRCF02 and MIRCF04 achieved higher equivalent viscous damping than the un-retrofitted specimen MIRCF01 with a drift increment under 0.25%. On the other hand, specimen MIRCF03 had a lower equivalent viscous damping compared to others. The equivalent viscous damping ranges from 0.07 to 0.22. However, when a drift increment was more than 0.5% the equivalent viscous damping of all retrofitted specimens were closed to 0.1.

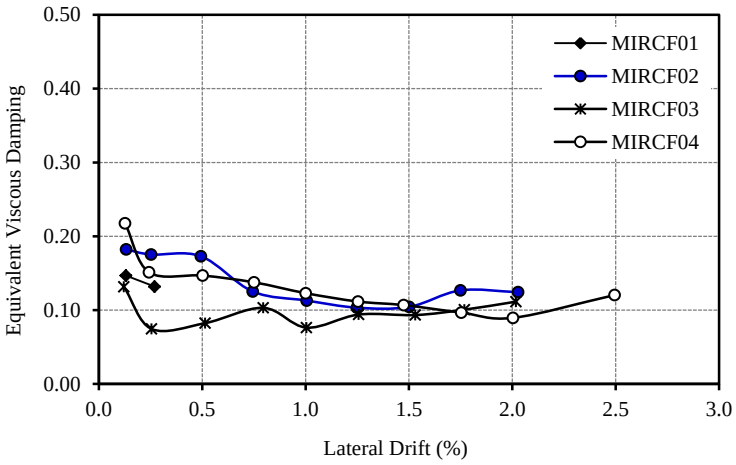

Figure 4-32. Equivalent viscous damping ratio with lateral drift

4.4 Strain in the steel reinforcement

In order to evaluate the structural response of the surrounding RC frames, strains in steel reinforcement were monitored during the experiment. Figure 4-33 shows the steel reinforcement strain measurement locations on the left side of test specimens. Because of geometric and loading symmetry, the results for only one side is shown in this section, which can give a pretty good picture on the response. The results for the other half is presented in Appendix. The corresponding drift ratio-strain relations of MIRCF01 are shown in Figure 4-34. It should be noted that two strain gauges were provided at a distance of 100 mm above the footing. Unfortunately, one of those was damaged during the casting. However, the remaining strain gauges yielded good results of the rebars. All the longitudinal steel bars in the columns of test specimen MIRCF01 did not yield, except one (SLC16) which reached its yield strain (yield strain was 1710 micro strain) because of buckling caused by shear failure of the column. The strains in the transverse reinforcement of the RC column were also measured. The location of those strain gages are illustrated in Figure 4-33. Unfortunately, the strain gages in the region which shear failure occurred (STC11 and STC12) were damaged during casting. The drift ratio and strain relations of remaining strain gages in transverse reinforcement of MIRCF01 are shown in Figure 4-35. All the transverse steel bars in the columns of specimen MIRCF01 did not yield during testing, because those strain gages were located outside the cracking regions.

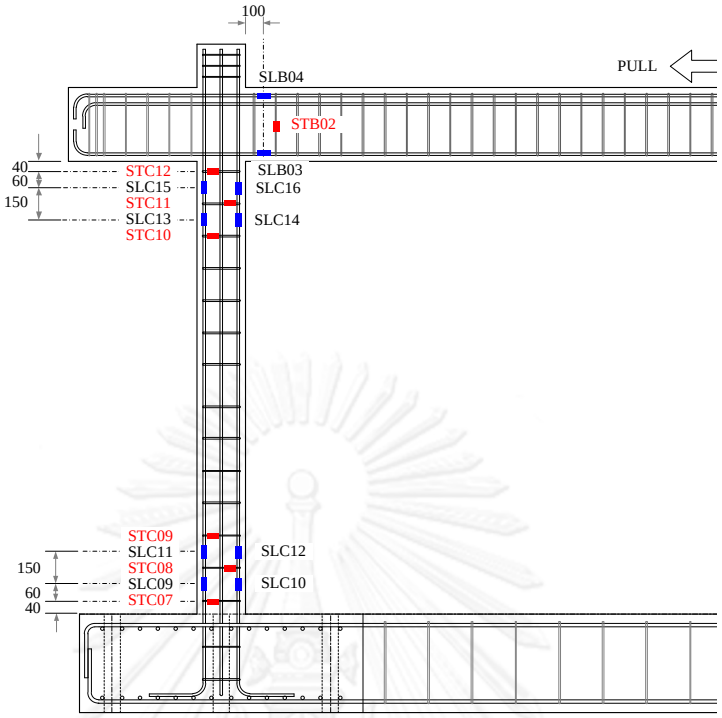

Figure 4-33. Strain measurement locations in the left side of test specimens

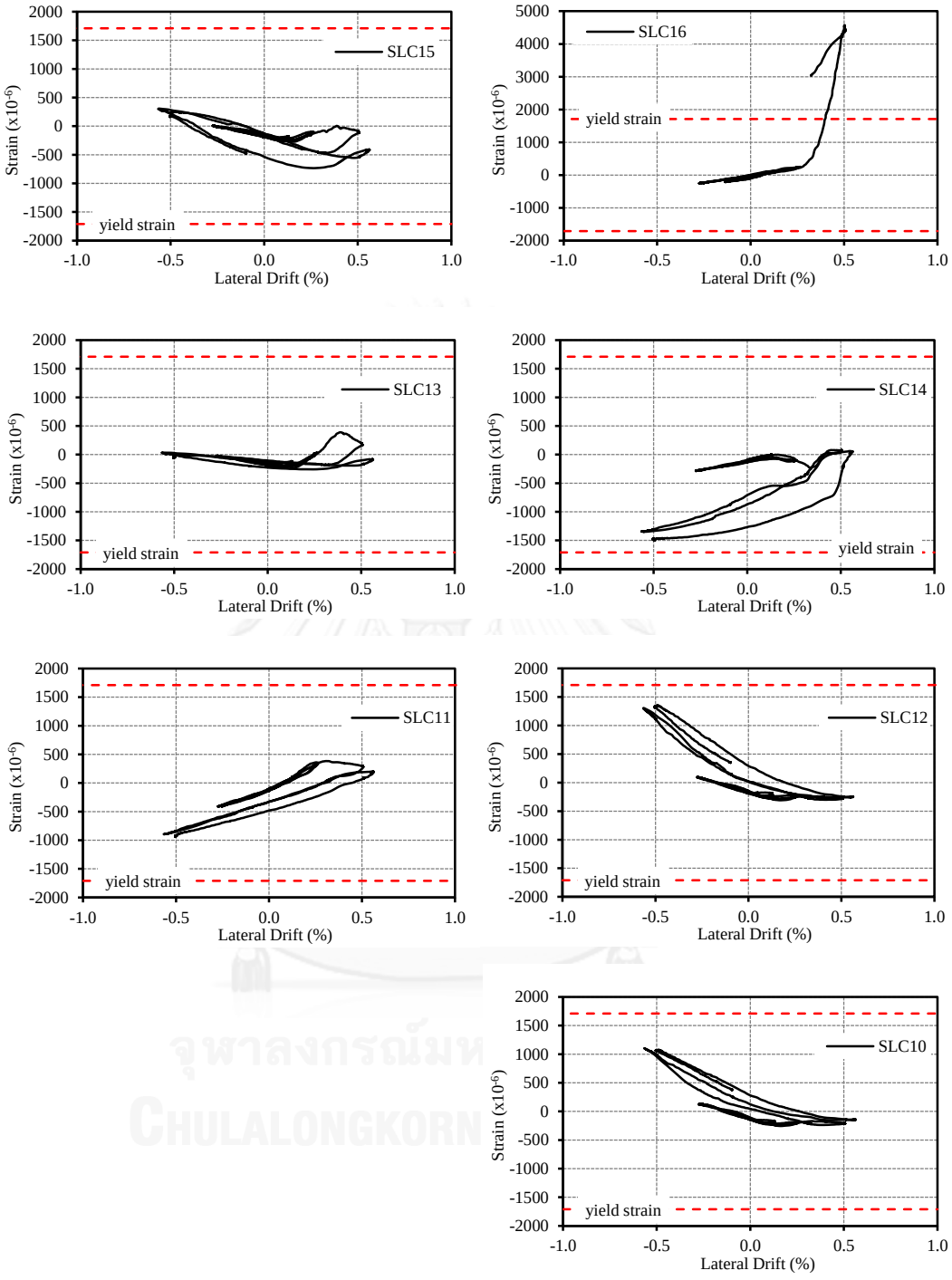

Figure 4-34. Drift ratio-strain relation of vertical rebars in the column of MIRCF01

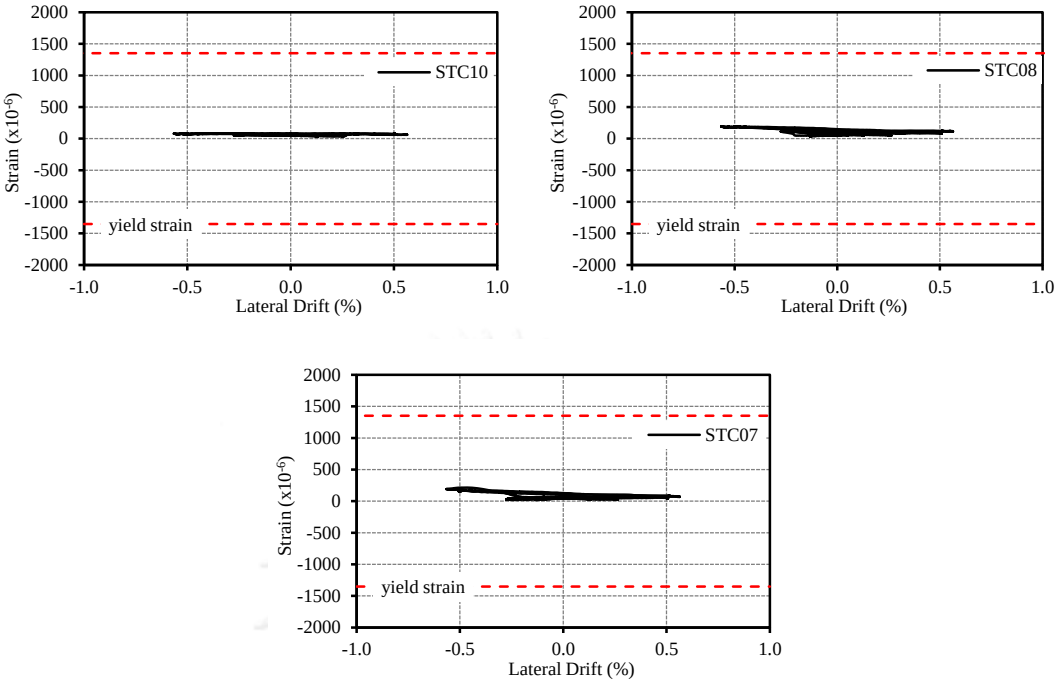

Figure 4-35. Drift ratio-strain relation of transverse rebars in the column of MIRCF01

The drift ratio-strain relations of steel reinforcement in the beam of MIRCF01 are shown in Figures 4-36 and 4-37. Since the test specimen experienced shear failure in the columns at a very small lateral drift of 0.5%, the beam was therefore subjected to only small deformation resulting in both longitudinal and transverse reinforcement not stressed to the yield level.

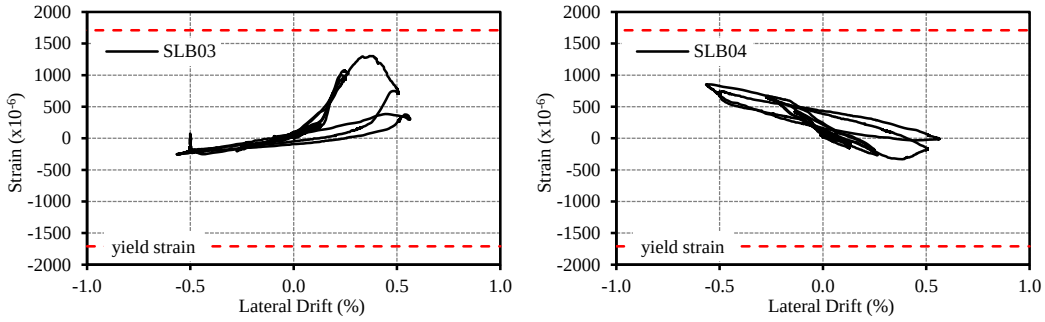

Figure 4-36. Drift ratio-strain relation of longitudinal rebars in the beam of MIRCF01

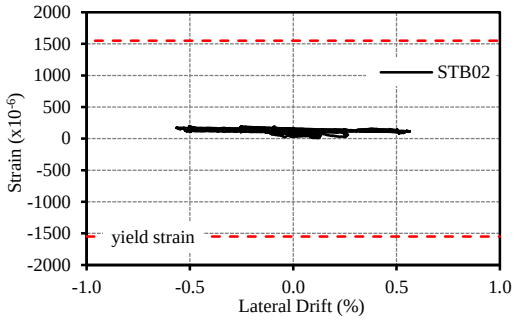

Figure 4-37. Drift ratio-strain relation of transverse rebar in the beam of MIRCF01

As shown in Figure 4-38, the retrofitted specimen (MIRCF02) could sustain a large drift of 2.0% and failed in flexural mode, as indicated by yielding of the longitudinal steel bars in the columns. As mentioned earlier, the RC frame of specimen MIRCF02 was the repaired one with all steel bars of specimen MIRCF01 retained in MIRCF02. Therefore, the strains in those bars of specimen MIRCF02 would contain the residual strains (if any) from the previous experiment. However, the residual strain effect can be ignored in all positions except SLC16 since the steel reinforcement buckled at this location whereas other rebars did not yield from the previous test as described in the previous section. Therefore, the drift ratio-strain relation of SLC16 of specimen MIRCF02 is discarded. The first yield was detected in specimen MIRCF02 at 0.75% drift level (see SLC14). The longitudinal reinforcement in the lower part of the column, SLC11 and SLC12, reached its yield strain at a drift ratio of 1.0%. Finally, all the longitudinal steel bars in the columns of test specimen MIRCF02 yielded, except SLC13.

The drift ratio-strain relations of the transverse reinforcements of MIRCF02 are shown in Figure 4-39. Although specimen MIRCF02 was loaded to the 2.0% drift ratio which was considerably higher than specimen MIRCF01, all the transverse steel bars in the columns still did not yield. It should be noted that the maximum value of transverse reinforcement strain was around 500 micro strains which corresponds to 37% of its yield strain. This result was consistent with the damage condition as described previously: only minor flexural-shear cracks developed in the lower part of the RC columns. Based on these results it can be concluded that the proposed retrofit scheme could prevent shear failure to occur in the RC columns.

The drift ratio-strain relations of steel reinforcements in the beam of MIRCF02 are shown in Figure 4-40. Both longitudinal and transverse reinforcements in RC beam of specimen MIRCF02 did not reach the yield strain, although one might expect yielding in some of the stirrups.

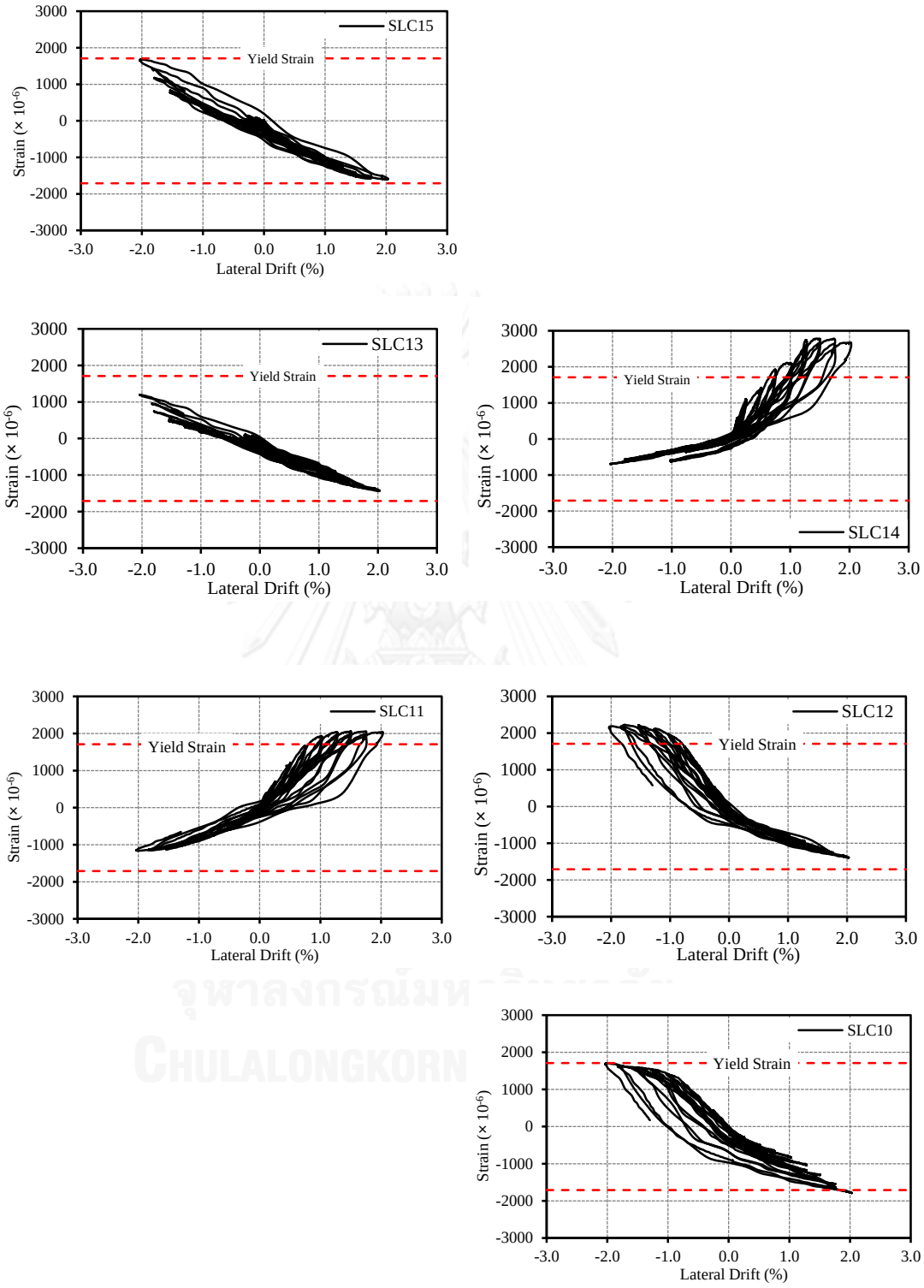

Figure 4-38. Drift ratio-strain relation of vertical rebars in the column of MIRCF02

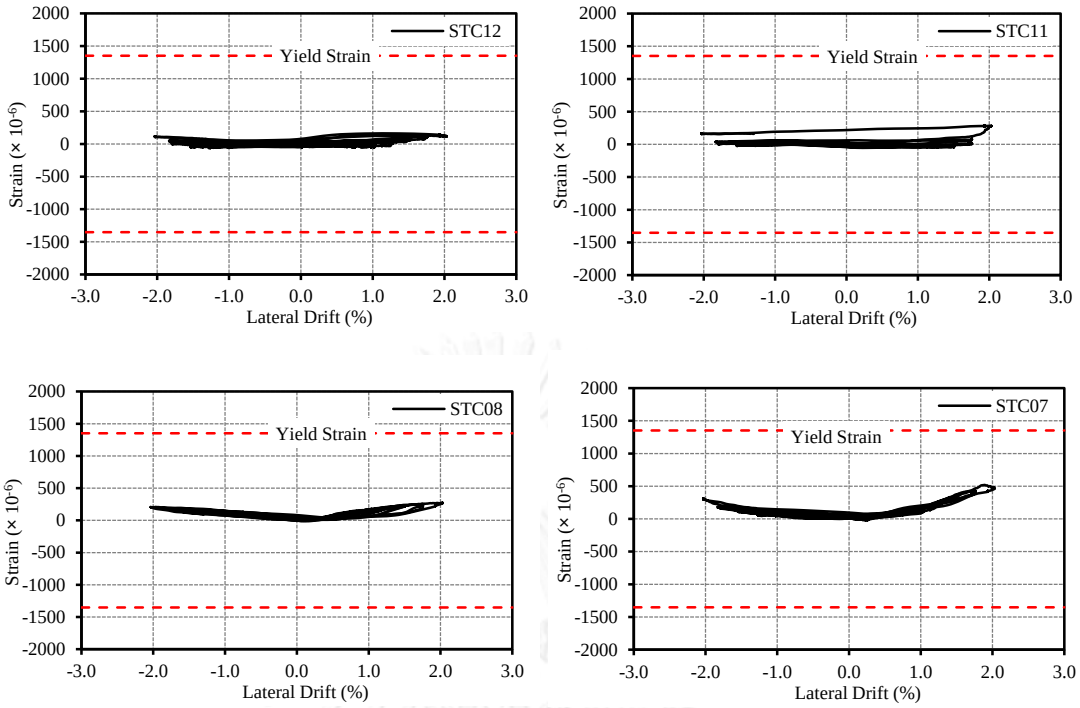

Figure 4-39. Drift ratio-strain relation of transverse rebars in the column of MIRCF02

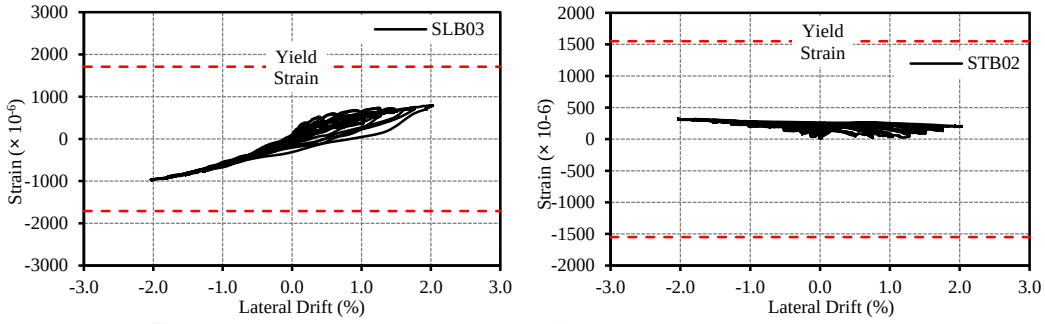

(a) (b)

Figure 4-40. Drift ratio-strain relation of steel reinforcement in the beam of MIRCF02: (a) longitudinal rebar; (b) transverse rebar

Figure 4-41 shows the drift ratio-strain relations of vertical rebars in the left column of specimen MIRCF03. Similar to specimen MIRCF02, the first yield of the longitudinal steel reinforcements at the base of the column was observed at the 0.75% drift (see SLC10). All the longitudinal steel bars in the columns of test specimen MIRCF03 reached its yield strain, except SLC13 at a drift ratio of 1.0%. Even

though the tested specimen was loaded to the maximum drift level of 2.5%, the steel reinforcement strains were recorded up to 1.75% drift ratio because of failure of the data acquisition system. The drift ratio-strain relations of the transverse reinforcements of MIRCF03 are shown in Figure 4-42. All the transverse steel rebars in the left columns did not yield during testing, except STC11 which reached its yield strain at 1.75% drift. Unlike specimen MIRCF02, there were more shear and flexural-shear cracks in the columns near the beam-column joints resulting in more severe demand in the column ties. With the limited resource of the data acquisition system used, strain measurement in the steel reinforcements of the beam was omitted.

As mentioned earlier, the RC frame of specimen MIRCF04 was also the repaired one with most of steel bars of specimen MIRCF03 retained in MIRCF04 except the longitudinal rebars that buckled which were replaced by the new steel reinforcement. Moreover, most of steel bars of specimen MIRCF03 reached its yield strain in the previous experiment. Therefore, the strains in those bars of specimen MIRCF04 would contain a significant amount of residual strains from the previous experiment. Consequently, the strain reading would yield erroneous picture of the strains in the rebars. Hence, the drift ratio-strain relation of vertical rebars of specimen MIRCF04 is not reported. The drift ratio-strain relations of the transverse reinforcement of MIRCF04 are shown in Figure 4-43. At a drift ratio under 2.0%, all the transverse steel bars in the left column of test specimen MIRCF04 remained elastic during testing. This result was consistent with fact that only minor flexural-shear cracks were observed in the RC columns. However, during the second cycle of the 2.5% drift the transverse rebar in the left column (STC08) yielded and fractured due to the abrupt flexural-shear failure of the column.

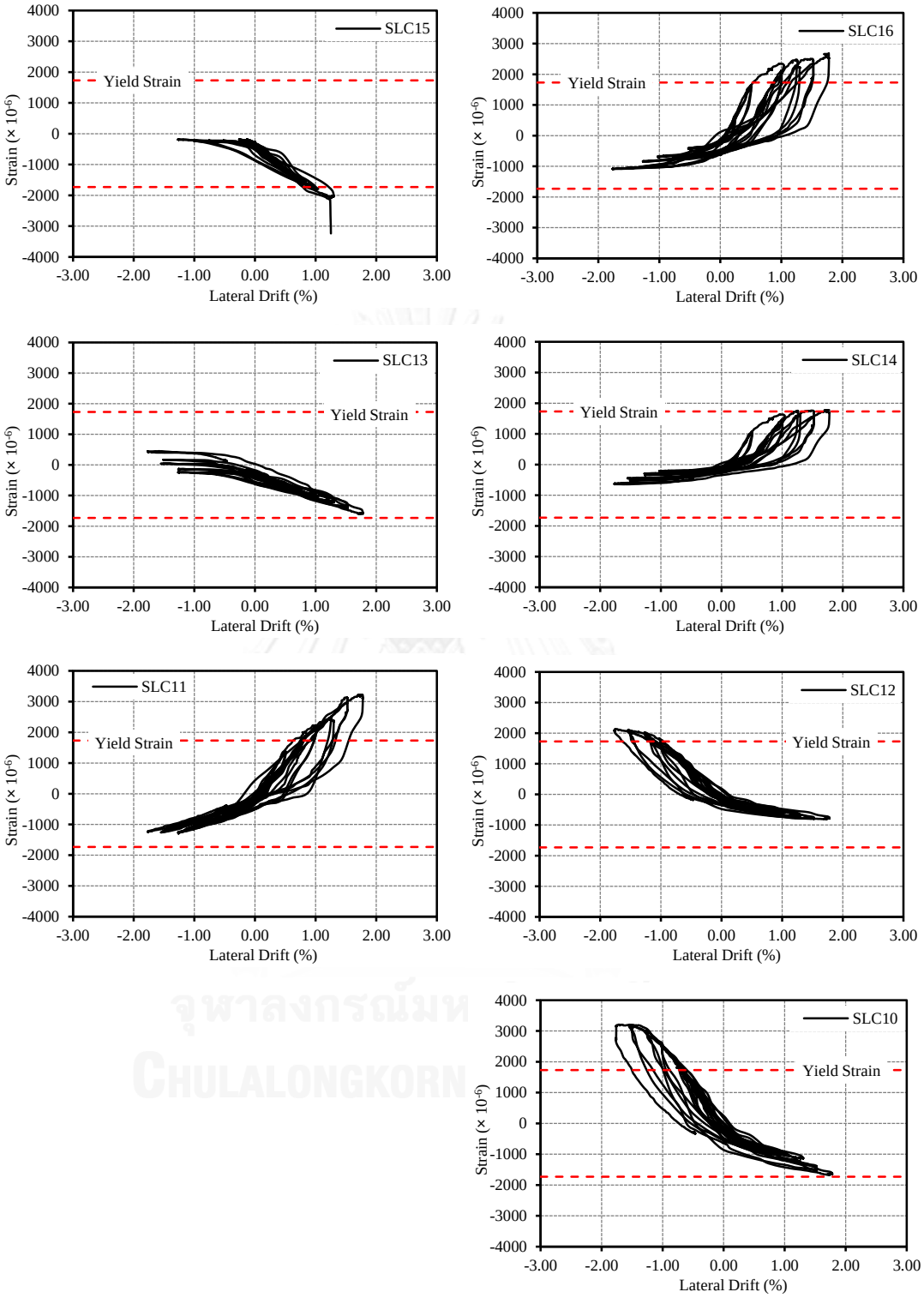

Figure 4-41. Drift ratio-strain relation of vertical rebars in the column of MIRCF03

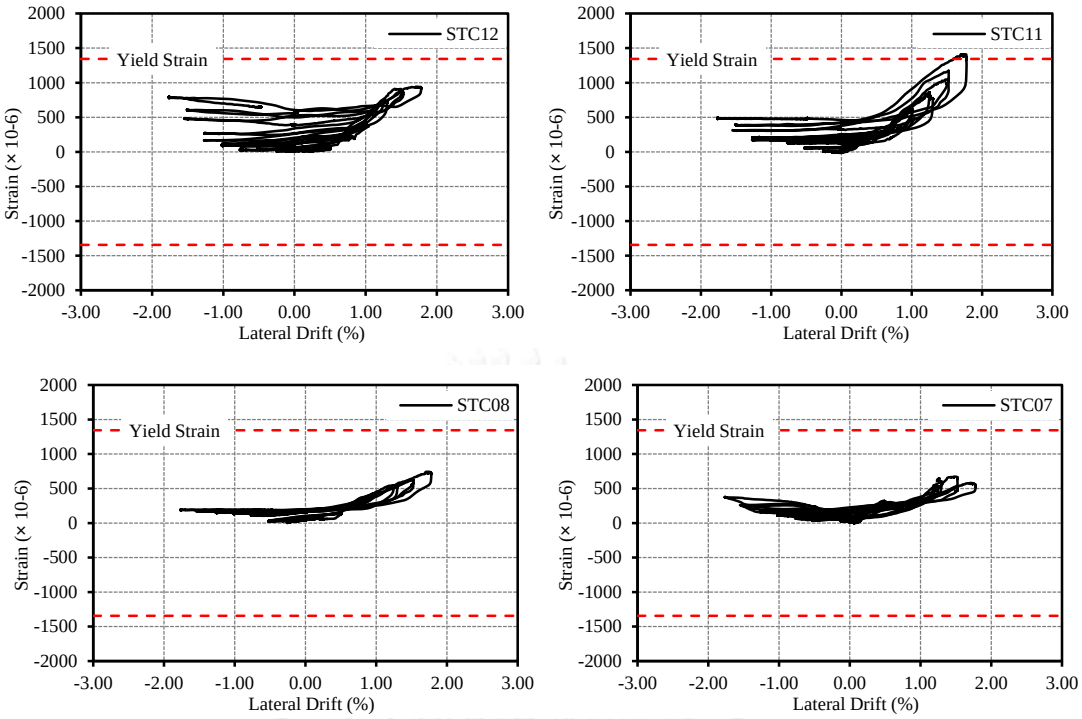

Figure 4-42. Drift ratio-strain relation of transverse rebars in the column of MIRCF03

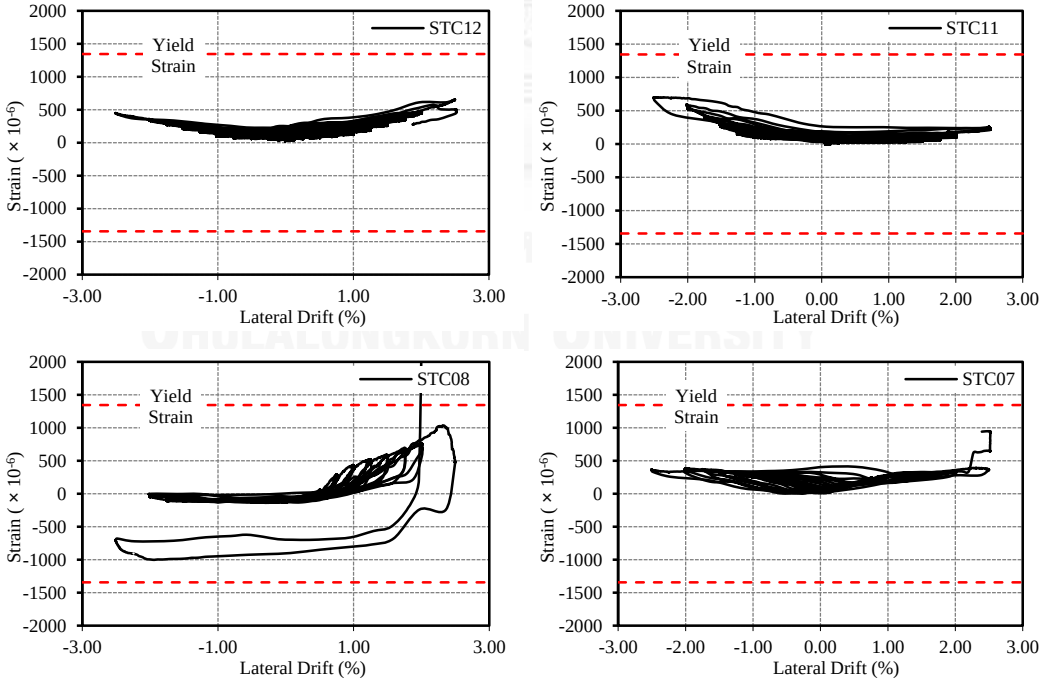

Figure 4-43. Drift ratio-strain relation of transverse re-bars in the column of MIRCF04

4.5 Shear force in reinforced concrete beam

In the proposed retrofit scheme, a large shear force evidently occurs in the beam due to the large strut force exerted by the URM panel. Since the beam was not strengthened, it is interesting to investigate if the shear demand in the beam exceeded its shear capacity. To this end, an elastic model of the assembly MIRCF02 was conducted with the surrounding reinforced concrete frame modelled using beam-column elements. An effective flexural rigidity of $0.5E_cI_g$ and an effective shear rigidity of $0.4E_cA_w$ were employed for the beam and columns in accordance with ASCE41-06 (ASCE, 2007). Here, E_c is modulus of elasticity of concrete, I_g is moment of inertia of gross concrete section and A_w is area of the web cross section. The beam-column joints were treated as rigid links. The capacity of the infill panel was estimated based on the diagonal strut analogy. An effective width of the equivalent diagonal strut was estimated according to ASCE41-06 (ASCE, 2007). Then the capacity of the diagonal strut corresponding to compression failure mode was determined. The expected capacity of the infill panel of 198 kN was applied on the beam and the lateral load corresponding to the maximum load capacity obtained from the experiment was also applied on the specimen. Therefore, the maximum shear demand in the beam was computed as 114 kN. However, the shear capacity of the beam calculated from ACI 318M-08 (ACI 2008) was 92 kN with the axial force in the beam taken into account. It should be noted that the axial compressive force in the beam close to the joint increased considerably due to the strut force from URM panel, with a consequence of increasing of shear capacity of the beam. Thus, the shear demand-to-capacity ratio of the beam was 1.24. This computed value indicated that severe damage due to shear should be expected in the beam at the peak load level. However, the experimental result shows no sign of imminent shear failure in the beam as evident in Figure 4-11. This is because of the conservative nature of shear models in codes and the building material over-strength effect.

It should be noted that in a multi-story building, the inclined force from the diagonal strut pushes upward to the floor above and downward to the floor below. In either case, the effect of the shear exerted by the infill panel to the beams should be determined, and an appropriate strengthening for the shear capacity of the beam segment between the load transfer bracket and the beam-column joint should be provided, if necessary.

4.6 Performance level of the test specimens

Under earthquake excitation, the degree of structural damage at a given earthquake hazard gives an indication of the structural performance. To determine the various performance states of a test specimen, a backbone curve and an idealized force-deformation curve of the specimen are constructed. The idealized force-deformation curves and structural performance levels are determined in accordance with ASCE41-06 standard (ASCE, 2007). For reinforced concrete frames with masonry infills, Collapse Prevention Performance Level (CP) is defined as the state when strength degradation begins, Life Safety Performance Level (LS) is taken as 3/4 of the deformation at CP, and Immediate Occupancy Performance Level (IO) is taken as 2/3 of the deformation at LS.

As shown in Figure 4-44, at the Life Safety Performance Level, the specimen MIRCF01 could sustain a lateral drift of about 0.22% (average value from positive and negative directions), whereas the drift capacity at CP was 0.29%. It should be noted that at LS level, the test specimen had not yet reached its peak lateral capacity. However, shear cracks of about 1 mm width developed in the surrounding RC frame. Moreover, impending crushing was also observed at one corner of the infill panel (see Figure 4-45).

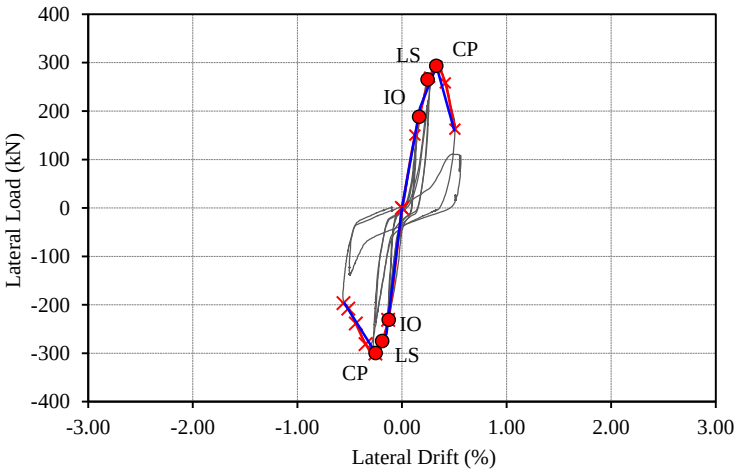

Figure 4-44. Performance level of specimen MIRCF01

Figure 4-45. Un-retrofitted specimen MIRCF01 at LS Performance Level

As can be seen from Figure 4-46, at the Life Safety Performance Level, the specimen MIRCF02 could sustain a lateral drift of about 1.0% (average value from positive and negative directions) with stable hysteretic loops, whereas the drift capacity at CP was 1.37%. Again, at LS level, the test specimen had not quite reached its peak lateral capacity, and only small cracks (less than 1 mm width) developed in the surrounding RC frame without spalling or impending signs of failure. As for the URM infill, although severe diagonal cracks formed in the URM panel as shown in Figure 4-47, there was no crushing or falling of the URM panel.

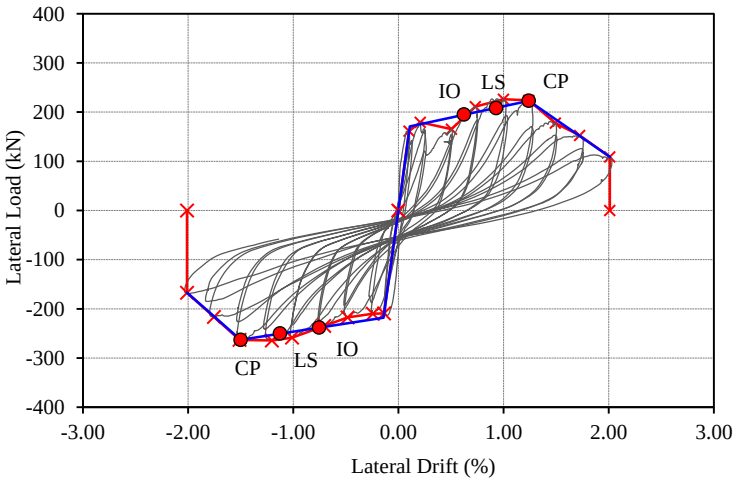

Figure 4-46. Performance level of specimen MIRCF02

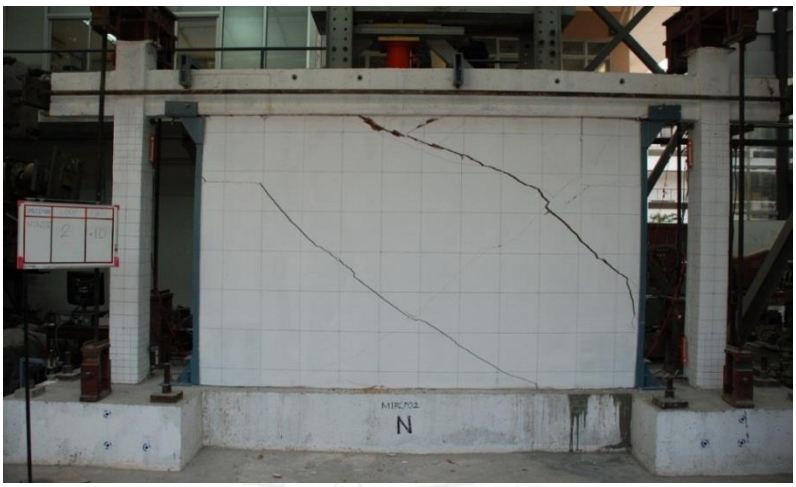

Figure 4-47. Retrofitted specimen MIRCF02 at LS Performance Level

For specimen MIRCF03, at the Life Safety Performance Level, the specimen could sustain an average lateral drift of about 1.24% close to the drift at peak capacity, with stable hysteretic loops, whereas the drift capacity at CP was 1.65% (see Figure 4-48). At LS level, flexural cracks, the largest one being about 1 mm wide, and visible shear cracks developed in the surrounding RC frame, while the URM infill suffered no diagonal cracks. However, a significant rocking occurred as shown in Figure 4-49, resulting in some crushing at one corner.

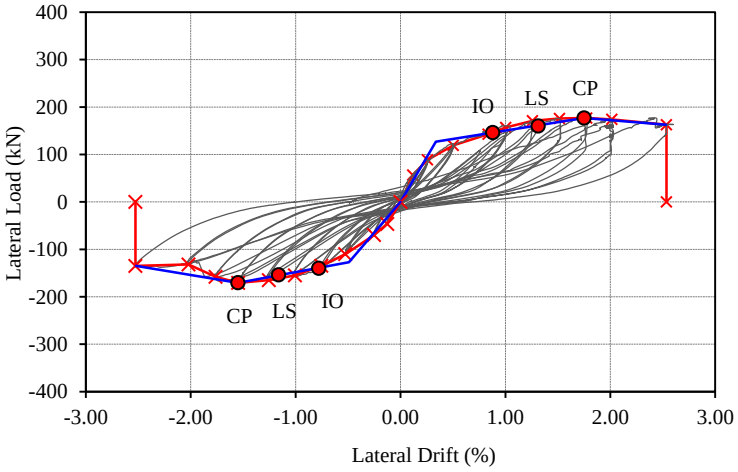

Figure 4-48. Performance level of specimen MIRCF03

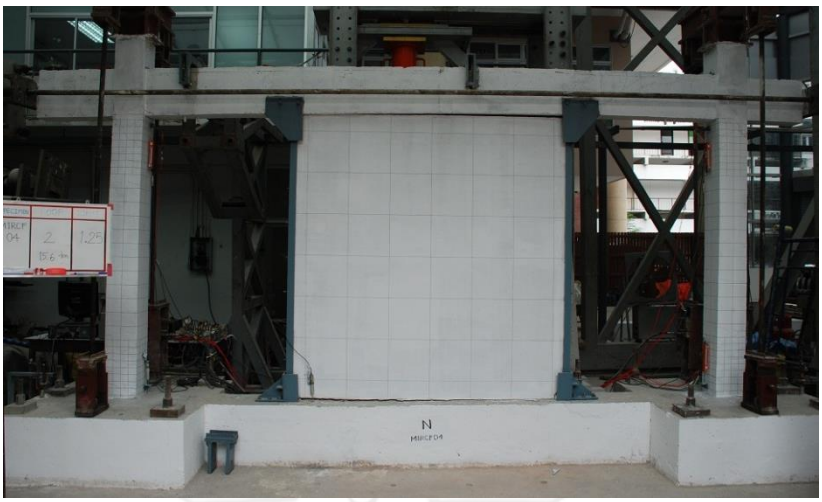

Figure 4-49. Retrofitted specimen MIRCF03 at LS Performance Level

As depicted in Figure 4-50, at the Life Safety Performance Level, the specimen MIRCF04 could sustain an average lateral drift of about 1.31% with stable hysteretic loops, whereas the drift capacity at CP was 1.75%. It should be noted that at LS level, although the test specimen reached its peak lateral capacity but only a slight degradation occurred. Furthermore, only minor flexural and flexural-shear cracks (about 0.5 mm width) developed in the surrounding RC frame without a sign of distress. Only minor diagonal cracks formed in the URM infill and minor corner crushing developed as depicted in Figure 4-51.

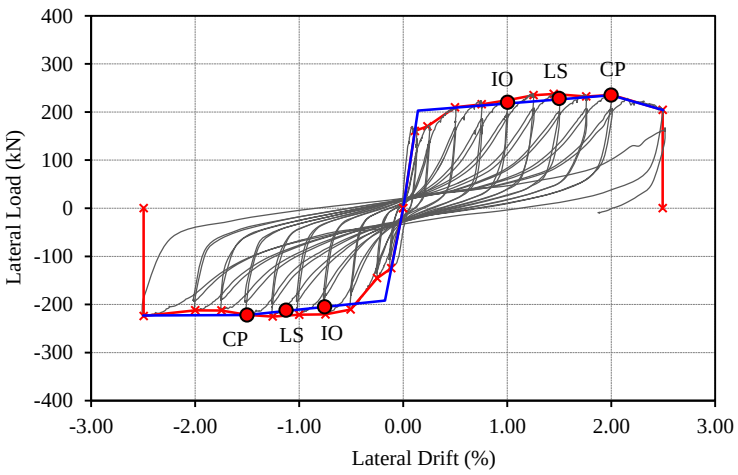

Figure 4-50. Performance level of specimen MIRCF04

Figure 4-51. Retrofitted specimen MIRCF04 at LS Performance Level

In conclusion, the retrofitted specimens (MIRCF02, MIRCF03, and MIRCF04) clearly performed significantly better than brittle URM infill wall as specified in ASCE41-06 in which the drift ratio is limited to 0.5% at LS. Also note that Eurocode 8 (CEN, 2004) specifies the story drift limit of 0.5% corresponding to the no-collapse state for structures with brittle non-structural elements attached to the frame. Therefore, the assembly satisfied the damage control level for LS specified in ASCE41-06. On the other hand, the un-retrofitted specimen (MIRCF01) did not satisfy the damage control level of those standards. Moreover, with slight steel wire mesh reinforcement provided in the masonry infill panel of specimen MIRCF04, the drift ratio at LS Performance Level increases by about 30% over specimen MIRCF02 which did not have steel reinforcement.

4.7 Comparison of different retrofit schemes

It is important to compare the performance of the proposed retrofit scheme to others researchers. As shown in Table 4-1, the retrofit scheme by using steel mesh reinforcement with plaster composite achieved the best drift capacity of about 1.2% at the 20% drop of peak capacity for the 2/3 scale specimen (Billington et al. 2009), while the best performance of the carbon fiber reinforced polymer retrofit was 1.7% (Yuksel et al. 2010). It should be noted that Yuksel used small size specimens of 1/3 scale. As indicated by Billington et al. (2009), significantly different results could be obtained from the small scale and large scale specimens. In their study, the best

drift capacity of 4.0% could be achieved in the 1/5 scale specimen. However the drift capacity drops to only 1.2% drift for the larger 2/3 scale specimen. This clearly indicates that size effect should be considered in an experimental investigation. In the present study, near full size specimens (3/4 scale) were tested. Without steel wire mesh reinforcement, a drift capacity of 1.5% at 20% drop in peak capacity was attained by specimen MIRCF02, and 1.75% by MIRCF03. With steel wire mesh reinforcement in the URM panel, a drift capacity as high as 2.0% could be expected.

Table 4-1. Comparison of different retrofit schemes

No	Samples by	Masonry panel L_w/H_w	Scale	Drift at 20% drop in capacity	Retrofit Scheme
1	Acun and Sucuoglu (2006)	1.72	1/3	0.75% - 1.1%	external mesh reinforcement with cover mortar
2	Erdem et al. (2006)	0.64 and 1.05	1/3	0.5%	diagonal CFRP strips
3	Altin et al. (2008)	1.73	1/3	0.6% - 1.0%	diagonal CFRP strips
4	Billington et al. (2009)	1.79	1/5	1.0% - 4.0%	sprayable ductile cement-based composites and welded wire fabric
			2/3	1.2%	
5	Yuksel et al. (2010)	1.17	1/3	1.0% - 1.7%.	various configurations of CFRP
6	Erol et al. (2012)	1.42	1/2	0.8%-1.4%	diagonal CFRP strips
7	This research MIRCF01	2.00	3/4	0.25%	un-reinforced panel
8	This research MIRCF02	1.60	3/4	1.50 %	URM panel separated from columns; load transfer brackets; corner strengthened

Table 4-1. Comparison of different retrofit scheme (continued)

No	Samples by	Masonry panel L_w/H_w	Scale	Drift at 20% drop in capacity	Retrofit Scheme
9	This research MIRCF03	1.00	3/4	1.75%	URM panel separated from columns; load transfer brackets; corner strengthened
10	This research MIRCF04	1.60	3/4	2.00%	Steel wire mesh reinforcement; panel separated from columns; load transfer brackets; corner strengthened

CHAPTER V
ANALYTICAL MODELING

5.1 Introduction

As described earlier the masonry infill panels provide significant lateral load resistance and affect the response of the structures. Under the seismic excitation, the separations between infill panels and surrounding RC frames rapidly occur and the openings length depends on the lateral deformation of the structure. Therefore, the complicated interaction between masonry infill panels and surrounding RC frames can cause a difficulty in structural response prediction. Moreover, several failure modes could occur in both masonry infill panels and surrounding RC frames which seriously affect the structural response. In the literature, a number of analytical approaches for RC frames with masonry infill panels have been proposed. An effective and simple approach called equivalent diagonal struts model is adopted in this study. Non-linear analytical model of non-ductile reinforced concrete frame with masonry infill panel is presented. The detail of the analytical model is described in the following section.

5.2 Nonlinear properties of the surrounding RC frame

A discrete frame element with nonlinearity lumped at each end was used to model beam and column components of the surrounding RC frame. To simulate various failure modes of the RC surrounding frame (flexural, flexural-shear, and shear failure modes) both flexural and shear plastic hinges were employed. An effective stiffness and plastic hinge moment-rotation relation proposed by Haselton and Deierlein (2007) were used. It should be noted that concrete crushing, steel reinforcement buckling, and bond failure of rebar are included in the Haselton-model. For a shear plastic hinge, the load-shear deformation relation proposed by Patwardhan (2005) was employed. However, to simplify the analysis, those plastic hinges will be modified and/or calibrated with relevant experimental results obtained in this study.

The flexural plastic hinge load-deformation curve is tri-linear (Figure 5-1). The response is linearly elastic up to the yield moment (M_y). In this range, the lateral stiffness of the element is defined as the effective stiffness. Afterwards, the load gradually increases until the maximum moment (M_c) is reached at the corresponding

chord rotation (θ_{cap}). At θ_{cap}, the strength degrades with softening stiffness (K_c) until the moment capacity drops to zero. The necessary parameters to construct the curve include the following

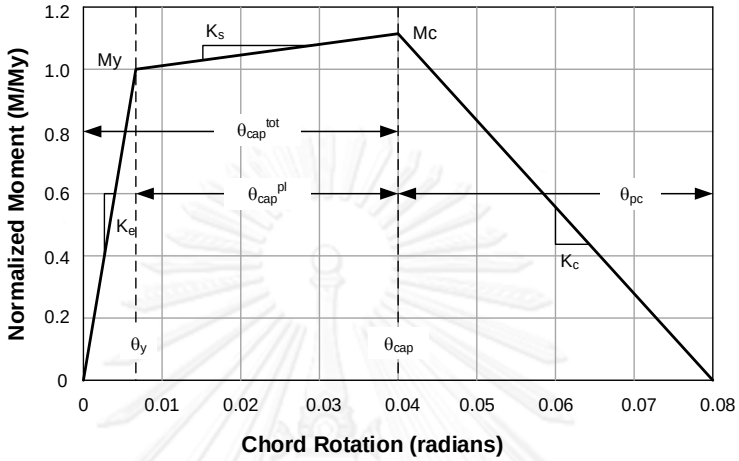

Figure 5-1. Moment-chord rotation of the member proposed by Haselton and Deierlein (2007)

The ratio of the effective stiffness at 40% of the yield capacity (EI_{stf40}) to gross elastic stiffness (EI_g) of an elastic frame element can be determined as follows (Haselton and Deierlein, 2007):

$$\frac{EI_{stf\,40}}{EI_g} = -0.02 + 0.98\left[\frac{P}{A_g f_c'}\right] + 0.09\left[\frac{L_s}{H}\right], \text{ where } 0.35 \le \frac{EI_{stf\,40}}{EI_g} \le 0.8 \qquad (5\text{-}1)$$

where P is axial load (kN), A_g is the gross section area of the member, f_c' is the compressive strength of concrete (MPa), L_s is shear span length (mm), and H is member sectional depth measured in the direction of loading (mm).

Figure 5-1 shows the moment-chord rotation relation of a member as proposed by Haselton and Deierlein (2007). The plastic rotation capacity (θ_{cap}^{pl}), total rotation capacity (θ_{cap}^{tot}), post-capping rotation capacity (θ_{pc}), and ultimate moment and yielding moment capacities ratio (M_c/M_y) can be determined as follows:

$$\theta_{cap}^{\ pl} = 0.12\left(\frac{\max\left(0.01, \frac{\rho_2 f_y}{f_c^{'}}\right)}{\max\left(0.01, \frac{\rho_1 f_y}{f_c^{'}}\right)}\right)^{0.225} (1+0.55a_{sl})(0.16)^{v}....$$

$$(0.02+40\rho_{sh})^{0.43}(0.54)^{0.01c_{units}f_c^{'}}(0.66)^{0.1s_n}(2.27)^{10.0\rho} \quad (5\text{-}2)$$

$$\theta_{cap}^{\ tot} = 0.12\left(\frac{\max\left(0.01, \frac{\rho_2 f_y}{f_c^{'}}\right)}{\max\left(0.01, \frac{\rho_2 f_y}{f_c^{'}}\right)}\right)^{0.175} (1+0.4a_{sl})(0.20)^{v}....$$

$$(0.02+40\rho_{sh})^{0.52}(0.56)^{0.01c_{units}f_c^{'}}(2.27)^{10.0\rho} \quad (5\text{-}3)$$

$$\theta_{pc} = (0.76)(0.031)^{v}(0.02+40\rho_{sh})^{1.02} \le 0.10 \quad (5\text{-}4)$$

$$\frac{M_c}{M_y} = (1.25)(0.89)^{v}(0.91)^{1.01c_{units}f_c^{'}} \quad (5\text{-}5)$$

where ρ is longitudinal reinforcement ratio (A_s/bd), ρ_1 is tension longitudinal reinforcement ratio (A_{s1}/bd), ρ_2 is compression longitudinal reinforcement ratio (A_{s2}/bd), ρ_{sh} is transverse reinforcement ratio (A_{sh}/sb); A_s, A_{s1}, A_{s2} are total , tension and compression longitudinal reinforcements area, respectively, b is the member cross-section width, d is the member cross-section effective depth, f_c' is concrete compressive strength (MPa), f_y is reinforcement yield strength (MPa), a_{sl} is bond slip indicator variable of reinforcement (a_{sl} = 1 when rebar slip is considered and a_{sl} = 0 when rebar slip is not considered), v is axial load ratio ($P/A_g f_c'$), c_{units} is a unit conversion variable that is 1.0 when the unit is MPa, s is transverse reinforcement spacing (mm), s_n is rebar buckling coefficient which is equal to $(s/d_b)\sqrt{(f_y/100)}$, and d_b is longitudinal reinforcement diameter (mm), f_y is yield strength of longitudinal reinforcement. Other parameters have been defined earlier.

As for the yielding moment, M_y, can be determined by several approaches (e.g., Whitney stress block approach). However, the Equations proposed by Panagiotakos and Fardis (2001) were suggested by Haselton and Deierlein (2007). The yielding moment of the column can be estimated by the following equations.

$$\frac{M_y}{bd^3} = \varphi_y \left\{ \begin{array}{l} Ec\frac{\xi_y^2}{2}\left(0.5(1+\delta_1) - \frac{\xi_y}{3}\right) + \ldots \\ \frac{E_s}{2}\left((1-\xi_y)\rho_1 + (\xi_y - \delta_1)\rho_2 + \frac{\rho_v}{6}(1-\delta_1)\right)(1-\delta_1) \end{array} \right\} \quad (5\text{-}6)$$

where ρ_v is web longitudinal reinforcement ratio, φ_y is yielding curvature, and ξ_y is ratio of neutral axis depth at yielding and effective depth that can be determined as follows:

$$\xi_y = (n^2A^2 + 2nB)^{1/2} - nA \quad (5\text{-}7)$$

$$n = \frac{E_s}{E_c} \quad (5\text{-}8)$$

where E_c and E_s are the moduli of elasticity of concrete and steel reinforcement, respectively, A and B are the parameters that depend upon sectional yielding condition which will be described in the following paragraph.

It should be noted that the yielding curvature (φ_y) and the ratio of neutral axis depth at yielding and effective depth (ξ_y) depends on yielding condition of the section. The section yielding of the RC members could be controlled by yielding of the tension reinforcement or nonlinearity of concrete in compression zone, depending on section properties and loading condition. The yielding curvature (φ_y) and the ratio of neutral axis depth at yielding and effective depth (ξ_y) determination of both cases are described below.

If the section yielding is controlled by tension reinforcement yielding, those parameters can be determined as follows:

$$\varphi_y = \frac{f_y}{E_s(1-\xi_y)d} \quad (5\text{-}9)$$

$$A = \rho_1 + \rho_2 + \rho_v + \frac{P}{bdf_y} \quad (5\text{-}10)$$

$$B = \rho_1 + \rho_2\delta_1 + 0.5\rho_v(1+\delta_1) + \frac{P}{bdf_y} \quad (5\text{-}11)$$

If section yielding is controlled by the nonlinearity of concrete in the compression zone, yielding curvature and the ratio of neutral axis depth at yielding and effective depth can be determined as follows:

$$\varphi_y = \frac{\varepsilon_c}{\xi_y d} \approx \frac{1.8 f_c^{'}}{E_s \xi_y d} \tag{5-12}$$

$$A = \rho_1 + \rho_2 + \rho_v - \frac{P}{\varepsilon_c E_s bd} \approx \rho_1 + \rho_2 + \rho_v - \frac{P}{1.8nbdf_c^{'}} \tag{5-13}$$

$$B = \rho_1 + \rho_2 \delta_1 + 0.5\rho_v(1+\delta_1) \tag{5-14}$$

$$\delta_1 = \frac{d_1}{d} \tag{5-15}$$

where b is the width of compression zone; d is sectional effective depth; d_1 is the distance from extreme compression fiber to centroid of compression reinforcement; P is axial force (positive for compression and negative for tension); ε_c is the elastic strain limit of concrete; and other parameters are as defined earlier.

In order to evaluate shear strength capacity of an RC column, a shear plastic hinge is considered in the model. A modeling proposed by Patwardhan (2005) is used. The load-displacement relation of the shear plastic hinge is depicted in Figure 5-2. The shear plastic hinge load-deformation curve is quad-linear. The response is linearly elastic up to the cracking strength (V_{cr}) at the cracking displacement ($\Delta_{v,cr}$). Beyond this level, the shear strength increases until the maximum capacity (V_n) is reached at the corresponding displacement ($\Delta_{v,n}$). The shear strength is maintained constant until the onset of shear strength degradation. After this level, the shear strength rapidly drops to zero when axial load failure occurs. The key parameters of the model are described as follows:

The cracking shear displacement ($\Delta_{v,cr}$) and shear strength (V_{cr}) are

$$\Delta_{v,cr} = \frac{P}{8898} + 0.155 \tag{5-16}$$

$$V_{cr} = \Delta_{v.cr} \frac{GA_g}{1000L} \tag{5-17}$$

where P is the axial force (kN), A_g is gross cross-sectional area of the column (mm^2), G is shear modulus of concrete (MPa), and L is the length of the column (mm). The units for $\Delta_{v,cr}$ and V_{cr} are mm and kN, respectively.

The shear displacement ($\Delta_{v,n}$) at the maximum shear strength (V_n) of the column can be determined as follows:

$$\Delta_{v,n} = \gamma_n L \tag{5-18}$$

Here γ_n is the average shear strain at maximum shear strength, which depends on the failure mode of the columns. For flexural-shear failure mode it is given by

$$\gamma_n = \frac{1}{227370} \frac{f_y \sqrt{\rho}}{\left(\frac{a}{d}\right)\sqrt{\frac{P}{A_g f_c'}}} - 0.0006 \tag{5-19}$$

For shear failure mode, the average shear strain at maximum shear strength is

$$\gamma_n = \frac{1}{172250} \frac{\left(\frac{a}{d}\right) f_{yt} \rho_{sh}}{\sqrt{\frac{P}{A_g f_c'}}} - 0.0011 \tag{5-20}$$

where a is the shear span-length of the column; f_y and f_{yt} are the yield strength of longitudinal and transverse reinforcements, respectively (MPa); ρ and ρ_{sh} are longitudinal and transverse reinforcement ratios, respectively (expressed in percentage), and other parameters are as described earlier.

The maximum shear strength (V_n) can be determined by a number of approaches. The shear strength prediction proposed by Sezen and Moehle (2004) was adopted by

Patwardhan (2005). However, the column aspect ratio (*a/d*) considered in the Sezen and Moehle model is limited to the range of 2 to 4. Therefore, the shear strength prediction suggested by ACI 318-08 (ACI, 2008) was used in this study instead. Hence, the maximum shear capacity of the column, V_n, becomes

$$V_n = 0.17\left(1+\frac{P}{14A_g}\right)\lambda\sqrt{f_c'}bd + A_{sh}f_{yt}\frac{d}{s} \quad (5\text{-}21)$$

Here *s* is the transverse reinforcement spacing, λ is the concrete unit weight correction factor (λ = 1 for normal weight), and other parameters are as defined previously. It should be noted that the unit of V_n is MN; the units of stresses is MPa; the unit of all dimensions is m.

Shear displacement ($\Delta_{v,u}$) of the column at the onset of shear strength degradation is given as

$$\Delta_{v,u} = \left(4-12\frac{(V_n/bd)}{f_c'}\right)\gamma_n L \quad (5\text{-}22)$$

Finally, the equation proposed by Elwood and Moehle (2005) was used to calculate the shear displacement at axial load failure ($\Delta_{v,f}$).

$$\Delta_{v,f} = \frac{4}{100}\frac{1+\tan^2\varphi}{\tan\varphi + P\left(\frac{s}{A_{sh}f_{yt}d_c\tan\varphi}\right)}L \quad (5\text{-}23)$$

where φ is the expected shear crack angle (φ = 65° was recommended by Elwood and Moehle 2005); d_c is the core-concrete depth which measures the center-to-center dimension of transverse reinforcement; and other parameters are as described earlier.

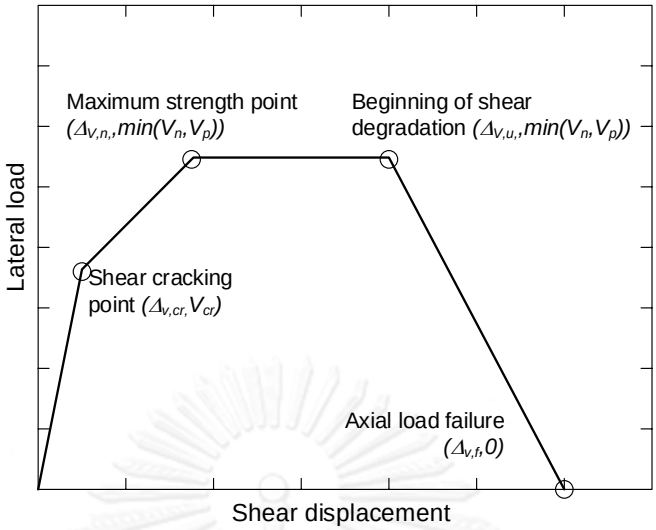

Figure 5-2. Load- displacement relation of the shear plastic hinge (Patwardhan 2005)

5.3 Analytical model of masonry infill panel

5.3.1 Load-deformation relation of masonry infill wall

In order to assess the behavior of masonry infill panel, a simplified lateral load-deformation relation of the panel specified by ASCE41-06 (ASCE, 2007) is modified and utilized in the analytical model. Although the load-deformation relation cannot provide a detailed local stress result, it is an efficient model to capture the overall behavior of the masonry infill panel. Figure 5-3 shows the skeleton of masonry infill panel load-deformation relation. The load-deformation curve consists of four linear segments. The response is elastic up to the yield strength. After this point, the load gradually increases until the maximum strength (V_{max}) is reached at corresponding lateral displacement (Δ_{max}). At the Δ_{max}, the strength degrades with softening stiffness (K_{sof}) until the residual strength (V_{res}) is reached. After this point, the strength is maintained constant. The necessary parameters to construct the curve include the following:

1) Initial stiffness (K_{ini})

   The initial stiffness of masonry infill panel represents the elastic stiffness of the panel and can be determined by a method described in Section 5.3.2.

2) Yield strength (V_y)

The yield capacity of masonry infill panel is normally initiated by the cracking of the masonry infill panel. According to extensive literature review by Uva et al. (2012), the yield capacity of masonry infill panel ranged from 0.6 to 0.8 times the maximum capacity. In this research, the yield strength of masonry infill panel is assumed as 0.8 times the maximum capacity.

3) Maximum strength (V_{max})

The maximum capacity of masonry infill panel can be determined by a method described in Section 5.3.3.

4) Lateral drift at maximum strength (Δ_{max})

In general, the lateral deformation at maximum capacity of masonry infill panel can be estimated based on the axial deformation of equivalent diagonal strut corresponding to the masonry prism compressive strain at the maximum strength (Mostafaei and Kabeyasawa 2004). However, in this research the lateral deformation at maximum capacity of masonry infill panel is estimated following the recommendation of ASCE41-06 standard (ASCE, 2007).

5) Residual strength (V_{res}) and lateral drift at residual strength is reached (Δ_{res})

As mentioned earlier, the strength and deformation of masonry infill panel depends on its failure mode. Therefore, the actual residual strength and deformation at residual strength cannot be estimated by a simple methodology. A number of researchers assume the residual capacity of masonry infill panel as a fraction of the maximum capacity, ranging from 0 to 0.35 times the maximum capacity (Uva et al. 2012). The lateral drift at residual strength can be calculated by assuming the softening stiffness (K_{sof}) of masonry infill panel as a fraction of the initial stiffness. Uva et al. (2012) proposed, based on the suggestion of Panagiotakos and Fardis (1996), the softening stiffness of masonry infill panel ranging from 0.005 to 0.1 times the initial stiffness. In this research, the residual capacity of masonry infill panel is assumed as 0.2 times the maximum capacity. For the softening stiffness of masonry infill panel, experimental results will be used to calibrate the values. The process is described in the next section.

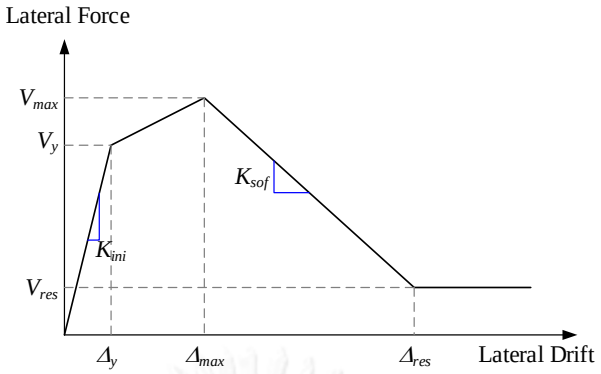

Figure 5-3. Lateral load-deformation relation of masonry infill panel (ASCE, 2007)

5.3.2 Initial lateral stiffness of masonry infill wall

Based on the equivalent strut model, the initial lateral stiffness of a masonry infill panel is represented by the axial stiffness of the equivalent diagonal strut. However, it has been found that the initial lateral stiffness of the masonry infill panel estimated by this approach is considerably lower than the stiffness given by experimental results. Mehrabi et al. (1996) reported that the initial lateral stiffness of the masonry infill panel estimated by the equivalent strut approach was about one-haft of that given by experimental results. An alternative method based on the conventional principle of mechanics introduced by Fiorato et al. (1970) for predicting the initial lateral stiffness of masonry infill panel can be used to improve the stiffness calculation. Therefore, this method is adopted in this research. The initial lateral stiffness of masonry infill panel can be expressed as

$$K_{ini} = \frac{1}{\frac{1}{K_{fl}} + \frac{1}{K_{sh}}} \tag{5-24}$$

where K_{fl} and K_{shl} are flexural and shear stiffness of a cantilever masonry panel, respectively, given by

$$K_{fl} = \frac{3E_m I_w}{h_w^3} \tag{5-25}$$

$$K_{sh} = \frac{A_w G_w}{h_w} \tag{5-26}$$

where E_m, I_w, h_w, A_w, and G_w are modulus of elasticity, moment of inertia, height, cross-sectional area, and shear modulus of the masonry panel. Shear modulus of masonry infill panel can be assumed as $0.4E_w$ (Stavridis and Shing, 2012).

5.3.3 Lateral capacity of masonry infill panel

The lateral resistance of a masonry infill panel has been elaborated in section 2.3.2. According to Asteris et al. (2011), only sliding along the bed-joint and corner crushing of the masonry infill panels are predominant failure modes. Therefore, the lateral capacity of the masonry infill panel will be taken as the smaller of the capacities associated with these two failure modes. It is important to note that the approach developed by Mostafaei and Kabeyasawa (2004) was used to estimate the lateral capacity of sliding along the bed-joint failure mode (V_{slide}). As for corner crushing failure mode, Al-Chaar (2002) stated that the effective width of a diagonal strut associated with the approach proposed by Mainstone (1971) given by Equation (2-1) is a lower bound of the expected effective width (Figure 5-4). The lateral capacity and lateral stiffness of the infill panel obtained using this approach may be significantly lower than those given by the experimental results. Alternatively, an upper bound estimation for the effective width of an equivalent diagonal strut was proposed by Smith and Carter (1969). The effective width of the equivalent diagonal strut can be determined using Equations 5-27 to 5-29. It should be noted that the relative stiffness of the surrounding frame and the masonry infill panel as well as the infill panel aspect ratio are considered in those Equations.

$$w = 0.0835Cd\left(1+\frac{2.574}{\lambda H}\right) \quad \text{for } \frac{L_w}{H_w} \geq 1.5 \tag{5-27}$$

where $$C = -0.3905\left(\frac{L_w}{H_w}\right)+1.7829 \tag{5-28}$$

$$w = 0.1106d\left(1+\frac{6.027}{\lambda H}\right) \quad \text{for } \frac{L_w}{H_w} = 1.0 \tag{5-29}$$

where d is infill panel diagonal length; H is column height (measures to centerlines of the beam); H_w is infill panel height; L_w is infill panel length; and λ is relative stiffness of the surrounding frame and the masonry infill panel.

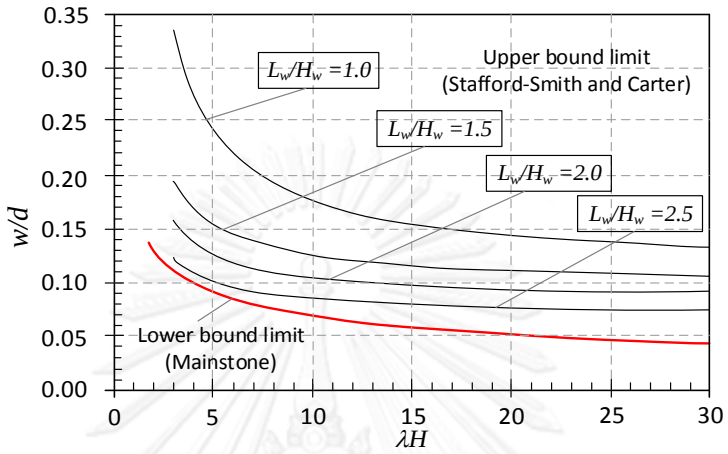

Figure 5-4. Upper- and lower-limit of a diagonal strut effective width (Al-Chaar 2002)

5.4 Calibration of the analytical model

To develop the analytical model, all components comprised in the model are calibrated with relevant experimental results in this section. The calibration detail for each component is summarized below.

5.4.1 Calibration of the column component

Since the performance of an RC member is affected significantly by its failure mode, the primary modes of failure (e.g. flexural, flexural-shear, and shear failure modes) should be incorporated into the model. A number of experimental results of the RC columns are available at the Pacific Earthquake Engineering Research Center website (PEER). In this study, the experimental results of the RC columns with rectangular cross-sections by Mo and Wang (2000), Sezen and Moehle (2004) and Lynn (1999) are considered. Those specimens were tested under lateral cyclic load and constant vertical load. The test specimens detailing, failure mode and material properties are listed in Table 5-1.

In this section, the analytical model of the RC columns were constructed and analyzed. Figure 5-5 shows the proposed analytical model of the RC column. The RC

column was modeled using elastic frame element with an effective stiffness. The effective stiffness at 40% of the yield capacity (EI_{stf40}) can be determined according to Equation 5-1. The nonlinear behavior of the column was captured by flexural and shear plastic hinges as described in Section 5.2. Axial load effect on moment capacity of the RC column was included through the axial load-moment (PM) interaction plastic hinge. The properties of those plastic hinges were calculated as described in Section 5.2, and the key modeling parameters are summarized in Table 5-2. Nonlinear push-over analyses were performed using SAP2000 structural analysis software (CSI 2011). It is important to note that the plastic hinges in SAP2000 are activated only if the element internal forces at the plastic hinges reach the yield strength. To simplify the analysis, the cracking point on load-displacement curve of the shear plastic hinge was excluded in this study. Therefore, the moment-chord rotation relation of flexural plastic hinge and the load-displacement relation of the shear plastic hinge can be simplified as depicted in Figures 5-6 and 5-7.

The comparison of the experimentally obtained load-deformation curves and the analytical results are shown in Figure 5-8. In all cases, the analytically obtained initial stiffness matches well with the experimental result up to 50% of yielding load. After this state the lateral stiffness obtained from analysis is considerably higher than that obtained from the experiment, especially in the case of flexural-shear failure specimen (see Figure 5-8 (c)). As a result, the analytically obtained yield displacement is lower than the actual yield displacement. However, the analytical model can capture the overall response of the RC columns reasonably well.

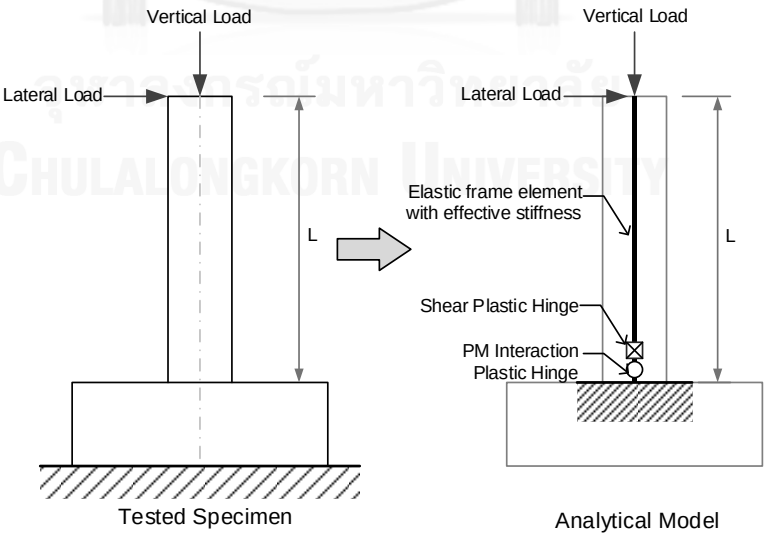

Figure 5-5. Analytical modeling of the RC column

Table 5-1. Tested specimens by Mo and Wang (2000), Sezen and Moehle (2004) and Lynn (1999)

Properties	Specimens		
	Lynn (1999)	Mo and Wang (2000)	Sezen and Moehle (2002)
Specimen	3SLH18	C1-2	No. 1
Section (mm)	457 × 457	400 × 400	457 × 457
Length (mm)	2946	1400	2946
Shear span (mm)	1473	1400	1473
Test configuration	Double curvature	Single curvature	Double curvature
Axial load ratio, ν	0.089	0.158	0.151
Longitudinal reinforcement ratio, ρ	0.0347	0.0243	0.0300
Transverse reinforcement ratio, ρ_{sh}	0.0007	0.0062	0.0017
Concrete compressive strength (MPa)	26.9	26.7	21.1
Longitudinal reinforcement yield strength (MPa)	331	497	434
Transverse reinforcement yield strength (MPa)	400	460	476
Failure mode	Shear	Flexural	Flexural-shear

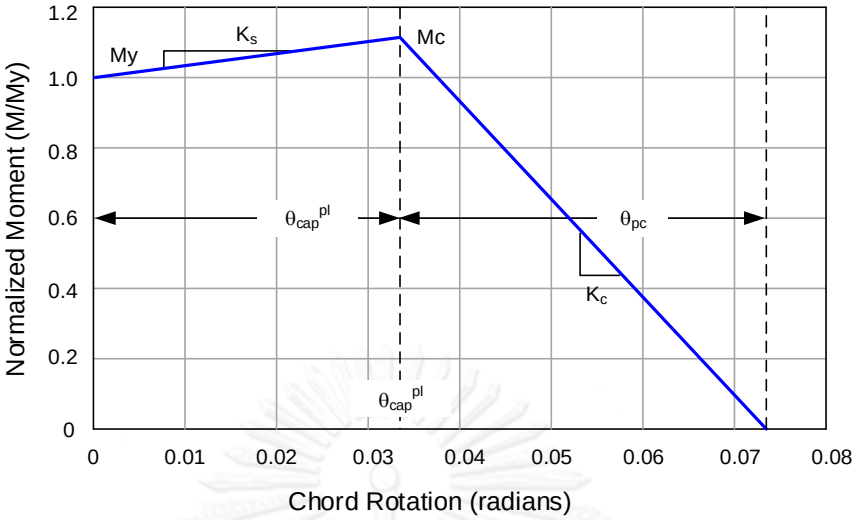

Figure 5-6. Moment- rotation relation of the flexural plastic hinge

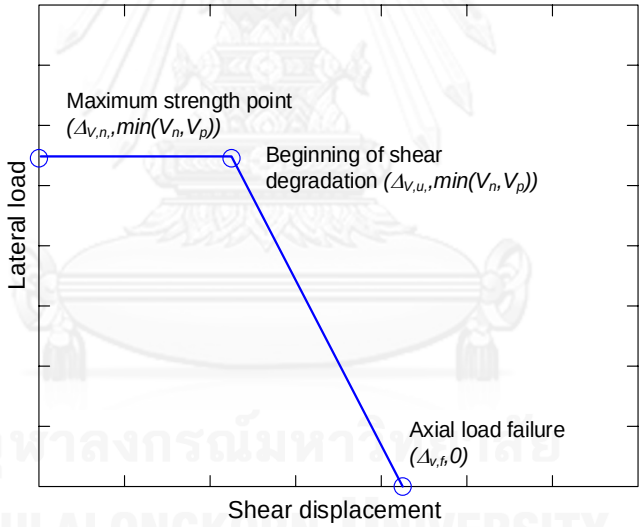

Figure 5-7. Load-displacement relation of the shear plastic hinge

Table 5-2. Modeling parameters of the tested specimens by; Mo and Wang (2000), Sezen and Moehle (2004) and Lynn (1999)

Properties		Specimens		
		Lynn (1999)	Mo and Wang (2000)	Sezen and Moehle (2002)
Element effective stiffness				
EI_{stf40}/EI_g		0.358	0.450	0.418
Flexural plastic hinge				
My	(kN-m)	405.5	318.0	430.0
Mc	(kN-m)	489.0	380.5	517.8
θ_y	(rad)	0.0100	0.0052	0.0123
θ_{cap}^{pl}	(rad)	0.0104	0.0415	0.0144
θ_{cap}^{tot}	(rad)	0.0204	0.0467	0.0267
θ_{pc}	(rad)	0.0247	0.1151	0.0382
Shear plastic hinge				
$\Delta_{v,n}$	(mm)	2.5	2.2	4.7
V_n	(kN)	238.6	560.4	307.8
$\Delta_{v,u}$	(mm)	8.5	4.8	13.9
$\Delta_{v,f}$	(mm)	92.8	103.7	141.2

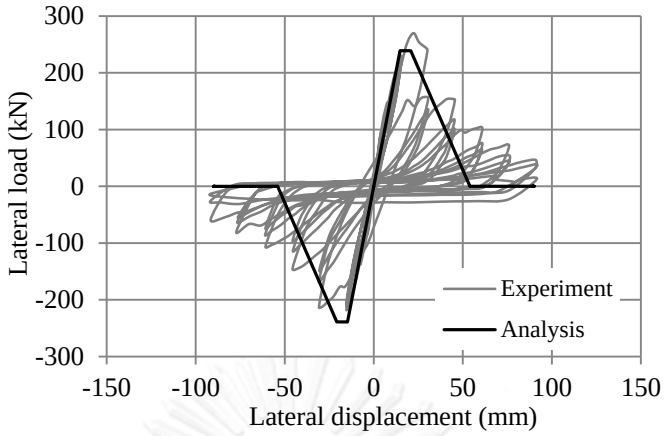

(a)

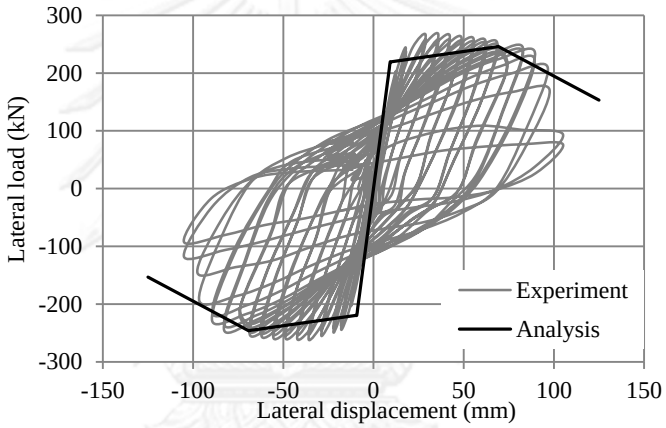

(b)

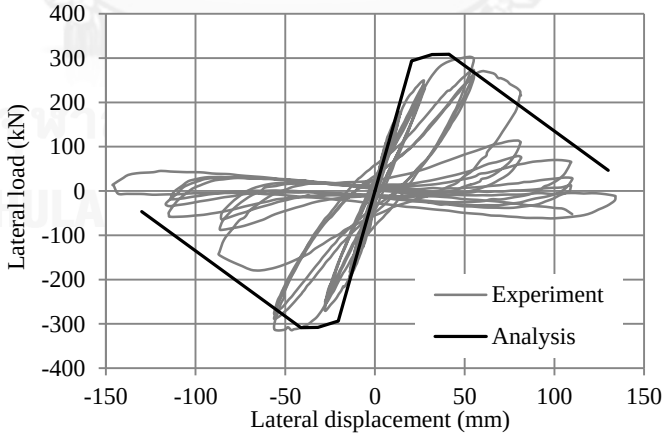

(c)

Figure 5-8. Comparison of experimental results and analytical results of the RC columns tested by: (a) Lynn (1999); (b) Mo and Wang (2000); and (c) Sezen and Moehle (2004)

5.4.2 Calibration of the masonry infill RC frame

In order to assess the structural behavior of the masonry infill RC frame, the analytical models were developed and calibrated with the relevant experimental results. The experimental results of 1/2-scale specimens of single-bay, single-story masonry infill RC frames reported by Mehrabi et al. (1996) were used. However, only three tested specimens out of twelve were selected to be the baseline for the calibration in this study. Those tested specimens consisted of the same non-ductile RC frame with two types of masonry infill panel and vertical load distribution. Lateral monotonic load and constant vertical load were employed for all specimens. The tested specimens details and material properties are given in Table 5-3.

Guided by an analytical model of the RC columns in the previous section, a non-linear analytical model of the RC frame was constructed as depicted in Figure 5-9. The columns and beam were modelled using elastic frame elements with an effective stiffness. Nonlinear behavior of those elements was represented by the lumped plastic hinges as described earlier. The axial load-moment interaction flexural plastic hinge was introduced at each end of the columns. To evaluate the shear capacity of the columns, shear plastic hinge was introduced at one end of the column members. In the case of beam component, only the flexural plastic hinge was introduced at each end of the member (axial load effect was excluded). The beam-column joints were treated as rigid. For the masonry infill panel, it was simplified using three diagonal struts as depicted in Figure 5-10. The total effective width of the diagonal struts (w) was calculated following the method proposed by Stafford-Smith and Carter (1969). The total capacity of the diagonal struts (V_{max}) was assumed to be the minimum value of the two failure modes of URM panel as described in section 5.3.1. The strut width and load resistant capacity of $0.6w$ and $0.6V_{max}$ were employed for the interior strut and $0.2w$ and $0.2V_{max}$ were employed for exterior struts. The exterior struts connect to the RC columns at a distant of $Z/2$ from the end of the RC columns (see Figure 5-10). Here, Z is the contact length between the RC columns and URM panel which can be calculated as $Z = \pi/2\lambda$ according to Stafford-Smith and Carter (1969). The load-deformation relation of those diagonal struts can be determined as described in Section 5.3.3. It should be noted that the load-deformation relation in Section 5.3.3 was defined for horizontal direction. Therefore all parameters must be transformed into those for the direction of the diagonal strut before using them in the computer software. The model parameters for the three tested specimens are shown in Tables 5-4 and 5-5.

Nonlinear push-over analyses were performed using SAP2000 structural analysis software (CSI2011).

Table 5-3. Tested specimens properties by Mehrabi et al. (1996)

Component	Properties	Specimens		
		No. 1 Bare frame	No. 3 Infill frame	No. 8 Infill frame
RC columns	Cross-section (mm)	178 × 178	178 × 178	178 × 178
	Longitudinal reinforcement ratio, ρ	0.0390	0.0390	0.0390
	Transverse reinforcement ratio, ρ_{sh}	0.0054	0.0054	0.0054
	Concrete compressive strength (MPa)	30.8	30.8	26.8
	Longitudinal reinforcement yield strength (MPa)	420	420	420
	Transverse reinforcement yield strength (MPa)	367	367	367
RC beam	Cross-section (mm)	229 × 152	229 × 152	229 × 152
	Longitudinal reinforcement ratio, ρ	0.0263	0.0263	0.0263
	Transverse reinforcement ratio, ρ_{sh}	0.0053	0.0053	0.0053
	Concrete compressive strength (MPa)	30.8	30.8	26.8
	Longitudinal reinforcement yield strength (MPa)	413	413	413
	Transverse reinforcement yield strength (MPa)	367	367	367
Infill wall	Type of masonry unit	-	solid concrete block	hollow concrete block
	Wall aspect ratio (L_w/H_w)	-	1.50	1.50
	Wall thickness (mm)	-	92	92
	Concrete compressive strength (MPa)	-	15.1	9.5
	Elastic modulus of masonry prism (MPa)	-	9515	5098
Failure mode		-Flexural	-Diagonal crack of wall -Extensive shear crack of RC column	-Diagonal crack of wall -Flexural failure of RC column

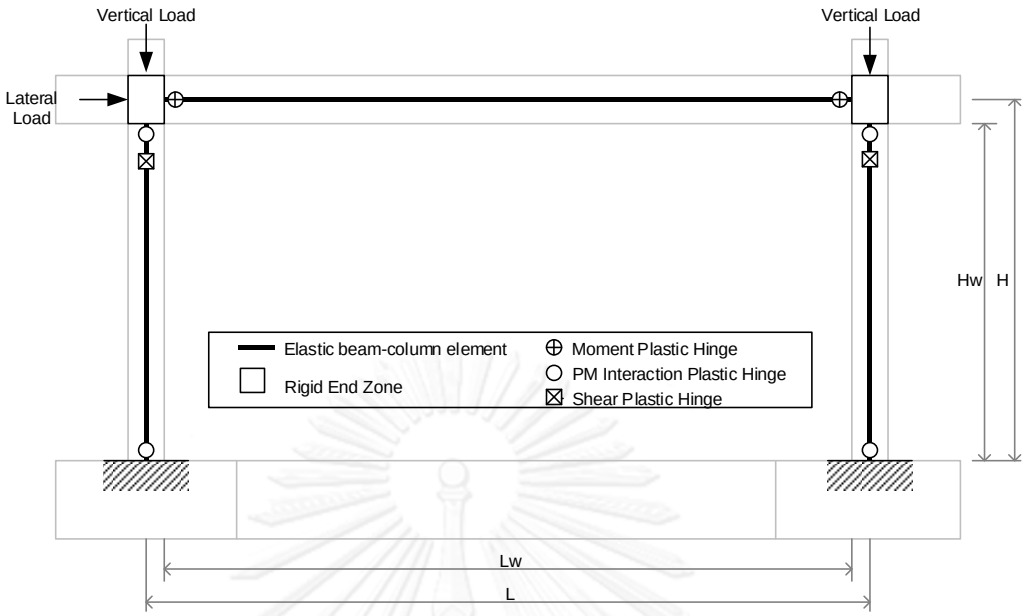

Figure 5-9. Analytical model of RC bare frame

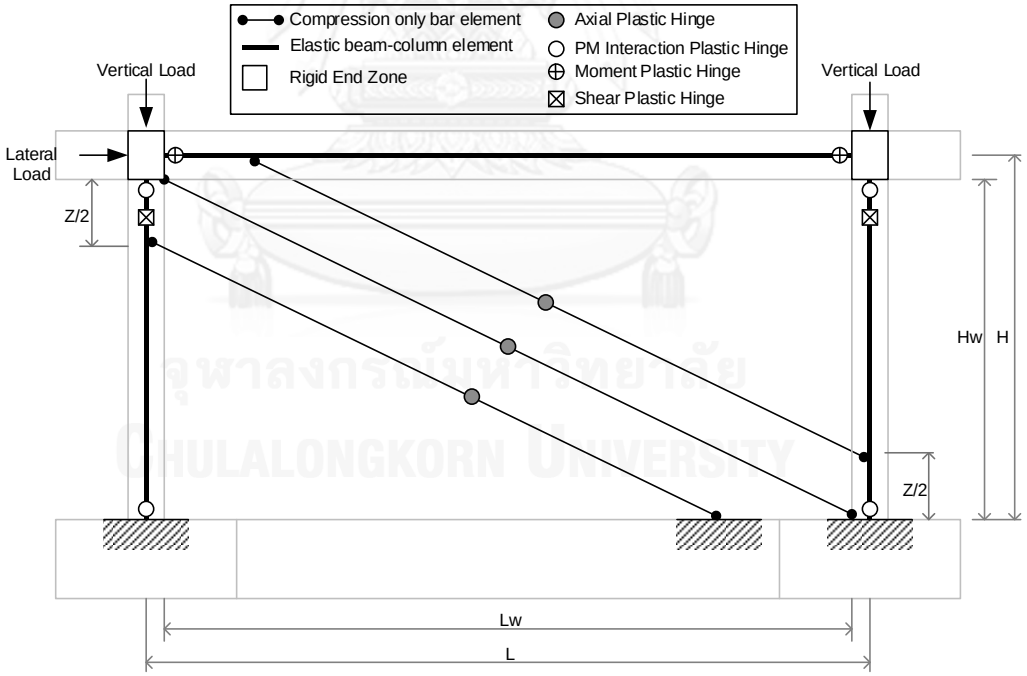

Figure 5-10. Analytical model of masonry infill frame

Table 5-4. Analytical model properties for RC surrounding frames

Component	Properties		Specimens		
			No.1 (bare frame)	No. 3	No. 8
RC columns	Element effective stiffness				
	EI_{stf40}/EI_g		0.487	0.487	0.509
	Flexural plastic hinge				
	My	(kN-m)	32.4	32.4	32.2
	Mc	(kN-m)	38.7	38.7	38.5
	θ_y	(rad)	0.0069	0.0069	0.0067
	θ_{cap}^{pl}	(rad)	0.0364	0.0364	0.0358
	θ_{cap}^{tot}	(rad)	0.0433	0.0433	0.0425
	θ_{pc}	(rad)	0.1040	0.1040	0.0962
	Shear plastic hinge				
	$\Delta_{v,n}$	(mm)	1.9	1.9	1.7
	V_n	(kN)	85	85	82
	$\Delta_{v,u}$	(mm)	5.2	5.2	4.4
	$\Delta_{v,f}$	(mm)	83.1	83.1	83.1
RC beam	Element effective stiffness				
	EI_{stf40}/EI_g		0.430	0.430	0.441
	Flexural plastic hinge				
	My	(kN-m)	32.5	32.5	32.6
	Mc	(kN-m)	39.2	39.2	39.5
	θ_y	(rad)	0.0108	0.0108	0.0107
	θ_{cap}^{pl}	(rad)	0.0403	0.0403	0.0404
	θ_{cap}^{tot}	(rad)	0.0511	0.0511	0.0511
	θ_{pc}	(rad)	0.1473	0.1473	0.1417

Table 5-5. Analytical model properties for URM panel

Properties		Specimens			
		No. 3		No. 8	
λ		0.00297		0.0027	
w	(mm)	418		432	
V_{slide}	(kN)	232		146	
V_{cc}	(kN)	480		315	
		Horizontal	Diagonal	Horizontal	Diagonal
K_{ini}	(kN/mm)	307	446	161	235
K_{sof}	(kN/mm)	9	13	5	7
V_{max}	(kN)	232	279	146	176
V_y	(kN)	186	224	117	141
V_{res}	(kN)	46	56	29	35
Δ_y	(mm)	0.61	0.50	0.72	0.59
Δ_{max}	(mm)	4.98	4.14	9.95	8.28
Δ_{res}	(mm)	25.18	20.95	33.65	28.00

Note: The softening stiffness (K_{sof}) of masonry infill panel was assumed as 3% of the initial stiffness (K_{ini})

The comparison of the experimentally obtained load-deformation curve and the analytical result of the RC bare frame (specimen No. 1) is shown in Figure 5-11. The analytical initial stiffness matches well with the experimental result up to 0.3% drift. After this state the lateral stiffness obtained from the analysis is considerably higher than the experimental result. Consequently, the analytically obtained displacement at the maximum lateral load is significantly lower than the actual value. Analytical result shows that the specimen reached its peak lateral strength at 1.2% drift. On the other hand, the experiment shows that the peak lateral strength of the tested specimen was observed at 3.0% drift. This difference may be due to the use of the effective stiffness at 40% of yield capacity (EI_{stf40}) of the elastic frame elements. Nevertheless, the analytical model can capture the lateral load capacity and failure mode of the tested specimen reasonably well.

As for the URM infill frame, the analytical model of the URM panel developed based on the approach described earlier was verified in this section. Figure 5-12 shows the load-story drift curves of the URM infill frame (specimen No. 8) obtained from analysis using various analytical models. According to the results, the analytical model using three diagonal struts and softening stiffness equal to 3% of the initial stiffness provided the best prediction. The result obtained using this analytical model matched well with the experimental result and this analytical model using three diagonal struts and softening stiffness equal to 3% of the initial stiffness was used to analyze specimen No. 3 and No. 8 in detail.

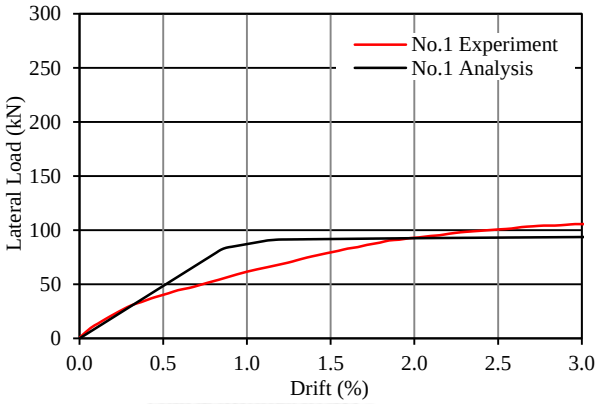

Figure 5-11. Comparison of experimental and analytical results of specimen No.1

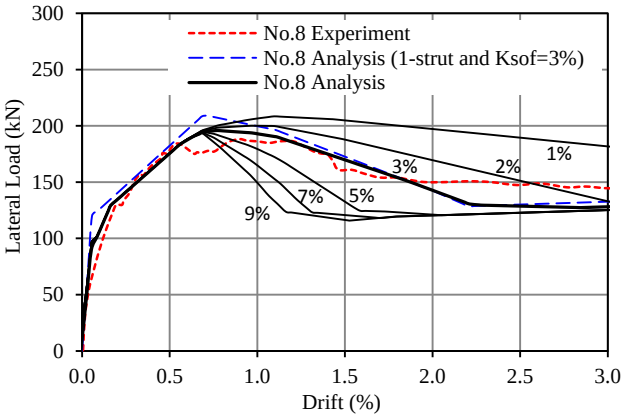

Figure 5-12. Comparison of experimental and analytical results using various models of specimen No.8

Figure 5-13 shows the comparison of experimental and analytical results of specimen No.3. The analytical initial stiffness matched well the experimental result up to 40% of the peak lateral load. After this state the lateral stiffness obtained from analysis was slightly higher than the experimental result. However, when the yielding in one of the struts occurred (point 1) the lateral stiffness significantly decreased. Analytical result shows that the specimen reached its peak lateral load at the similar drift compared with the experiment. However, the peak lateral load of the tested specimen obtained by analytical model was lower than that of the experimental results by approximately 10%. Nevertheless, the analytical model could reasonably capture the overall response of the tested specimen. Moreover, failure pattern of the surrounding RC frame was comparable with the experimental result although the model could not capture the shear crack observed in the RC columns.

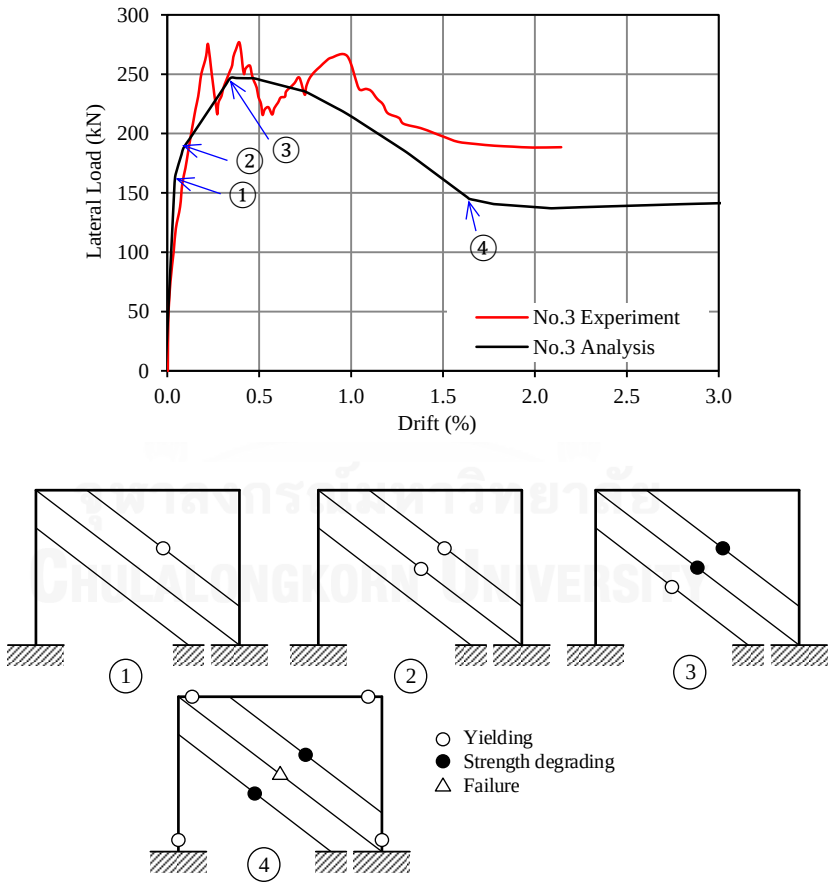

Figure 5-13. Analytical result of specimen No.3

Figure 5-14 shows the comparison of experimental and analytical results of specimen No.8. The analytical result matched well with the experimental result in terms of strength and stiffness up to 1.8% drift. After this level, the lateral capacity obtained from analysis was lower than that of the experimental result by approximately 12%. Analytical result shows that the specimen reached its peak lateral load at the similar drift compared with the experiment. However, the peak lateral load of the tested specimen obtained by the analytical model was slightly higher than the experimental results. At this state (point 3) strength degradation of two diagonal struts, interior and top-exterior, were observed. As for a surrounding RC frame, only yielding occurred at the bottom end of the right column. According to the results, the analytical model can capture the overall response of the specimen. Moreover, failure pattern of the surrounding RC frame was comparable with the experimental result.

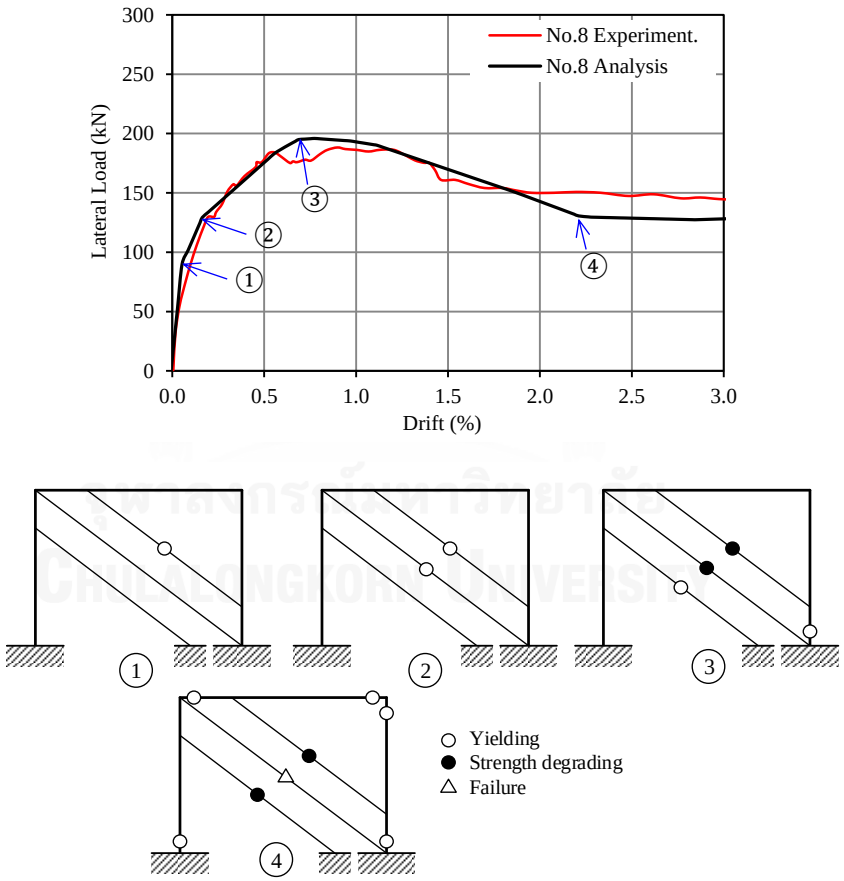

Figure 5-14. Analytical result of specimen No.8

5.5 Analytical study of un-retrofitted and retrofitted masonry infill frames

In this section the analytical evaluation of un-retrofitted and retrofitted masonry infill RC frame specimens are conducted and compared with the experimental results reported in Chapter IV.

5.5.1 Modelling description

The analytical model described in the previous sections was used. However, some parameters were modified and validated to improve the accuracy of the model, especially in the case of retrofitted specimens. The analytical models of the un-retrofitted and retrofitted specimens were constructed as depicted in Figure 5-15 and Figure 5-16, respectively. The test specimens detailing and material properties were described in Chapter III. Modeling parameters for the surrounding RC frame of both the un-retrofitted and retrofitted specimens are shown in Table 5-6. They were determined from the relevant formulas in section 5.2. As for the URM infill panel capacity estimation following the formulas described earlier, the lateral capacity of MIRCF01 corresponding to sliding along the bed-joint and corner crushing failure modes were 125 kN and 280 kN, respectively. Hence, the predicted failure mode of the un-retrofitted specimen was sliding along the bed-joint whereas the experimental result showed that corner crushing was the actual failure mode. Thus, the sliding capacity was larger than 280 kN. This discrepancy may be due to the much conservatism in the empirical formulas for the cohesive capacity (τ_0) and friction coefficient (μ) of masonry infill panel in the estimation of the capacities. Therefore, the experimentally obtained lateral capacity of URM panel was used to calibrate the parameters for computing sliding capacity of the URM infill panel. To this end, the lateral resistance capacity of MIRCF01 was taken as the lower bound of the sliding capacity, and a lower bound of the cohesive capacity (τ_0) of 0.6 MPa was determined from back-calculation using from Equation 2-18. It is interesting to note that, according to ASTM standard (ASTM, 2010), the cohesive capacity (shear strength at zero normal stress state) of a masonry panel can be determined from a diagonal tension test. In fact, this testing method was conducted on the masonry assemblages representative of test specimens in this study, and the cohesive capacity obtained ranged from 1.0 to 1.2 MPa (see Table 3-5). These values agreed with the estimated lower bound cohesive capacity of masonry panel presented above. Therefore, for conservatism, the lower bound cohesive capacity (0.6 MPa) was used to estimate the

lateral resistance capacity of sliding along the bed-joint failure mode for all test specimens. Accordingly, the modeling parameters for the URM infill panel of the un-retrofitted specimen are determined and listed in Table 5-7.

For the retrofitted specimens MIRCF02, MIRCF03, and MIRCF04, some adjustment was made in the determination of the diagonal strut effective width. Due to the gap between the infill panel and the RC columns, the infill panel was less confined than MIRCF01. So a lower bound of the diagonal strut effective width was used as given by Equation (2-1) proposed by Mainstone (1971). Employing the lower bound cohesive capacity (0.6 MPa) and the adjusted effective width of the strut leads to agreement of the expected failure modes of all specimens with the experimental results as shown in Table 5-8.

The URM drift at maximum capacity, Δ_{max}, is more difficult to assign. For the un-retrofitted specimen, the ASCE 41-06 (ASCE, 2007) recommendation of 0.3% was adopted. Obviously, the test results of the retrofitted specimens, revealed much improved displacement ductility as reported in Chapter IV. The strengthening schemes thus have a significant effect on load-deformation relation and failure mechanism of the infill panel. A trial and error approach was used to estimate the drift at maximum capacity of the masonry infill panel. As a result, the drift at maximum capacity of the masonry infill panel of approximately 2 times of the ASCE41-06 recommended value yields a reasonable agreement with the experimental results. The URM infill panel modeling properties of retrofitted specimens are listed in Table 5-8.

Finally, the softening stiffness (K_{sof}) affects the descending branch of the push-over curve. Figures 5-17 and 5-18 show the push-over curves for various softening stiffnesses. To capture the sudden drop in lateral capacity of the un-retrofitted specimen MIRCF01 following corner crushing, the softening stiffness (K_{sof}) of 10% of the initial stiffness is seen to be appropriate. For retrofitted specimens without steel wire mesh reinforcement, it appears that the softening stiffness equal to 3% of the initial stiffness yields satisfactory results. With steel wire mesh reinforcement employed in the infill panel, the significantly improved ductility leads to a much more gradual drop in the peak load. Therefore, the softening stiffness equal to 1% of the initial stiffness is more appropriate for the reinforced infill panel.

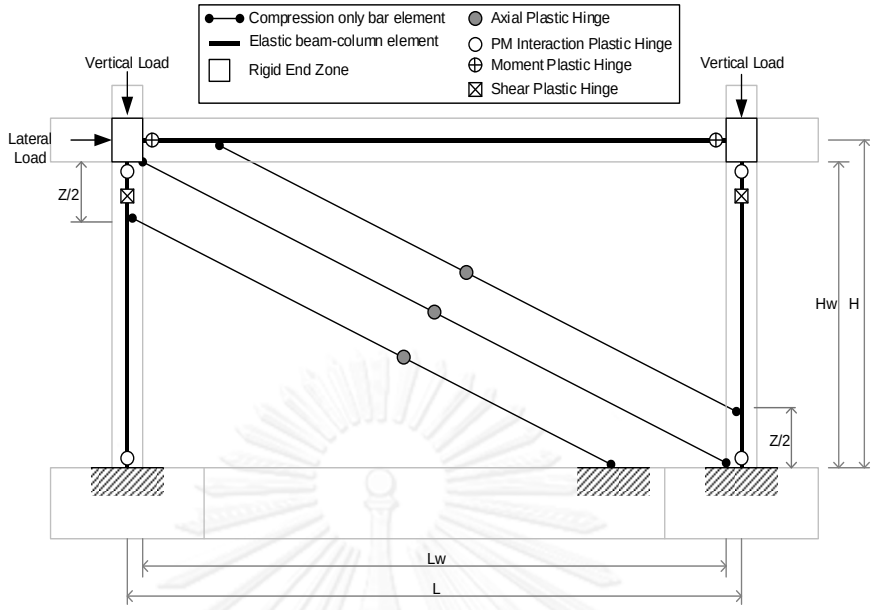

Figure 5-15. Analytical model of the un-retrofitted specimen

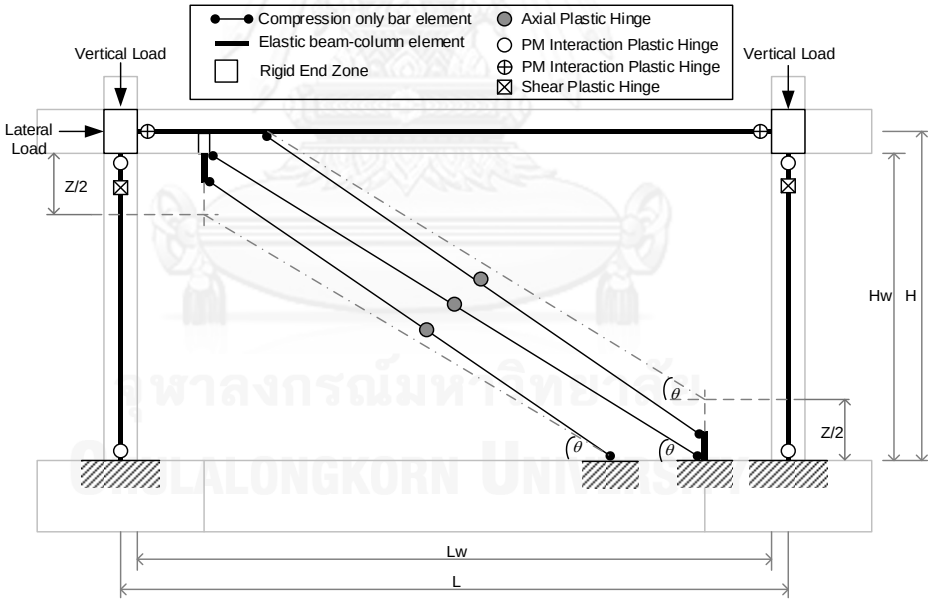

Figure 5-16. Analytical model of the retrofitted specimens

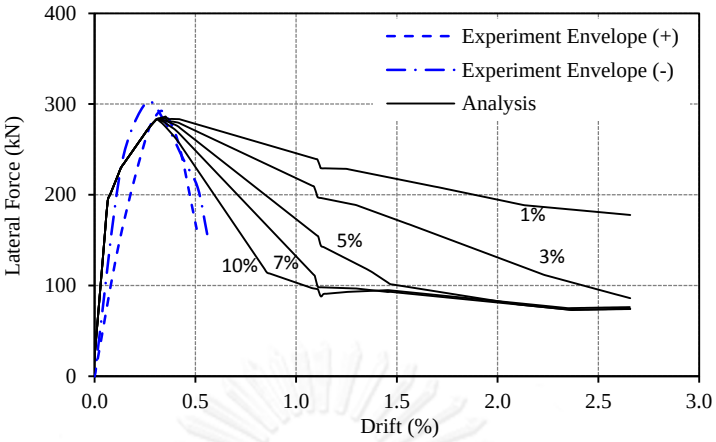

Figure 5-17. Comparison of experimental and analytical results using various models of specimen MIRCF01

Table 5-6. Analytical modeling properties for the RC frame of un-retrofitted and retrofitted specimens

Component	Properties		Specimens			
			MIRCF01	MIRCF02 (retrofitted)	MIRCF03 (retrofitted)	MIRCF04 (retrofitted)
RC columns	Element effective stiffness					
	EI_{stf40}/EI_g		0.598	0.598	0.587	0.587
	Flexural plastic hinge					
	My	(kN-m)	41.0	41.0	39.6	39.6
	Mc	(kN-m)	49.0	49.0	47.3	47.3
	θ_y	(rad)	0.0090	0.0090	0.0088	0.0088
	θ_{cap}^{pl}	(rad)	0.0088	0.0088	0.0092	0.0092
	θ_{cap}^{tot}	(rad)	0.0178	0.0178	0.0180	0.0180
	θ_{pc}	(rad)	0.0173	0.0173	0.0181	0.0181
	Shear plastic hinge					
	$\Delta_{v,n}$	(mm)	0.7	0.7	0.6	0.6
	V_n	(kN)	51	51	52	52
	$\Delta_{v,u}$	(mm)	2.3	2.3	2.1	2.1
	$\Delta_{v,f}$	(mm)	26.1	26.1	25.8	25.8

Table 5-6. Analytical modeling properties for the RC frame of un-retrofitted and retrofitted specimens (continued)

Component	Properties	Specimens			
		MIRCF01	MIRCF02 (retrofitted)	MIRCF03 (retrofitted)	MIRCF04 (retrofitted)
RC beam	Element effective stiffness				
	EI_{stf40}/EI_g	0.619	0.732	0.674	0.738
	Flexural plastic hinge				
	My (kN-m)	39.9 -57.2	55.0 -71.1	44.6 -61.0	54.8 -69.8
	Mc (kN-m)	48.7 -69.7	66.2 -85.6	54.0 -73.9	65.8 -83.8
	θ_y (rad)	0.0184 -0.0164	0.0157 -0.0165	0.0164 -0.0126	0.0150 -0.0160
	θ_{cap}^{pl} (rad)	0.0310 -0.0249	0.0251 -0.0249	0.0288 -0.0255	0.0252 -0.0253
	θ_{cap}^{tot} (rad)	0.0494 -0.0413	0.0408 -0.0414	0.0452 -0.0414	0.0402 -0.0413
	θ_{pc} (rad)	0.1063 -0.1063	0.0713 -0.1067	0.0876 -0.1058	0.0697 -0.1074

Table 5-7. Masonry infill panel modeling properties of un-retrofitted specimen

Properties		Un-retrofitted specimens	
		MIRCF01	
λ		0.00153	
w	(mm)	675	
V_{slide}	(kN)	280	
V_{cc}	(kN)	280	
		Horizontal	Diagonal
K_{ini}	(kN/mm)	157	194
[1)] K_{sof}	(kN/mm)	15.7	19.4
V_{max}	(kN)	280	311
V_y	(kN)	224	249
V_{res}	(kN)	56	62
Δ_y	(mm)	1.42	1.27
Δ_{max}	(mm)	6.24	5.61
Δ_{res}	(mm)	18.29	16.46

[1)] The softening stiffness is assumed as 10% of the initial stiffness

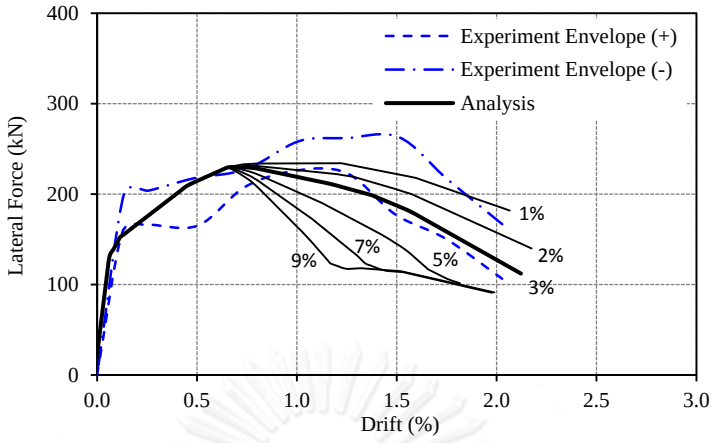

(a)

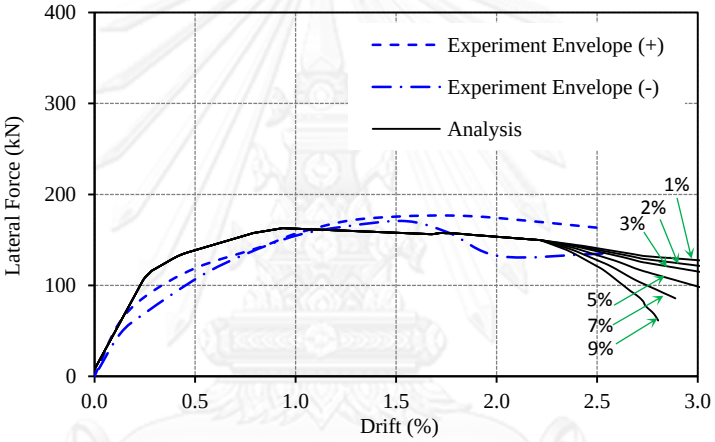

(b)

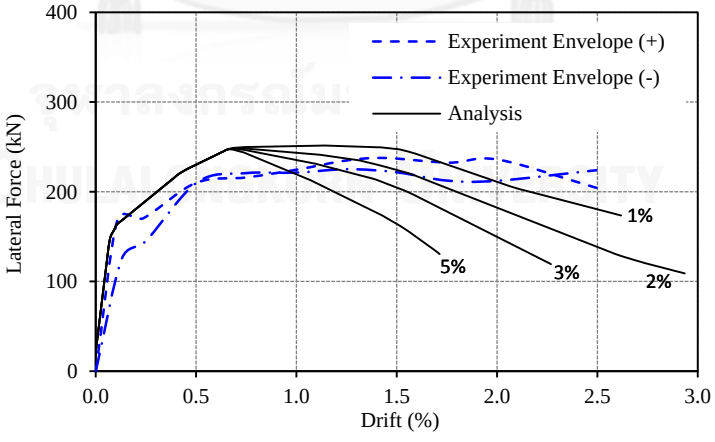

(c)

Figure 5-18. Comparison of experimental and analytical results using various models for specimens: (a) MIRCF02; (b) MIRCF03 and (c) MIRCF04

Table 5-8. Masonry infill panel modeling properties of retrofitted specimens

Properties		Retrofitted specimens					
		MIRCF02		MIRCF03		MIRCF04	
λ		0.00157		0.0159		0.00155	
[1] w	(mm)	424		309		426	
V_{slide}	(kN)	265		334		264	
V_{cc}	(kN)	**168**		**106**		**183**	
		Horizontal	Diagonal	Horizontal	Diagonal	Horizontal	Diagonal
K_{ini}	(kN/mm)	110	150	39	78	108	148
[2] K_{sof}	(kN/mm)	3.3	4.5	1.2	2.3	1.1	1.5
V_{max}	(kN)	168	196	106	150	183	214
V_y	(kN)	134	157	85	120	146	171
V_{res}	(kN)	34	39	21	30	37	43
Δ_y	(mm)	1.22	1.05	2.18	1.54	1.35	1.15
[3] Δ_{max}	(mm)	13.93	11.92	33.28	23.53	13.93	11.92
Δ_{res}	(mm)	54.74	46.82	106.77	75.50	149.76	128.10

[1] The effective width of diagonal strut calculated by Equation (2-3)

[2] The softening stiffness is assumed as 3% and 1% of the initial stiffness for unreinforced and reinforced masonry infill panel, respectively.

[3] Maximum drift of the masonry infill panel is assumed as 2 times of the ASCE41-06 recommended values.

5.5.2 Results and discussion

The lateral force versus story drift relation and the damage pattern of specimen MIRCF01 (un-retrofitted) from the analysis is shown in Figure 5-19. In addition, the experimentally obtained envelope curves were utilized to compare with the analytical results. According to the figure, an analytical initial stiffness is considerably higher than experimentally obtained one, especially when compared with the positive envelope curve. Consequently, the story drift, in elastic range, obtained from analysis was considerably smaller compared with the experimental results. However, after the exterior diagonal strut yielded (point 1), the stiffness of the tested specimen decreased significantly and was lower than the experimental value. As indicated in the figure, the analytically obtained story drift at peak lateral load matched well with the experimental result. At point 3, the onset of strength degradation in both exterior and interior diagonal struts was observed as well as shear failure of the RC column

also occurred. After this state the lateral capacity of the tested specimens obtained by the experiment decreased faster than that of the analytical result. Based on the comparison, the analytical model could reasonably capture the overall response of the un-retrofitted specimen although the considerable difference of analytically and experimentally obtained was observed in the strength degradation range. Besides, the analytically obtained failure mechanism of the surrounding RC frame was consistent with the experimental observed.

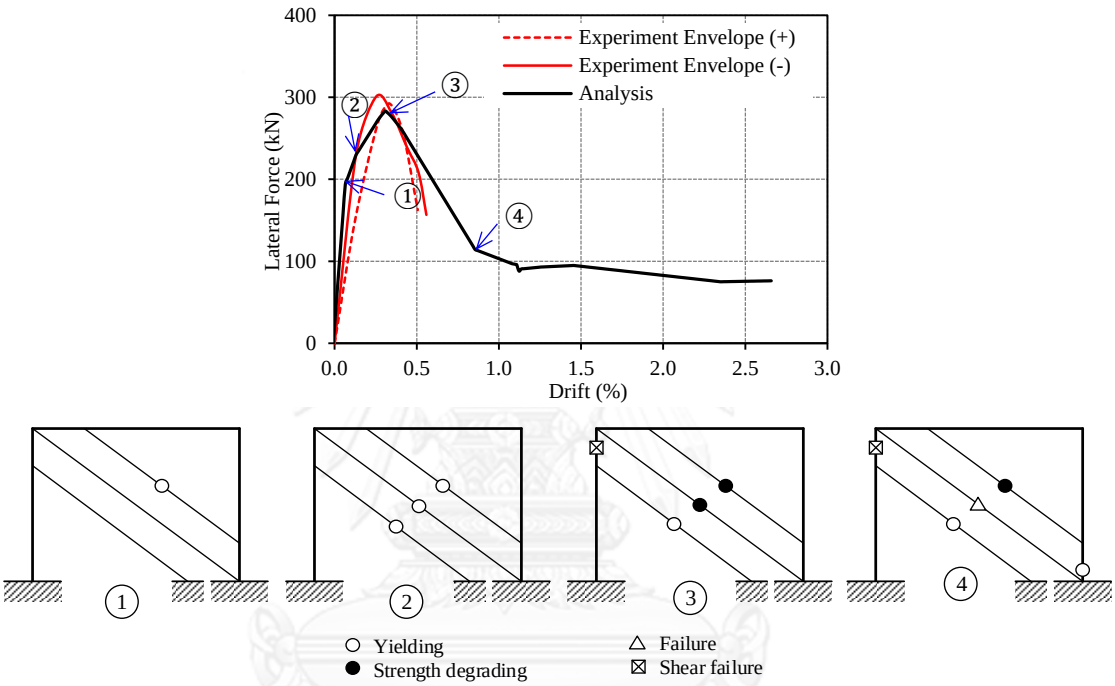

Figure 5-19. Analytical result of specimen MIRCF01

Figure 5-20 shows the comparison of the lateral force versus story drift relation of the retrofitted specimen MIRCF02. Damage pattern corresponding to the important state were included in the figure. It can be seen that the analytical initial stiffness was matched well with the experimentally obtained. After the onset of yielding on the exterior diagonal strut (point 1), the lateral stiffness of the specimen decreased slightly. At the point 2, both exterior and interior diagonal struts yielding were observed. Consequently, the lateral stiffness of the specimen decreased significantly. It should be noted that this point was identical with a cracking of the infill panel in experimentally observed. The analytical result shows that the specimen reached its peak lateral capacity at 0.7% drift which the drift ratio was considerably smaller than that of the experimentally obtained. Nevertheless, the

analytical model could capture an average peak lateral load of the specimen. According to the experimental observation, only the flexural yielding was occurred in the RC columns. Therefore, the proposed analytical model could simulate the overall failure mechanism of the tested specimen as well.

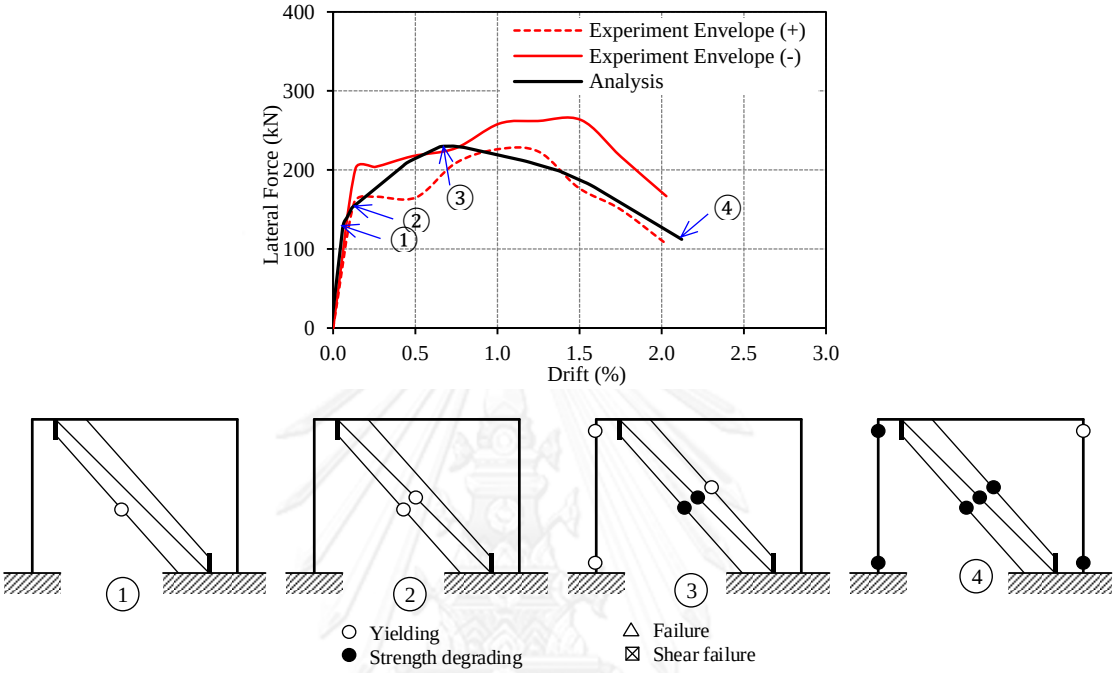

Figure 5-20. Analytical result of specimen MIRCF02

Figure 5-21 shows the comparison of the lateral force versus story drift relation of the retrofitted specimen MIRCF03. Damage pattern corresponding to the important states were also included in the figure. It can be seen that an analytical initial stiffness matched well with the experimental result when a story drift smaller than 0.125%. After this state, an analytical lateral stiffness was measurably larger compared with the experimentally obtained. However, after an interior diagonal strut yielded (point 1), the lateral stiffness of the specimen considerably decreased. Moreover, when the yielding introduced in an exterior diagonal strut (point 2), the analytical lateral stiffness of the specimen was consistent with the experimental result. The analytical result shows that the specimen reached its peak lateral load at 0.9% drift. This story drift was considerably smaller than that of the experimental observation. However, an analytical model could capture an average peak lateral load of the specimen. In addition, a softening lateral stiffness obtained by analytical

procedure reasonably matched the experimental envelope curves. According to the experimental results, only the flexural yielding was observed in the RC columns, which it consistent with the analytical result.

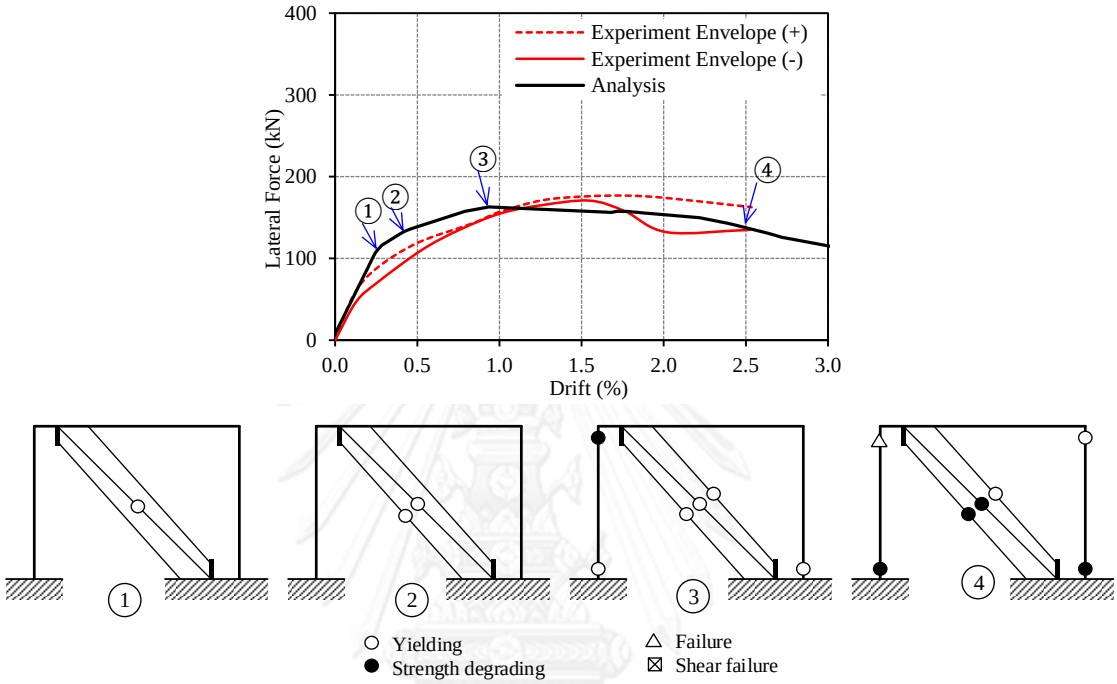

Figure 5-21. Analytical result of specimen MIRCF03

The comparison of the lateral force versus story drift relation of specimen MIRCF04 is illustrated in Figure 5-22. Damage pattern corresponding to the significant state were also included in the figure. It can be seen that an analytical initial stiffness matched well with the experimental result, especially when compared with the experimental positive envelope curve. However, an analytical initial stiffness was considerable larger when compared with the experimental negative envelope curve. The experimental results revealed that the lateral strength of the tested specimen slightly dropped due to a diagonal cracking of the infill panel. At a similar story drift, the bottom exterior and interior diagonal struts yielding (point 2) were observed in the analytical investigation. Consequently, the lateral stiffness of the specimen MIRCF04 considerably decreased without lateral strength deterioration. It can be concluded that the proposed analytical model could not capture the lateral strength

deterioration caused by a diagonal crack of the infill panel. The analytical result shows that the specimen reached its peak lateral load approximately at 1.15% drift. This drift was slightly smaller when compared with the experimental result. Moreover, the peak lateral strength obtained by the analytical procedure was slightly higher when compared with the experimentally obtained. The lateral strength deterioration of the analytical curve was observed at 1.5% drift which reasonable agree with the experimental curves. In addition, a softening lateral stiffness obtained by analysis acceptable matched the experimental envelope curves. Similar to the experimental result, only the flexural failure was observed in the RC columns. The analytical model shows that it can be used to investigate the overall response of the specimen MIRCF04.

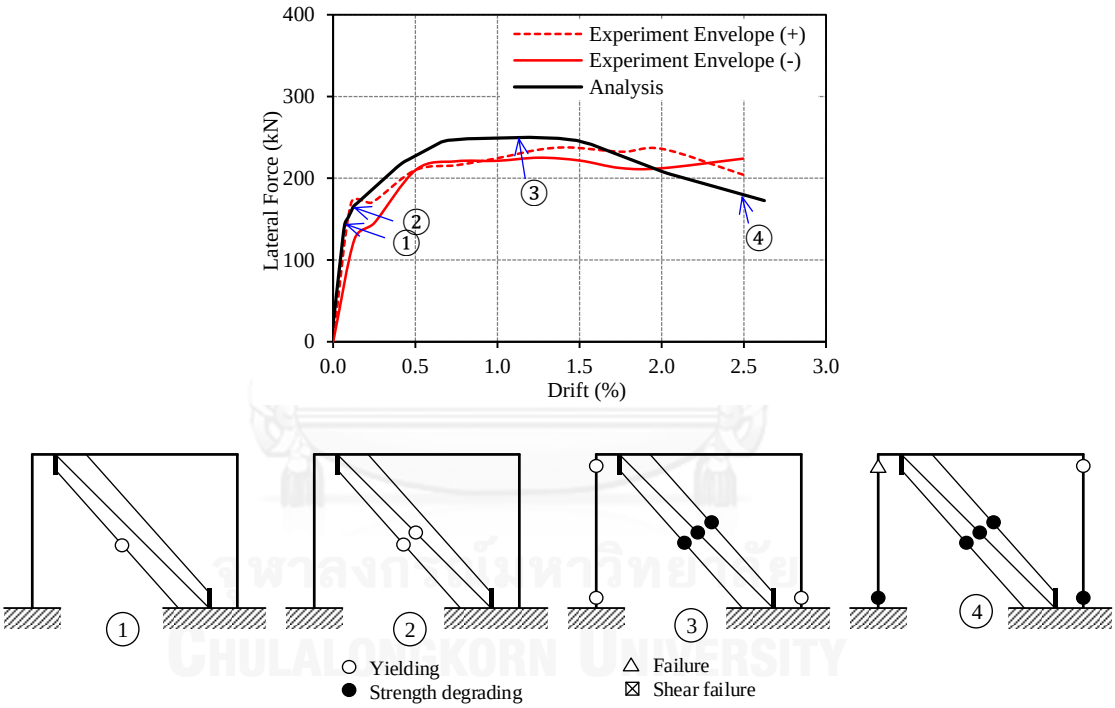

Figure 5-22. Analytical result of specimen MIRCF04

CHAPTER VI
CONCLUSIONS

In order to investigate the seismic performance of masonry infilled RC frames, experimental and analytical investigations were carried out. An exterior RC frame of a three-bay, three-story, typical commercial building had been selected as a prototype structure. To represent existing buildings which do not meet the current seismic design code, a prototype structure was designed to resist only gravity and wind loads. The RC frame was typical of non-ductile detailing in Thailand, with light transverse reinforcement. Four 3/4-scale models of single-bay, single-story non-ductile RC frame with masonry infill panels were tested under lateral cyclic loading. Finally, the nonlinear pushover analyses were performed and compared with the experimental results. The main findings can be summarized as follows:

The un-retrofitted specimen MIRCF01 suffered shear cracks in the columns and beam-column joints at very small drift following corner crushing of the infill panel. This frame assembly attained an average peak load at 0.33% drift, after which the capacity suddenly dropped due to the large shear cracks in RC columns and beam-column joints as well as corner crushing of the masonry infill. The life safety performance level of the un-retrofitted sub-assemblage could be attained only at a very small story drift of 0.22%

Guided by failure mechanisms observed from the literature and experimental results of an un-retrofitted specimen, a retrofit scheme was proposed for resolving weaknesses of the non-ductile infilled URM RC frames. The masonry infill panel was separated from the columns and steel brackets were used to transfer the interactive forces between the panel and the beams, thereby totally eliminating the transfer of large strut force to the columns. Small vertical steel members were anchored to the vertical boundaries of masonry infill to prevent the sliding along the bed-joint failure of the masonry panel and the corners of the infill were reinforced with steel wire meshes and high strength mortar.

For the specimen tested with the proposed retrofit scheme implemented, the life safety performance level could be attained at a story drift of more than 1.0% with much better performance than that stipulated in building standards which allow only a drift of 0.5% for the masonry unit. Furthermore, a drift capacity of 1.5% and 1.75% could be achieved at a sustainable lateral load capacity of 80% in the case of

retrofitted unreinforced masonry infill panels of panel aspect ratio of 1.6 and 1.0, respectively. As for the specimen with the masonry infill panel reinforced with steel wire mesh, it could attain a drift capacity of 2.0% at 20% drop in peak capacity even with a small reinforcement ratio of 0.11%. Moreover, the assembly with reinforced masonry infill panel exhibited much better post-peak performance than the specimen infilled with unreinforced masonry panel. It is interesting to note that the peak lateral load capacity was reduced approximately in proportion to the reduction in the area of the URM panel. With 20% of the masonry infill panel removed the retrofitted specimens MIRCF02 and MIRCF04 could attain secant stiffness of more than 80% of the un-retrofitted one at 0.125% drift. A 70% reduction in secant stiffness was observed in the test specimen MIRCF03 with 50% of the panel removed. As for the energy dissipation capacity, all retrofitted specimens attained much higher total energy dissipation capacities than the un-retrofitted one. The retrofitted scheme clearly results in superior performance over other schemes in the literature which could achieve a drift capacity in the 1.4% range in general.

A discrete frame element with nonlinearity lumped at each end was applied for modelling the surrounding RC frame. Although this type of element cannot provide detailed results but it can capture the overall response of the structure. In order to simulate the various failure modes of the RC frame, both the flexural and shear plastic hinges were employed. The plastic hinge model proposed by Haselton and Deierlein (2007) and Patwardhan (2005) were utilized to model the flexural and shear plastic hinges, respectively. The comparison of analytical and previous experimental load-displacement curves of the RC columns and RC frame exhibited the acceptable correlations. This modeling could capture the main failure mechanisms and peak capacity of those specimens as well.

For the URM infill panel, a simplified model using three diagonal struts yielded satisfactory results. It can generate an additional shear force in the adjacent column consistent with the actual behavior of the URM infill RC frames. A successful model has to be able to predict with reasonable accuracy the peak capacity and associated drift. It should be able to capture the predominant failure mode. The URM panel lateral load capacity depends on the effective of the diagonal struts and the masonry properties. For un-retrofitted specimens, total effective width of diagonal strut (w) based on the method proposed by Stafford-Smith and Carter (1969) is appropriate approach. However, due to the less confinement of infill panel in the retrofitted specimens, a smaller expected diagonal strut effective width computed form the lower bound estimation proposed by Mainstone (1971) should

be used. As for the load resistance capacity associated with both corner crushing and sliding along the bed-joint failure modes, the formulas suggested by Mostafaei and Kabeyasawa (2004) yielded good correlation with experimental results, provided an appropriate value of the cohesive capacity (τ_0) is assigned. The ASCE 41-06 standard (ASCE, 2007) specified value of τ_0 was found to be much under-estimated for the specimens tested. By using the un-retrofitted specimen as a calibrating specimen, the lower bound of cohesive capacity (τ_0) of URM panel was back-calculated and found to be 0.6MPa which better agreed with the values obtained from diagonal tension tests in accordance with ASTM E519-10 standard. Based on the adjusted cohesive capacity and the adjusted strut effective width, the predicted failure mode of the URM panels were consistent with the experimental results.

The URM drift at maximum lateral load capacity, Δ_{max}, obviously has a significant effect on the lateral load-drift relation of the URM infilled RC frame. For the un-retrofitted specimens, the lateral drift at maximum capacity of the masonry infill panel recommended by ASCE41-06 (2007) matches reasonably well with the experimental results. However, the strengthening schemes have a significant effect on load-deformation relation and failure mechanism of the infill panel, and the drift at maximum capacity of the masonry infill panel of approximately 2 times of the ASCE41-06 recommended value yields a reasonable agreement with the experimental results. The softening stiffness of the masonry panel has to be selected properly. For an un-retrofitted specimen vulnerable to corner crushing leading to shear failure in the column, the the softening stiffness (K_{sof}) of 10% of the initial stiffness is seen to be appropriate. For retrofitted specimens without steel wire mesh reinforcement, it appears that the softening stiffness equal to 3% of the initial stiffness yields satisfactory results. For a retrofitted specimen with wire mesh reinforcement, a softening stiffness of 1% of the initial stiffness could account for the gradual drop in the descending branch of the load-deformation curve.

The analytical model of masonry infill RC frames presented could simulate the lateral load-displacement relation of the tested specimens reasonably well. The peak capacities of the test specimens were predicted to within 3% to 8% of the average peak capacities obtained from the experiments. However, the estimated lateral drifts at the peak capacities were considerably lower than those of the experimental results by about 5% to 44%.

REFERENCES

ACI. 2008. Building code requirements for structural concrete and commentary (ACI 318-08). American Concrete Institute,Farmington Hills, MI

Acun, B. and Sucuoglu, H. Strengthening of masonry infill walls in reinforced concrete frames with wire mesh reinforcement. 10 8th US National Conference on Earthquake Engineering 2006, 18–22 April 2006 San Francisco, CA. 6022-6031.

Al-Chaar, G. 2002. Evaluating strength and stiffness of unreinforced masonry infill structures. *In:* ERDC/CERL-TR-02-1, N. (ed.). Engineering Research and Development Center, US Army Corps of Engineers.

Al-Chaar, G., Issa, M. and Sweeney, S. 2002. Behavior of masonry-infilled nonductile reinforced concrete frames. *Journal of Structural Engineering,* 128**,** 1055-1063.

Altin, S., Anil, Ö., Kara, M. E. and Kaya, M. 2008. An experimental study on strengthening of masonry infilled rc frames using diagonal cfrp strips. *Composites Part B: Engineering,* 39**,** 680-693.

Angel, R., Abrams, D., Shapiro, D., Uzarski, J. and Webster, M. 1994. Behavior of reinforced concrete frames with masonry infills. *Rep. UILU-ENG-94-2005.* Department of Civil Engineering, University of Illinois, Urbana-Champaign.

ASCE. 2007. Seismic rehabilitation of existing buildings (ASCE/SEI 41-06). American Society of Civil Engineers,Reston, VA

Asteris, P., Antoniou, S., Sophianopoulos, D. and Chrysostomou, C. 2011. Mathematical macromodeling of infilled frames: State of the art. *Journal of Structural Engineering,* 137**,** 1508-1517.

ASTM. 2010. Standard test method for diagonal tension (shear) in masonry assemblages (ASTM E519-10). ASTM International, West Conshohocken, PA

Bertero, V. and Brokken, S. 1983. Infills in seismic resistant building. *Journal of Structural Engineering,* 109**,** 1337-1361.

Billington, S., Kyriakides, M., Blackard, B., Willam, K., Stavridis, A. and Shing, P. 2009. Evaluation of a sprayable, ductile cement-based composite for the seismic retrofit of unreinforced masonry infills. *Improving the seismic performance of existing buildings and other structures.*

Calvi, G. M. and Bolognini, D. 2001. Seismic response of reinforced concrete frames infilled with weakly reinforced masonry panels. *Journal of Earthquake Engineering,* 5**,** 153-185.

CEN. 2004. European standard en 1998-1:2004 Eurocode 8:Design of Structures for Earthquake Resistance, Part 1: General rules, Seismic actions and Rules for buildings. Comite Europeen de Normalisation.,Brussels

Centeno, J., Ventura, C., Foo, S. and Lara, O. Seismic performance of gravity load designed reinforced concrete frames with unreinforced masonry infill walls. 314, 2008 Vancouver, BC.

Corte, G. D., Fiorino, L. and Mazzolani, F. 2008. Lateral-loading tests on a real rc building including masonry infill panels with and without frp strengthening. *Journal of Materials in Civil Engineering,* 20**,** 419-431.

Crisafulli, F. J. 1997. *Seismic behaviour of reinforced concrete structures with masonry infills.* Ph.D. Thesis, University of Canterbury.

Crisafulli, F. J. and Carr, A. J. 2007. Proposed macro-model for the analysis of infilled frame structures. *Bulletin of the New Zealand National Society for Earthquake Engineering,* 40.

Dolšek, M. and Fajfar, P. 2002. Mathematical modelling of an infilled rc frame structure based on the results of pseudo-dynamic tests. *Earthquake Engineering & Structural Dynamics,* 31**,** 1215-1230.

El-Dakhakhni, W., Elgaaly, M. and Hamid, A. 2003. Three-strut model for concrete masonry-infilled steel frames. *Journal of Structural Engineering,* 129**,** 177-185.

Elwood, K. J. and Moehle, J. P. 2005. Axial capacity model for shear-damaged columns. *ACI Structural Journal,* 102**,** 578-587.

Erdem, I., Akyuz, U., Ersoy, U. and Ozcebe, G. 2006. An experimental study on two different strengthening techniques for rc frames. *Engineering Structures,* 28**,** 1843-1851.

Erol, G., Karadogan, H. F. and Cili, F. Seismic strengthening of infilled reinforced concrete frames by cfrp. 15th World Conference on Earthquake Engineering, 24–28 September 2012,Lisbon, Portugal.

Fardis, M. N. and Panagiotakos, T. B. 1997. Seismic design and response of bare and masonry-infilled reinforced concrete buildings. Part ii: Infilled structures. *Journal of Earthquake Engineering,* 1**,** 475-503.

FEMA. 1998. Evaluation of earthquake-damaged concrete and masonry wall building-basic procedures manual (FEMA306). Federal Emergency Management Agency,Washington, D.C.

Fiorato, A. E., Sozen, M. A. and Gamble, W. L. 1970. An investigation on the interaction of reinforced concrete frames with masonry filler walls. *Report UILU-ENG 70-100.* University of Illinois – Urbana Champaign.

Gómez-Martínez, F., Pérez-García, A., De Luca, F., Verderame, G. M. and Manfredi, G. Preliminary study of the structural role played by masonry infills on rc building performances after the 2011 lorca, spain, earthquake. 15th World Conference on Earthquake Engineering, 24–28 September 2012 Lisbon, Portugal.

Haselton, C. B. and Deierlein, G. G. 2007. Assessing seismic collapse safety of modern reinforced concrete momentframe buildings. *Report No. 152.* California: John A. Blume Earthquake Engineering Center, Stanford University.

Hashemi, A. and Mosalam, K. M. 2007. Seismic evaluation of reinforced concrete buildings including effects of masonry infill walls. *PEER Report 2007/100.* Pacific Earthquake Engineering Research Center.

Hassan, A. F. and Sozen, M. A. 1997. Seismic vulnerability assessment of low-rise buildings in regions with infrequent earthquakes. *ACI Structural Journal,* 94**,** 31-39.

Holmes, M. 1961. Steel frames with brickwork and concrete infilling. *ICE Proceedings.*

Kakaletsis, D. J. and Karayannis, C. G. 2008. Influence of masonry strength and openings on infilled r/c frames under cycling loading. *Journal of Earthquake Engineering,* 12**,** 197-221.

Kaushik, H. B., Rai, D. C. and Jain, S. K. A rational approach to analytical modeling of masonry infills in reinforced concrete frame buildings. The 14th World Conference on Earthquake Engineering, 12–17 October 2008 Beijing, China.

Kyriakides, M. A. and Billington, S. L. Seismic retrofit of masonry-infilled non-ductile reinforced concrete frames using sprayable ecc. Paper (No. 05-04-0063) Proceedings of the 14th World Conference on Earthquake Engineering, 12–17 October 2008,Beijing, China.

Lee, H. S. and Woo, S. 2002. Effect of masonry infills on seismic performance of a 3-storey r/c frame with non-seismic detailing. *Earthquake Engineering and Structural Dynamics,* 31**,** 353-378.

Lukkunaprasit, P. and Srechai, J. A low cost retrofit scheme for masonry-infilled non-ductile reinforced concrete frames. Paper (No. 4279) presented at the 15th World Conference on Earthquake Engineering, 24–28 September 2012 Lisbon, Portugal.

Lynn, A. 1999. *Seismic evaluation of existing reinforced concrete building colums.* Ph.D. Thesis, University of California at Berkeley, Berkley.

Magenes, G. and Pampanin, S. Seismic response of gravity-load designed frame systems with masonry infills. 13th World Conference on Earthquake Engineering, 1-6 Aug 2004 Vancouver, BC, Canada.

Mainstone, R. J. 1971. On the stiffnesses and strengths of infilled frames. *ICE Proceedings, Suppl.*

Mehrabi, A., Benson Shing, P., Schuller, M. and Noland, J. 1996. Experimental evaluation of masonry-infilled rc frames. *Journal of Structural Engineering,* 122**,** 228-237.

Mo, Y. and Wang, S. 2000. Seismic behavior of rc columns with various tie configurations. *Journal of Structural Engineering,* 126**,** 1122-1130.

Mostafaei, H. and Kabeyasawa, T. 2004. Effect of infill masonry walls on the seismic response of reinforced concrete buildings subjected to the 2003 bam earthquake strong motion: A case study of bam telephone center. *Bulletin of the Earthquake Research Institute,* 73.

Negro, P. and Verzeletti, G. 1996. Effect of infills on the global behaviour of r/c frames: Energy considerations from pseudodynamic tests. *Earthquake Engineering & Structural Dynamics,* 25**,** 753-773.

Panagiotakos, T. B. and Fardis, M. N. Seismic response of infilled rc frames structures. the 11th world conference on earthquake engineering, 23-28 June 1996 Acapulco, Mexico. Paper No. 225.

Panagiotakos, T. B. and Fardis, M. N. 2001. Deformations of reinforced concrete members at yielding and ultimate. *ACI Structural Journal,* 98**,** 135-147.

Patwardhan, C. 2005. *Shear strength and deformation modeling of reinforced concrete columns.* Master Thesis, The Ohio State University.

Paulay, T. and Priestly, M. J. N. 1992. *Seismic design of reinforced concrete and masonry buildings.* New York: John Wiley & Sons, Inc.

Pinto, A. V. and Taucer, F. 2006. Assessment and retrofit of fullscale models of existing rc frames. *Advances in Earthquake Engineering for Urban Risk Reduction.* Dordrecht: Springer.

Polyakov, S. V. 1960. On the interaction between masonry filler walls and enclosing frame when loading in the plane of the wall. *Translation in earthquake engineering.* Earthquake Engineering Research Institute (EERI), San Francisco.

Priestley, M. J. N., Seible, F. and Calvi, G. M. 1996. *Seismic design and retrofit of bridges*, John Wiley & Sons.

Pujol, S. and Fick, D. 2010. The test of a full-scale three-story rc structure with masonry infill walls. *Engineering Structures,* 32**,** 3112-3121.

Saneinejad, A. and Hobbs, B. 1995. Inelastic design of infilled frames. *Journal of Structural Engineering,* 121**,** 634-650.

Sezen, H. and Moehle, J. P. 2004. Shear strength model for lightly reinforced concrete columns. *Journal of Structural Engineering,* 130**,** 1692-1703.

Sezen, H., Whittaker, A. S., Elwood, K. J. and Mosalam, K. M. 2003. Performance of reinforced concrete buildings during the august 17, 1999 kocaeli, turkey earthquake,

and seismic design and construction practise in turkey. *Engineering Structures,* 25**,** 103-114.

Shing, P., Stavridis, A., Koutromanos, I., Willam, K., Blackard, B., Kyriakides, M., Billington, S. and Arnold, S. 2009. Seismic performance of non-ductile rc frames with brick infill. *Improving the seismic performance of existing buildings and other structures.*

Shing, P. B. and Mehrabi, A. B. 2002. Behaviour and analysis of masonry-infilled frames. *Progress in Structural Engineering and Materials,* 4**,** 320-331.

Smith, B. S. and Carter, C. 1969. A method of analysis for infilled frames. *ICE Proceedings* [Online], 44. Available: http://www.icevirtuallibrary.com/content/article/10.1680/iicep.1969.7290.

Srechai, J. and Lukkunaprasit, P. 2013. An innovative scheme for retrofitting masonry-infilled non-ductile reinforced concrete frames. *The IES Journal Part A: Civil & Structural Engineering,* 6**,** 277-289.

Stafford Smith, B. 1966. Lateral stiffness of infilled frames. *Journal of the Structural Division,* 88**,** 183-199.

Stavridis, A. 2009. *Analytical and experimental study of seismic performance of reinforced concrete frames infilled with masonry walls.* Ph.D. Thesis, University of California, San Diego.

Stavridis, A. and Shing, P. B. Simplified modeling of masonry-infilled rc frames subjected to seismic loads. Paper (No. 5484) presented at 15th World Conference on Earthquake Engineering, 24–28 September 2012 Lisbon, Portugal.

Uva, G., Raffaele, D., Porco, F. and Fiore, A. 2012. On the role of equivalent strut models in the seismic assessment of infilled rc buildings. *Engineering Structures,* 42**,** 83-94.

Yuksel, E., Ozkaynak, H., Buyukozturk, O., Yalcin, C., Dindar, A. A., Surmeli, M. and Tastan, D. 2010. Performance of alternative cfrp retrofitting schemes used in infilled rc frames. *Construction and Building Materials,* 24**,** 596-609.

Zovkic, J., Sigmund, V. and Guljas, I. 2013. Cyclic testing of a single bay reinforced concrete frames with various types of masonry infill. *Earthquake Engineering and Structural Dynamics,* 42**,** 1131-1149.

APPENDIX

APPENDIX

STRAIN IN STEEL REINFORCEMENT

Figure A-1 shows the steel reinforcement strain measurement locations in the right side of test specimens, and the corresponding drift ratio-strain relations of all tested specimens are shown in Figures A-2 to A-6. It should be noted that some strain gauges were damaged during casting. Moreover, as mentioned earlier, the RC frame of some specimens were the repaired one. Therefore, the re-bars of those specimens would contain the residual strains from the previous experiment. Therefore, the remaining strain gauges did give a bad picture of the strains in the re-bars. Hence, the drift ratio-strain relation of the re-bars of repaired specimens is discarded in some locations.

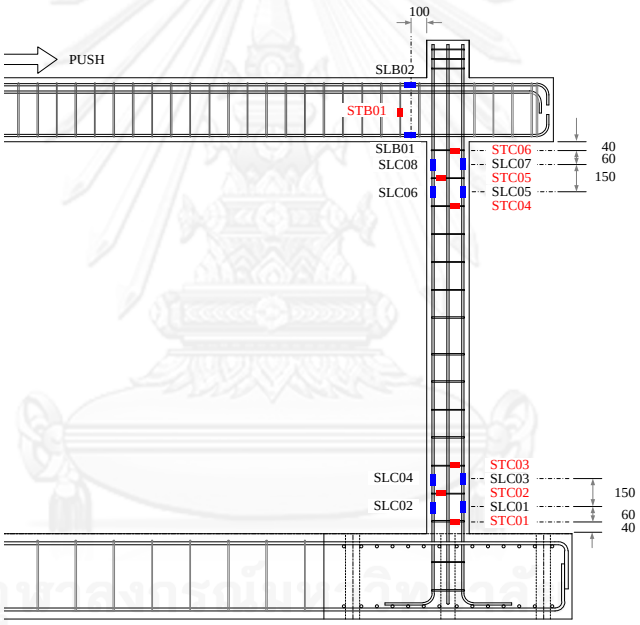

Figure A-1. Strain measurement locations in the left side of test specimens

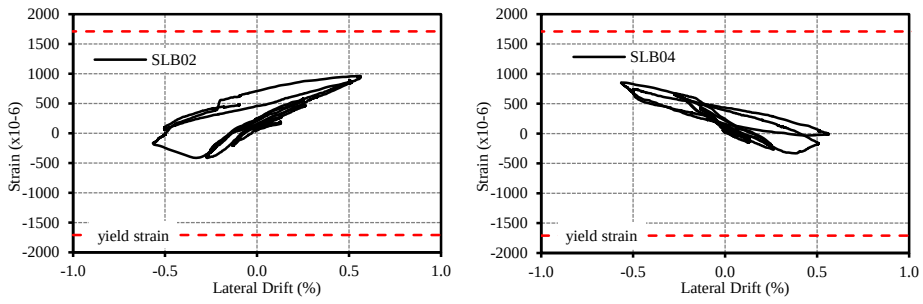

Figure A-2. Drift ratio-strain relation of re-bars in the beam of MIRCF01

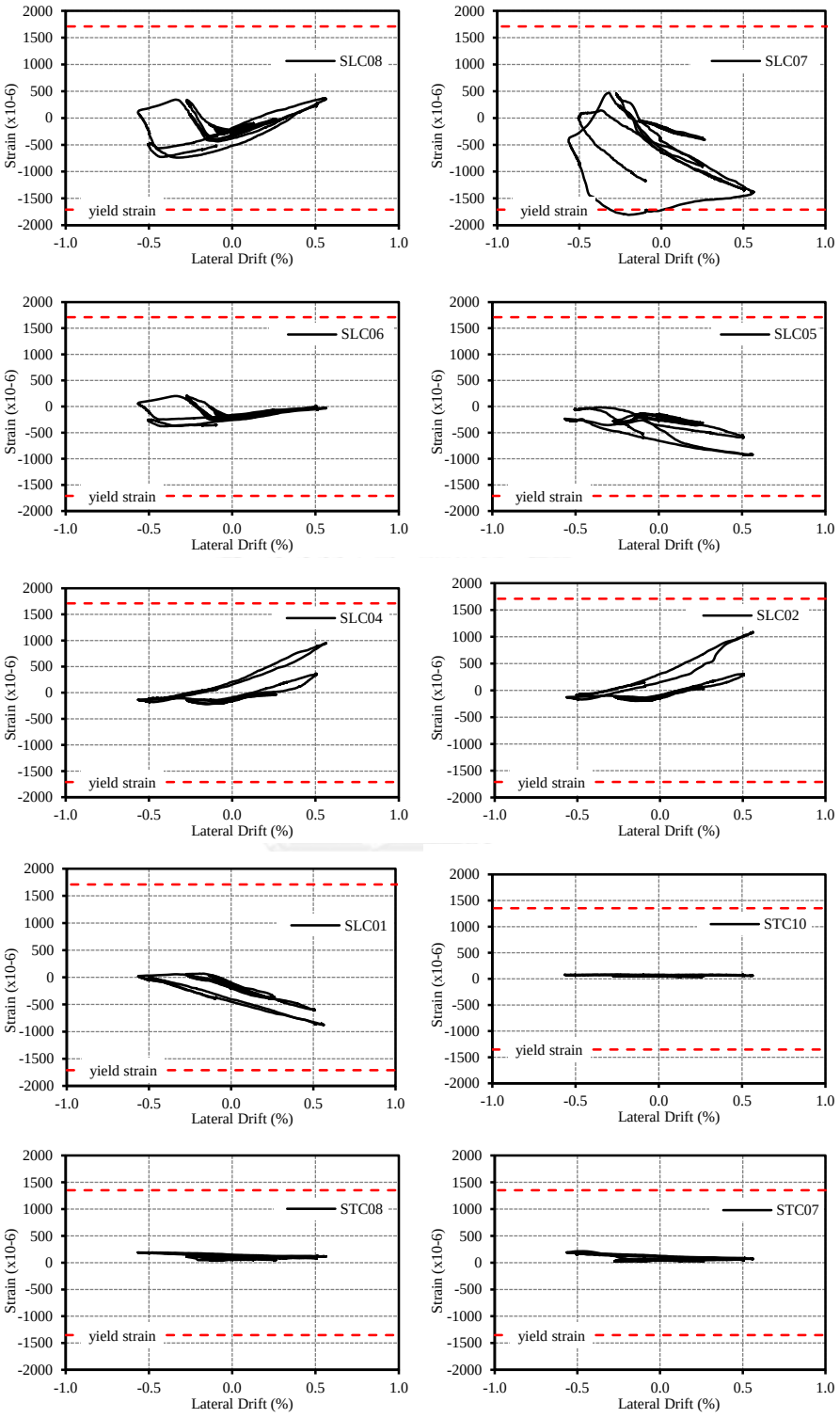

Figure A-3. Drift ratio-strain relation of re-bars in the column of MIRCF01

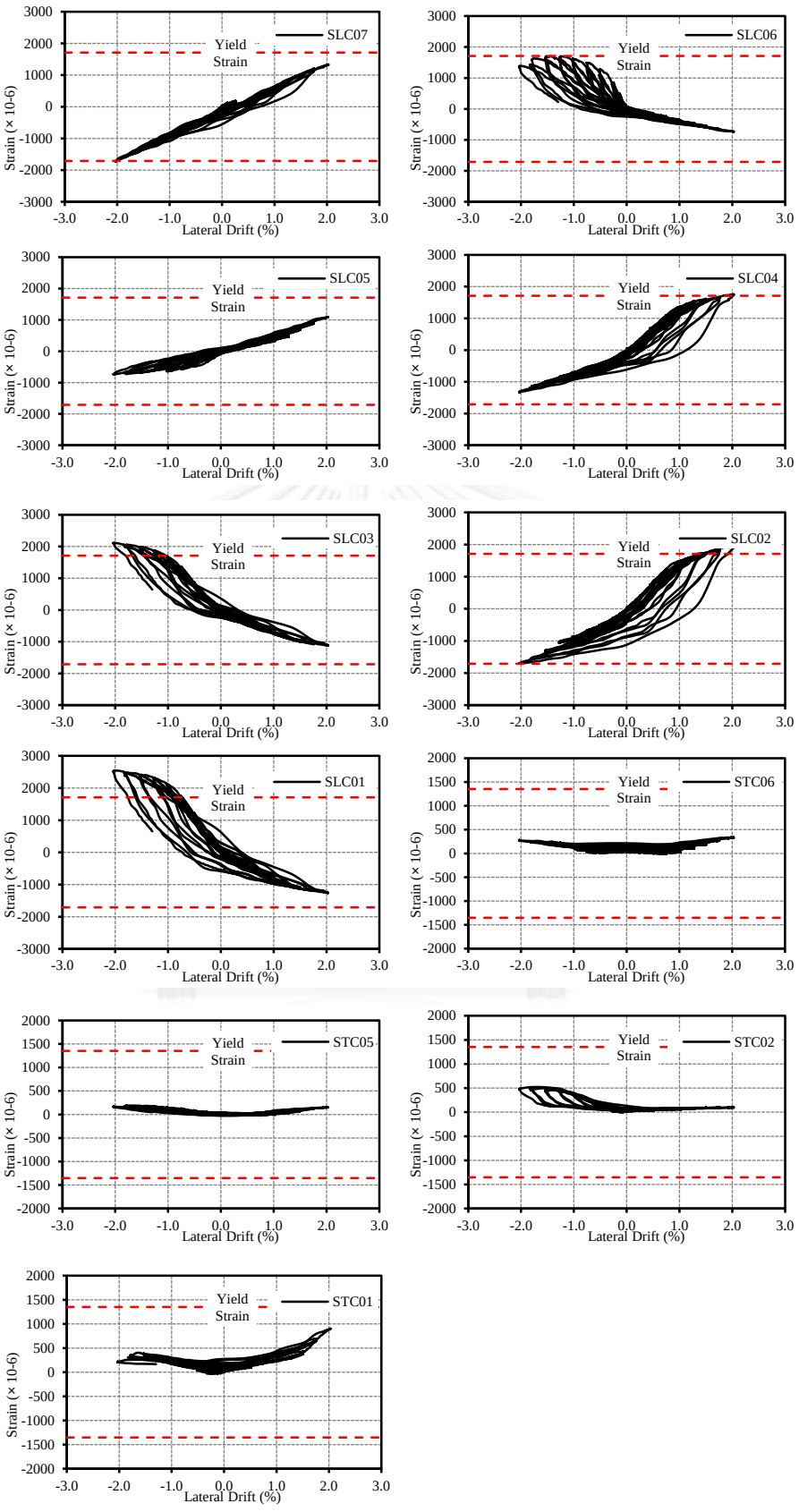

Figure A-4. Drift ratio-strain relation of re-bars in the column of MIRCF02

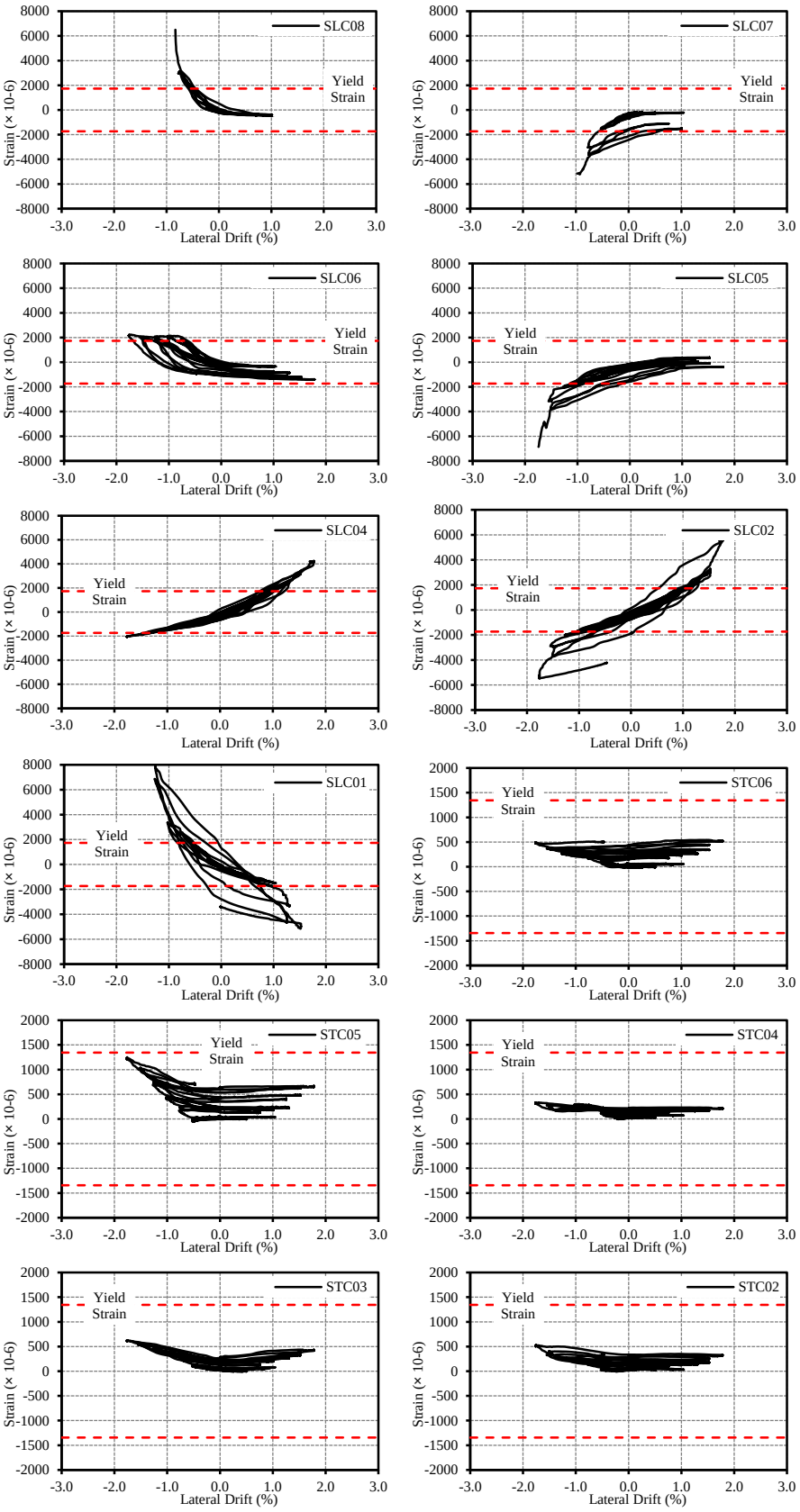

Figure A-5. Drift ratio-strain relation of re-bars in the column of MIRCF03

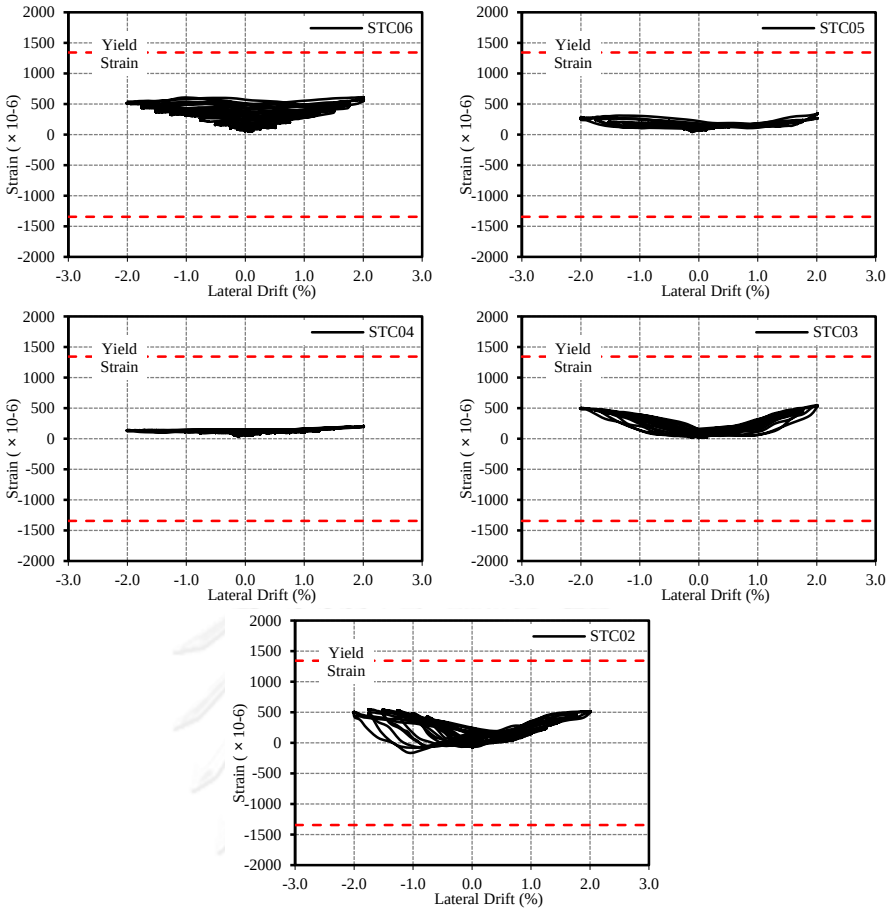

Figure A-6. Drift ratio-strain relation of transverse re-bars in the column of MIRCF04

VITA

My name is JARUN SRECHAI. I was born in Trang province, Thailand, on February 25, 1982. For the secondary school and vocational certificates, I studied at Ratsada Nupradit Anusorn School and Trang Technical College, respectively. In 2002, I completed the program for the Diploma of Civil Technology from Rajamangala Institute of Technology Southern Campus. Then, I moved to Bangkok and had a chance to study in the Bachelor's and Master's programs of Civil Engineering at King Mongkut's University of Technology Thonburi where I graduated in 2005 and 2007, respectively. In the following year, I received a scholarship from the Commission on Higher Education of Thailand-AUN/SEED-Net to study in the Ph.D. program at Department of Civil Engineering, Chulalongkorn University. In 2011, I got an exchange doctoral student scholarship from the European Commission funded project EU-NICE. With this support, I had an opportunity to carry out my research at the University of Chieti-Pescara, Italy.